DESIGN AND DEVELOPMENT OF PZT BASED MICROPUMP FOR MICROFLUIDIC APPLICATIONS

Fathima Rehana Munas

148054T

Thesis submitted in fulfillment of the requirements for the degree of Master of Philosophy

Department of Mechanical Engineering

University of Moratuwa
Sri Lanka

January 2020

DECLARATION

I declare that this is my own work and this thesis does not incorporate without acknowledgement any material previously submitted for a Degree or Diploma in any other University or institute of higher learning and to the best of my knowledge and belief it does not contain any material previously published or written by another person except where the acknowledgement is made in the text.

Also, I hereby grant to University of Moratuwa the non-exclusive right to reproduce and distribute my dissertation, in whole or in part in print, electronic or other medium. I retain the right to use this content in whole or part in future works (such as articles or books).

Signature Date

The above candidate has carried out research for the MPhil thesis under my supervision.

Name of the supervisor: Dr. Y.W.R. Amarasinghe

Signature of the supervisor: Date

ABSTRACT

The present technical context is promptly growing in implementing onsite microfluidic utensils utilized in microfluidics owing to their great demand. The microfluidics mainly involves in implementing minuscule devices to deal with minute volumes of fluids. Manufacturing these microfluidic devices like micropumps is a great challenge and micropumps are very much indispensable to regulate and convey fluid in minute scale.

In this research a PZT based micropump was designed and developed for microfluidic applications. A PZT actuated brass diaphragms and a comprehensive flow arrangement are the important elements of this micropump structure. Basically, the design prominences on a cross junction, engendered by a nozzle jet with a pump chamber and two inlet and an outlet channel respectively. In this sense, the fluid flow rectification is done by nozzle jet feature to expedite the fluid path within the system during every vibration cycle of PZT diaphragm. This micropump device was developed with layer by layer fabrication of polymethyl methacrylate (PMMA) plates using laser cutters and all the layers were squeezed in to attain required structure.

In order to recognize the physiognomies of flow and to verify the experimental outcomes with simulated data, numerical simulation analysis in ANSYS were carried out. In addition, the PZT diaphragms were under taken for eigenfrequency study analysis in COMSOL Multiphysics as well. In this sense, the applied frequency of the piezoelectric diaphragms was varied by using the prescribed control system developed for this device. As per the test results, the maximum flow rate of 31.15 ml/min achieved at the frequency of 100 Hz. In addition, the thin film deposition techniques and the thermo elastic damping analysis on PZT actuators were also analyzed to identify the performance enhancement of this micropump.

Since monitoring pressure and getting response is vital in microfluidic devices, design and simulation of MEMS based piezoresistive pressure sensor has been carried out. According to the piezoresistive structural coupled field analysis, the optimal diaphragm structure was chosen among three kinds of diaphragms considered for this study. Further, the thermo mechanical behavior of piezoresistive pressure sensors have also been considered in this research.

At last, the complete numerical simulation was done for the micropump fluid flow coupled with the designed pressure sensor. According to this analysis, the pressure sensor gives the favorable sensitivity variation over micropump discharge pressure. Hence the developed micropump is not only for a specific application but also worthwhile in a wide range of microfluidic applications.

Keywords: PZT, valveless, micropump, MEMS, Piezoresistive, Pressure Sensor

DEDICATION

This thesis work is dedicated to my family and my teachers. A special feeling of gratitude to my loving parents, who have always loved me unconditionally and whose good examples have taught me to work hard for the things that I aspire to achieve. Also, I am truly thankful to my husband who has been a constant source of support and encouragement during the challenges.

ACKNOWLEDGMENT

I take this great opportunity to express my profound gratitude and deep regards to my research supervisor Dr. Y.W.R. Amarasinghe for his exemplary guidance, monitoring and constant encouragement throughout my research. Without his keen supervision none of this work would have been possible for myself alone.

I consider myself very fortunate for being able to work with such a resourceful individual. I also express my sincere gratitude to my co-supervisors Dr. Van Thanh Dau and Dr. Pubudu Kumarage for their cordial support, valuable information and guidance, which helped me to carryout simulations in this task through various stages.

I also would like to remind Prof. Dzung Viet dao and Dr. Van Thanh Dau for their valuable feedbacks and guidance in my publications even they are busy with their schedule.

Moreover, I'm particularly grateful to the Head of the Department of Mechanical Engineering as well as one of the panel members of this research Prof. R.A.R.C. Gopura, for his tremendous support and guidance. Furthermore, I would like to extend my utmost gratefulness to Dr. A.G. Buddhika P. Jayasekara who is the chair of the progress review panel appointed for this research, for his valuable comments and advices given to me throughout this research. I also thankful to Dr. Damith Chathuranga who is the research coordinator of the Department of Mechanical Engineering.

I would like to especially thank to the Final year project students N.H.R.G. Melroy, G.C.B. Abeynayake and H.L. Chathuranga who helped me in the fabrication process.

I also thank to the staff of the Mechatronics and MEMS/NEMS laboratory of Department of Mechanical Engineering for providing me the facility required for conduction my research works whenever required.

I especially thank to Mr. Eranga De. Silva, Mr. Isururu Udayange, Mr. Pesan Sampath, Mr. Janaka Basnayake and Mr. Uditha Roshan for their valuable support in the mechatronic laboratory. I also owe my thankfulness to the Head of the Department of Mechanical Engineering, Faculty of Engineering, South Eastern University of Sri Lanka for his great support.

Last but not the least I express my sincere gratitude to everyone who supported me throughout my research work.

Fathima Rehana Munas,
MPhil Postgraduate,
Department of Mechanical Engineering,
University of Moratuwa.

TABLE OF CONTENTS

LIST OF FIGURES

LIST OF TABLES

LIST OF ABBREVIATIONS

Abbreviation	Description
DRIE	Deep Reactive Ion Etching
EHD	Electro Hydro Dynamic
EO	Electro Osmotic
EW	Electro Wetting
FEM	Finite Element Method
FI	Fluid Inertia
ICPF	Ion Conductive Polymer Films
ITO	Indium Tin Oxide
KOH	Potassium Hydroxide
LOC	Lab On a Chip
MEMS	Micro Electro Mechanical System
MHD	Magneto Hydro Dynamic
μTAS	Micro Total Analysis System
PCB	Printed Circuit Board
PDMS	Poly Di-Methyl Siloxane
PEEK	Polyether Ether Ketone
PGA	Polyglycolide/ Polyglycolic Acid
PLA	Polylactide/ Polylactic Acid
PMMA	Poly methyl methacrylate
POCT	Point Of Care Testing
PZT	Lead Zirconate Titanate
SDM	Shape Deposition Manufacturing

Abbreviation	Description
SFF	Solid Free Form Fabrication
SL	Stereo Lithography
SMA	Shape Memory Alloys
SOI	Silicon On Insulation

CHAPTER 1.0 INTRODUCTION

The present technical context is promptly growing in developing onsite biomedical devices used in microfluidic applications owing to their mandatory requirements. The microfluidics mainly involve implementing minuscule devices to deal with minute volumes of fluids. Even manufacturing biomedical devices such as microneedles, micropumps, micro pressure sensors and others for microfluidics is great challenge. Micropumps are very much indispensable to regulate and convey fluid in minute scale and they have the prior opportunity in different applications of biomedicine amongst all the devices utilized in microfluidics.

Macroscopic pumps such as water pumps and fuel pumps are used in realistic day to day applications. Micropumps are developed by scaling down the macroscopic pumps where micromachining techniques are used to develop these diminished features of the micropumps [1][2][3]. In addition, micropumps are very much useful in various sectors like biomedical, food and beverages, aerospace, printing, microelectronics, automotive, chemical processing and consumer products. Also, the demand for micropumps in biomedical applications as well as in industries are extensive.

Based on the operation principles, micropumps are categorized as mechanical and non-mechanical micropumps. Generally, a physical actuator is indispensable to actuate these mechanical micropumps. Meanwhile, non-mechanical micropumps are used to increase the momentum of the working fluid in micro devices due to the addition of energy [4][1][2][3]. Therefore, mechanical micropumps are very much useful in biomedical applications.

To standardize the fluid flow in micropumps, valving techniques are substantial and hence, they are subcategorized as micropumps with or without valves. In valve type micropumps, an exterior actuation technique is required to regulate the flow through it. Valve type micropumps are immensely complicated in integrated microfluidic systems even though monitoring the valves is relatively easy. On the other hand, diffuser/nozzle components are the key factors for flow monitoring in valveless micropumps [4].

Mechanical micropumps with valveless arrangement comprise a pump chamber enclosed with periodically oscillating elastic diaphragm. An actuation technique is

used to drive this periodic oscillation of the diaphragm and this roots a periodic variation in the fluid volume and pressure inside the pump chamber [1][5]. The diffuser/nozzle elements attached to the pump chamber will guide the fluid motion to flow in a proper path [1][2][6][7][8][9][10].

Micropumps are used to deliver fluid from one place to another place in a controllable manner. However, some applications need high precision and compact designs. Considering the historical data of micropumps, first micropump was made in 1975 [11]. In 1978, a publication on the "Design and development of a micropump for release of insulin" was produced. This design was carried out with miniature piezoelectric diaphragm and active valves controls techniques to control insulin delivery [12].

In 1990, silicon etching techniques by adapting normal silicon processing methods used in manufacturing integrated circuits was used to fabricate micropump. In this micropump, the maximum speed of 100 μl/min and a 60 cm of pressure in water column was achieved. Here, the driving frequency was one of the key element in determining the speed of pumping [13].

In 2016, design and simulation analysis of Poly Dimethyl Siloxane (PDMS) membrane based piezoelectric micropump was carried out. In this micro pump, the flow rectification is done by the valveless diffuser with the divergence angle of 15˚ and the flow rate of about 0.75m/s. Also this pump works in low Reynolds's numbers varying from 5 to 40 [14].

From 1975 to 2016, numerous researches have been carried out on the "Design and simulation of micropumps" where some of the researches had gone beyond the development of the micropump for the bio medical applications. The micropumps can be classified by their actuating mechanism, the structural component as well as their applications.

A number of micropumps are developed with different kinds of actuation principles for diverse applications. But it is essential to measure discharge pressure feedback in portable devices like micropumps. There are yet no devices developed till now that use pressure feedback mechanism although it is worthwhile to develop a micropump with such technique for microfluidic applications.

Therefore, the research in this thesis describes the design and development of PZT actuated micropump for microfluidic applications. The Figure 1 shows the proposed design of the micropump. In this sense, there are several areas to be focused in developing the micropumps. Some of them are actuating principles, working principles, modelling and simulation, fabrication, characterization as well as signal conditioning which are described in detail.

The remainder of this chapter consist of aim and objectives of this research. The layout of the thesis are also provided.

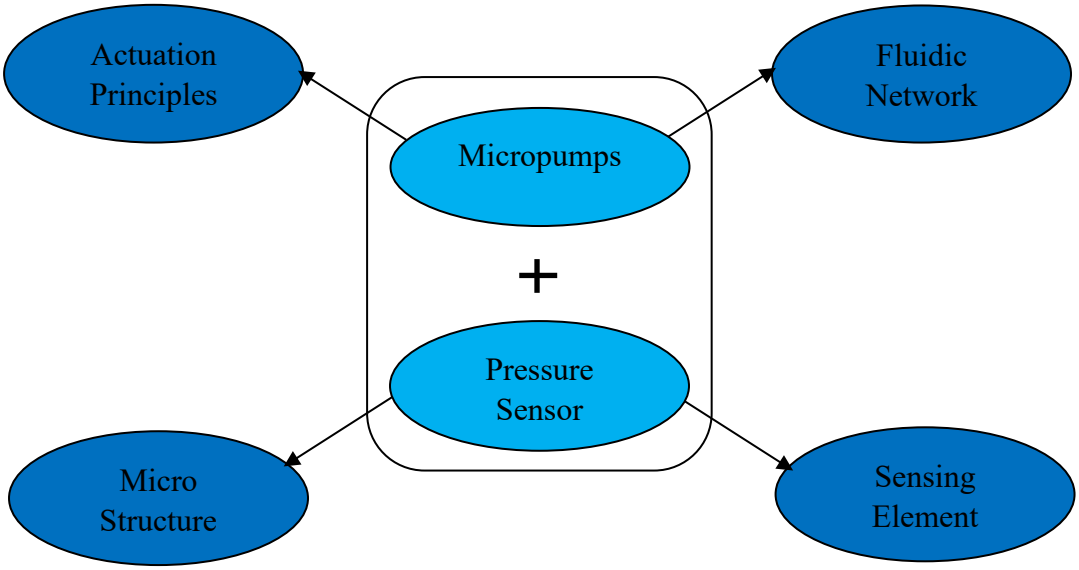

Figure 1: Proposed design of the micropump

1.1 Aims and Objectives

1.1.1 Aim:

The principle aim of this research is to develop a performance enhanced PZT based micropump for microfluidic applications.

1.1.2 Objectives:

- Identify the working principles, performance factors, governing laws and parameters as well as different types of actuating mechanisms of micropumps.
- Propose a novel suitable structure for the micropump.
- Design and simulate the micropump using FEM tools to complete the theoretical analysis.
- Fabricate the micropump with suitable fabrication techniques.
- Testing and validating the overall system through a simple electrical circuit.

- Performance enhancement of PZT actuated micropumps.
- Design and simulate a MEMS based pressure sensor to couple with the micropump for the pressure monitoring and feedback requirements.
- Complete the numerical simulation for the entire system consisting micropump coupled with pressure sensor to analyze the applicability of the system.

When developing PZT based micropump for microfluidic applications, it is very essential to conduct a literature review. This literature review is mainly based on the micropumps. The pressure sensors used for pressure monitoring and feedback to identify current stage in the development of these micropumps. Therefore, in this thesis, Chapter Two consists of the details about the conducted literature review.

As an initial step, design and simulation studies were carried out for a PZT actuated micropump. Hence the Chapter Three of this thesis consists the details about the design and simulation of PZT actuated micropump. The proposed PZT based valveless micropump was fabricated using suitable fabrication techniques. Hence the fabrication of this micropump is explained in Chapter Four. The signal conditioning and electrical circuitry is essential for the easy operation and control of the fabricated micropump which are presented in Chapter Five of the thesis. The testing and validation of the fabricated micropump within the prescribed ranges is also vital. Thus, the Chapter Six explains the testing and validation procedure with the results to examine the feasibility to use this device for microfluidic applications. It is necessary to analyze the performance enhancement of the fabricated micropump. Thus, it is briefly discussed in Chapter Seven of the thesis. Since the pressure monitoring and feedback of this micropump is an additional advantage for this device, design and simulation studies were performed for a MEMS based piezoresistive pressure sensor to be integrated with this micropump. Hence the Chapter Eight of this thesis consist the details about the Design and Simulation Analysis of MEMS based piezoresistive pressure sensor. As the next stage, numerical simulation analysis was performed for this entire system consisting of micropump coupled with pressure sensor to analyze the applicability of the system. These fine points are discussed in Chapter Nine. Finally, the Chapter Ten presents the discussion of this research work.

CHAPTER 2.0 LITERATURE REVIEW

2.1 Micropumps and microfluidic applications

This literature articulates various kinds of micropumps based on their operation principles and their applications in microfluidics. Also, this review is mainly concentrated on existing micropumps and their operation principles with their pros and cons. The main components of the micropump and their feature are also discussed under this section. The eminence of this literature is to discuss about actuation methods, working principles, performance parameters and their medical applications described in the literature. In addition, brief explanation about commercially available micropumps is also done.

2.1.1 What is Micropump

Many researchers in literature have defined micropump in several ways. An exemplary micropump is a source that has actuation technique used to transmit fluid in a precise manner [7][15][16]. The Figure 2.1.1 a illustrates the schematic diagram of a micropump. Like in macro-sized pumps, micropumps are also designed to move fluids. But because of their minute scale in size, non-mechanical methods can also be applicable to pump fluids to exploit the physical characteristics of fluids at the micro-scale. According to this concept, micropumps are categorized as mechanical and non –mechanical micropumps [2][16].

The exertions in developing micropumps are directed to fabricate various types of micropumps as per the requirements and specifications [3][7]. In addition, the Figure 2.1.1 b shows photographs of micropumps used in various applications.

The design of micropumps is mainly based on valve mechanisms such as valve based and valve less. In addition, there are several actuating mechanism that would also be used in designing a micropump such as piezoelectric, electrostatic, thermo-phenumatic, electromagnetic, Bimetallic and others [17][18]. This will be discussed in detail in the following chapters. Mainly microfluidic structures require pump with size comparable to the volume to be pumped. On the other hand, the root factors such as reliability, power consumption, actuation voltage, ease and cost of fabrication,

biocompatibility and a dosing accuracy are also factors to be considered in microfluidic applications [19][20][21].

As micropumps in biomedical applications mainly deal with the human where the resources used for fabrication has to satisfy bio-compatibility and bio-stability necessities [22]. Therefore, bio-compatible material selection is an important factor in developing these kinds of micropump. Silicon is a good bio-compatible material for extensive use in microfluidic applications especially in biomedicine. However, polymers are commonly used in biomedical applications and suitable for human implantation. Polymethyl Methacrylate (PMMA), Poly Dimethyl Siloxane (PDMS) and SU-8 photo resist have good biocompatibility that are presently used in fabrication of micropumps [2].

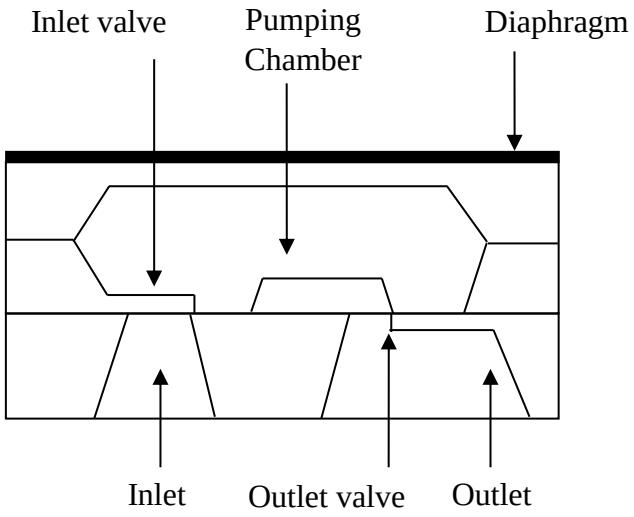

Figure 2.1.1 a: Schematic illustration of a micropump [23]

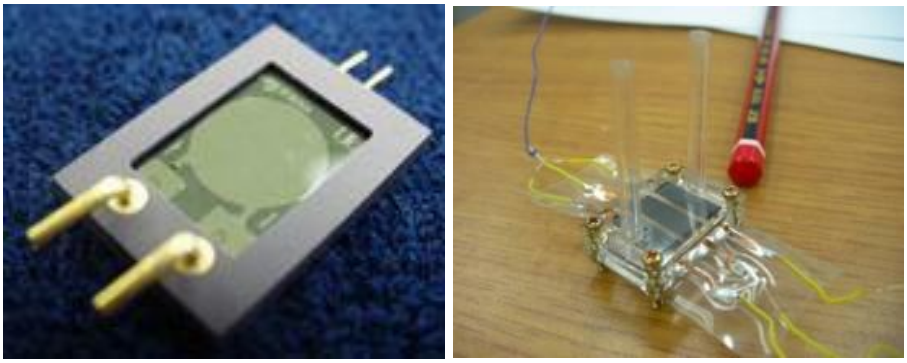

Figure 2.1.1 b: Photographs of micropump [20][24]

2.1.2 Applications of Micropumps

Pioneering work on micropumps is initiated in 1970s. In order to implant them into the human body, the very first miniaturized micropump was developed in 1975 by Thomas and Bessman [2]. The fabrication of this device was carried out by using basic conventional methods [2]. Then, Smith designed and developed a peristaltic micropump consisting of three valves with piezoelectric actuation by using silicon micro fabrication techniques for insulin delivery in early 1980s [2][19].

Though micropumps are being developed for many motives, the key objectives are reduction of weight and the ability to handle trivial capacities [2]. Because of their reduced dimensions, micropumps weigh less and use less space than their macroscopic counterparts. They also have the ability to handle small volumes of liquid very efficiently. In addition, these pumps can be applied in various activities such as transmitting fluids, mingling fluids, safe handling of perilous fluid and waste separation. There are many benefits of micropumps in industries and the application of these micropumps are categorized into four main areas which is illustrated in Figure 2.1.2.

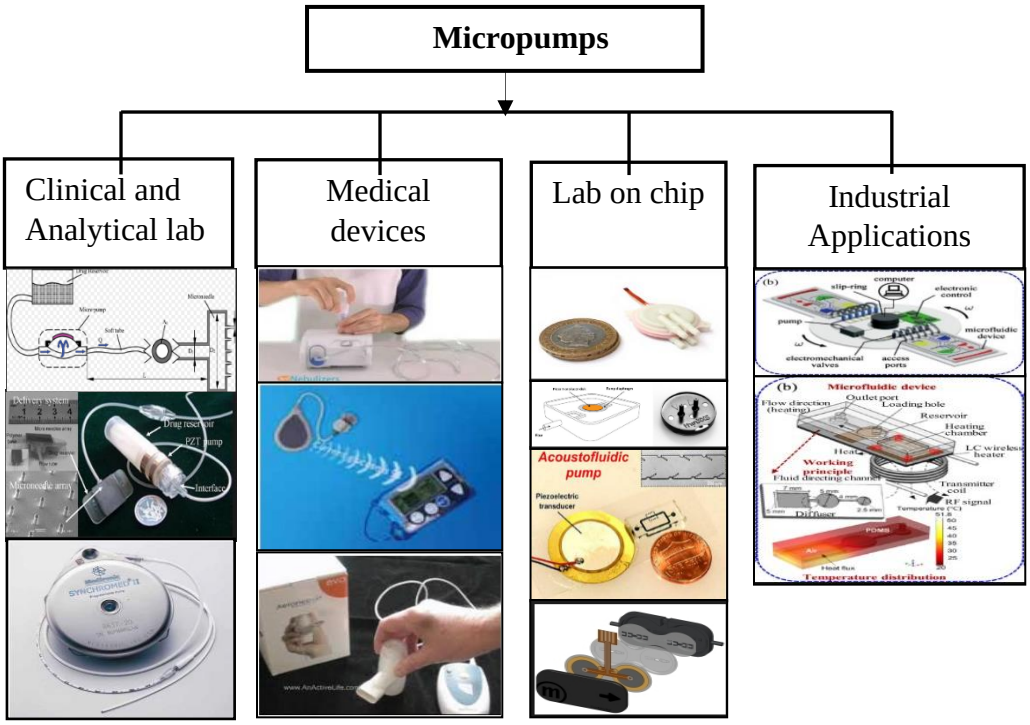

Figure 2.1.2: Application areas of micropumps

However, the bio medical sector is most attracted to these giant characteristics. It is very crucial in formulating models for therapeutic analyses and distributing exact dosages of prescriptions. By using a micropump, a small drop of blood also can be extracted from a patient and distributed on a chip for analysis. Micropumps have precise distribution and dosages with fast dynamic response. Micropumps are also developed so that they can be used in vivo or internal to the pump. These pumps are used to deliver medications for variety of purposes.

In addition to this, micropumps are very useful in DNA hybridization to shuttle flow through micro channel [25]. Also, these are ideal for hazardous environment and low power consumption.

2.1.3 Commercial availability of micro pumps for microfluidic applications

Though researches have been carried out from 1975 to 2016 in biomedical industry for microfluidics, commercial availability of these micro pumps are very few. The Dolomite Company fabricated micropumps with the dimensions of 25 x 25 x 4.8 mm respectively [26]. Figure 2.1.3 shows the micropump developed by Dolomite Company. Also Bartels Company manufactured micro pump with check valves named as “mp6” [27]. In addition to this, it is mentioned that, these two commercially available pumps need micro pump controller (signal generator) to control the flow rate.

Figure 2.1.3: Micropump produced by Dolomite company[27]

2.1.4 Classification of Micropumps

Currently micropumps are categorized as mechanical and non-mechanical micropumps. In general, mechanical micropumps are defined as mechanically actuated pumps and they are literally scaled down versions of their macroscopic counter parts with a distinct pumping technique. But non-mechanical micropumps are typically not found in the macroscopic world. However, these are commonly used in micro devices because they can take advantage of some of the physical properties of the fluids when the volume decreases to microliter level. These kinds of micropumps constantly add energy to the referencing fluid in order to proliferate the momentum. Due to the exposed energy transfer, dynamic pumps can engender steady and constant flows.

Based on the actuation techniques and operating principles, micropumps are characterized into numerous sub- sets. The Figure 2.1.4 illustrates the classification of micropumps.

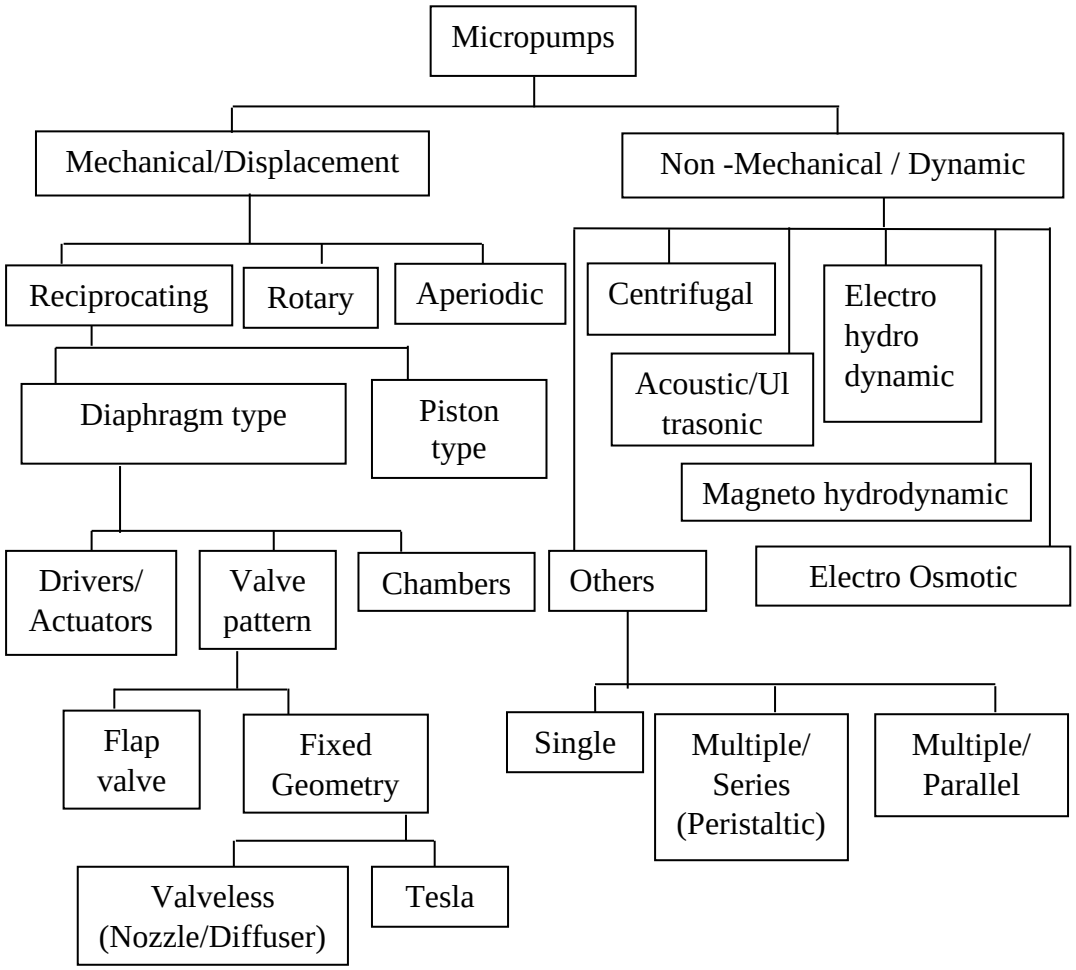

Figure 2.1.4 Classification of micropumps[19]

2.1.5 Design specifications and parameters

To ensure the success of the proper design of micropumps in real world uses, it is vital to comprehend about valves, actuators, reservoir, nozzle/diffuser mechanism and pumping parameters [1] [19].

2.1.5.1 Actuator

The actuator is the essential component of a micropump which transmutes energy into motion. In this sense, the actuator receives energy from electricity, heat, liquid pressure, air pressure and translates it into motion [1]. In literature, most of the designs has actuation disk which is attached to the membrane. Membranes are fabricated in such a way that it produces energy itself. However in peristaltic micropumps, more than one actuator is fabricated sequentially [1].

2.1.5.2 Valves

In microfluidic applications, active and passive valves have been described to control the fluid flow [1] [2] [17]. Although actuation mechanisms are not applicable in passive valves, the control of fluid flow is reliant based on the difference in pressure. Also the fluid flow is in unique path through these kind of valves [2].

On the other hand, active components are operated by an external actuation source in active valves and the very first active valve was reported in 1988 by Van Lintel [2] [19].

2.1.5.3 Chamber or Reservoir

Considering the microfluidic systems, chamber design is crucial, and it has significant impact on the pressure characteristics, stroke volume and nozzle-diffuser loss coefficients. In literature, it is observed that micropumps have single chamber as well as multiple chamber arrangement. In peristaltic pumps, chambers are arranged in series /parallel manner to improve the performance [2] [17] [28].

2.1.5.4 Nozzle/Diffuser Element

Nozzle/diffuser element is a modulator to flow in valveless micropumps. In 1993, Stemme and Stemme presented the nozzle/diffuser action in a valveless micropump as

a first time [2][19]. Basic principle of the nozzle/diffuser element is the large quantity of fluid enters into the chamber through an inlet than fluid exiting the outlet during the suction. In the meantime, the action will be reversed during the compression [2]. The nozzle/diffuser action in micropumps is shown in Figure 2.1.5.4. The pressure loss Δp at a rectification structure is also given by:

$$\Delta p = \varsigma \frac{\rho u^2}{2} \qquad (2.1.5.4)$$

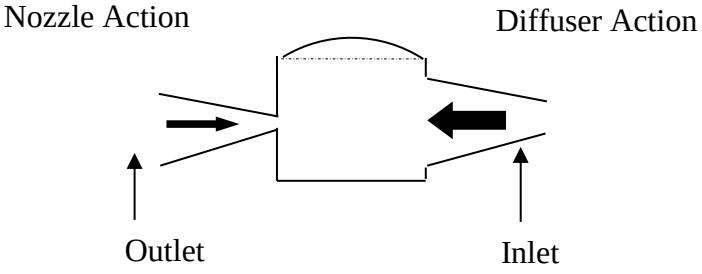

a

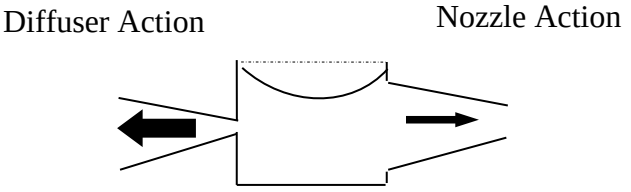

b

Figure 2.1.5.4: Schematic diagram of nozzle/diffuser element [17][28]
(a. Expansion stroke/Supply mode b. Compression stroke/Pump)

2.1.5.5 Pumping Parameters

Optimizing the pumping parameters such as maximum flow rate (Q_{max}), pump power (P_{pump}), maximum back pressure (h_{max}) and pump efficiency (η) is very much essential for the better performance of the micropumps. At zero $h_{max,}$ Q_{max} is optimum and at the highest value of h_{max}, Q_{max} is zero. For incompressible flow, the pump head (h) can be calculated from the steady flow energy equation[2][15][17]:

$$h = \left(\frac{P}{\gamma} + \frac{u^2}{2g} + Z \right)_{exit} - \left(\frac{P}{\gamma} + \frac{u^2}{2g} + Z \right)_{entrance} \quad (2.1.5.5\ a)$$

The efficiency of the pump η is expressed in terms of power as follows:

$$\eta = \frac{P_{pump}}{P_{actuator}} \quad (2.1.5.5\ b)$$

Here, the efficiency is governed by fluid leakage losses, frictional losses and losses due to imperfect pump construction [1] [17].

Then the total efficiency is expressed as:

$$\eta_t = \eta_m \eta_v \eta_h \quad (2.1.5.5\ c)$$

2.1.6 Mechanical Micropumps

In mechanical micropumps, periodic movement of mechanical components pushes the fluid from inlet to outlet [2]. Initially, these micropumps are developed with the actuation method of reciprocating piston [8]. Here the intermittent operation of moving boundaries gives impact on the working fluid during suction and compression. In most of the macroscale mechanical pumps, moving boundaries are pistons. Whereas in mechanical micropumps, actuated diaphragms which are glued around its perimeter are the moving elements. The fabrication of these diaphragms are carried with glass, PDMS and silicon. In addition, these diaphragms enclose the pumping chamber of the micropump with various kinds of actuation methods [2].

Here, the periodic oscillation of the diaphragm generates pressure difference (Δ P) which is a function of stroke volume (ΔV) of the micropump [1][2][3][17]. Hence the compression ratio (ε) is defined by the equation:

$$\varepsilon = \frac{\Delta V}{V_o} \quad (2.1.6)$$

Where (V_o) is the dead volume of the pumping chamber.

One of the main applications of a mechanical diaphragm micropump is the delivery of insulin to diabetes patients to regulate their blood sugar. It was primarily developed in 1990s. In addition, this mechanical micropump can also be used in the “lab on a chip” (LOC). Here, LOC refers to a chip on which several laboratory functions have been

integrated in MEMS technology. Though LOC handles extremely small fluid volumes (picolitres or less), micropumps are used to remove a drop of blood from a patient and distribute on to the LOC [19].

According to the present and past experiences, the performance of these kinds of pumps are normally limited by its different actuation principles, their applications, construction and fabrication parameters [1][2][15][19].

2.1.7 Actuation Principles

There are various kinds of actuation techniques such as electrostatic, piezoelectric, thermo-pneumatic, electromagnetic, shape memory alloy as well as bimetallic techniques which are discussed in various kinds of micropumps. These actuation principles are explained below in a detailed manner.

2.1.7.1 Electrostatic Actuation

These actuation techniques are vital for micropumps used for microfluidic applications. When applying voltage between two plates, coulomb attraction will be generated [2]. Hence, the electrostatic force induced by electric field is the electrical force of attraction and repulsion [2][3][20][17][28]. Further, the electrostatically actuated micropump is illustrated in Figure 2.1.7.1.

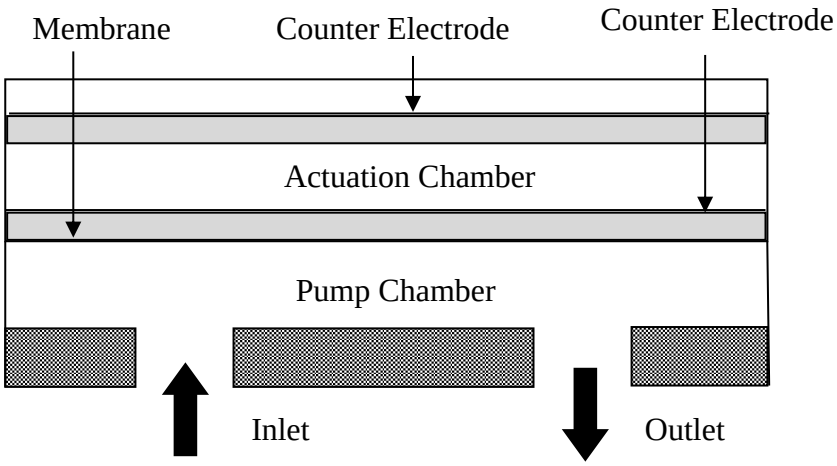

Figure 2.1.7.1: Electrostatic principle of actuation [2]

When applying high voltage to the capacitor electrodes, pump diaphragm is electrostatically attracted, and the diaphragm goes for deflection. The volume of the chamber and the pressure within the micropump vary during the intermittent oscillation of the membrane and this allows the fluid to push in to the pump chamber in a unique direction [2]. The equation 2.1.7.1 a explains the capacitance between the diaphragm and the electrode:

$$C = \frac{\varepsilon A}{l} \qquad \text{(2.1.7.1 a)}$$

Also the developed electro static force between the two electrodes is given by:

$$F = \frac{1}{2}\frac{\partial C}{\partial l}V^2 = -\frac{\varepsilon A}{2l^2}V^2 \qquad \text{(2.1.7.1 b)}$$

Where A is the Area, ε is permittivity of the medium, l is the distance between the plates and V is the voltage.

As per the described equations, the selection of the medium is considerable though the electrostatic force depends on it as well. The past records reveal that the research and development studies had been carried on these actuation techniques.

The positive impact of these micropumps are fast response and low power consumption [2][23][17][28]. However, the significant weakness is the considerably small displacement. In addition, the electrode degradation would occur after the long-term operation and this leads to the reduction in electric field strength. In order to avoid these issues, researches are constantly conducted to introduce bipolar techniques with more complex electronic drive systems [8].

2.1.7.2 Piezoelectric Actuation

Piezoelectric actuation technique is mostly applicable in biomedical applications [2][20][28]. This mechanism is paramount due to its sophisticated features. In this technique, the piezoelectric effect is used to convert electrical energy to mechanical energy [2]. When an electric field is applied on a piezoelectric crystal, the strain will be developed. The Figure 2.1.7.2 shown below represents the piezo electric principles of actuation. In these actuation technique, stroke volume and actuation force are

significantly high. Not only this, it is very simple with fast mechanical response although fixing the PZT material on the micropump membrane is a bit of difficulty and the construction is complicated. In addition high actuation voltage is required [2][3][17][28].

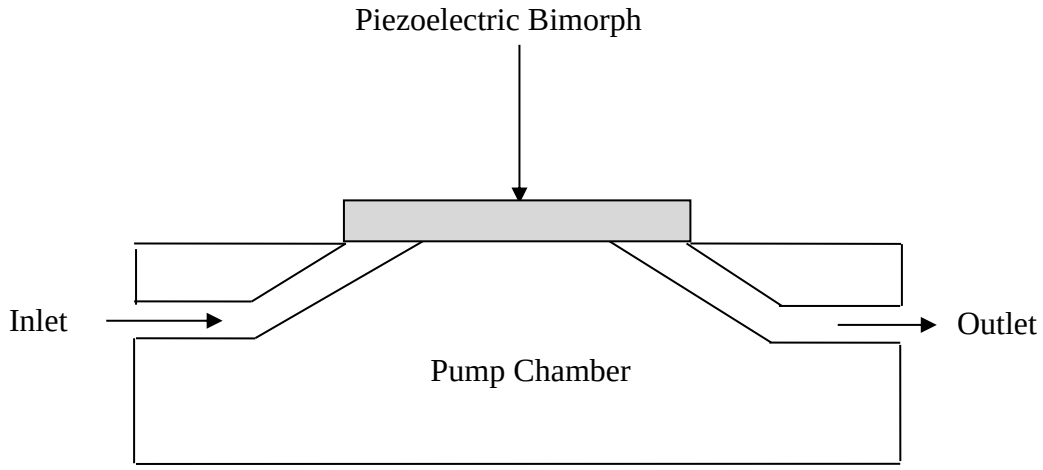

Figure 2.1.7.2: Piezoelectric principle of Actuation[2]

2.1.7.3 Thermo-pneumatic Actuation

In thermo-pneumatic actuation technique, a pair of heater and cooler is used to expand and compress air inside the chamber in a periodic and consecutive manner. Due to the periodic change in the volume of the chamber, the membrane gets regular momentum to allow the fluid flow. These pumps stimulate relatively large diaphragm displacement and induced pressure [2][3]. Here, the increase of pressure in liquids is expressed as [2][3].:

$$\Delta P = E\left(\beta \Delta T - \frac{\Delta V}{V}\right) \qquad (2.1.7.3)$$

Thermo pneumatic micropumps have the ability to make compact and small design, with several 100 micrometers of membrane displacements. Hence the flow rate throughout the pump is huge. Also the fabrication and integration are easy by using silicon technology [2]. But thermo pneumatic actuation has relatively long thermal time constant, which is vital during the cooling process. This actuation exhibits a high-power consumption and this leads to the heating of transport medium. Hence it is

essential to maintain the driving power at constant and specific level. The Figure 2.1.7.3 represents the thermo pneumatic micropump actuation.

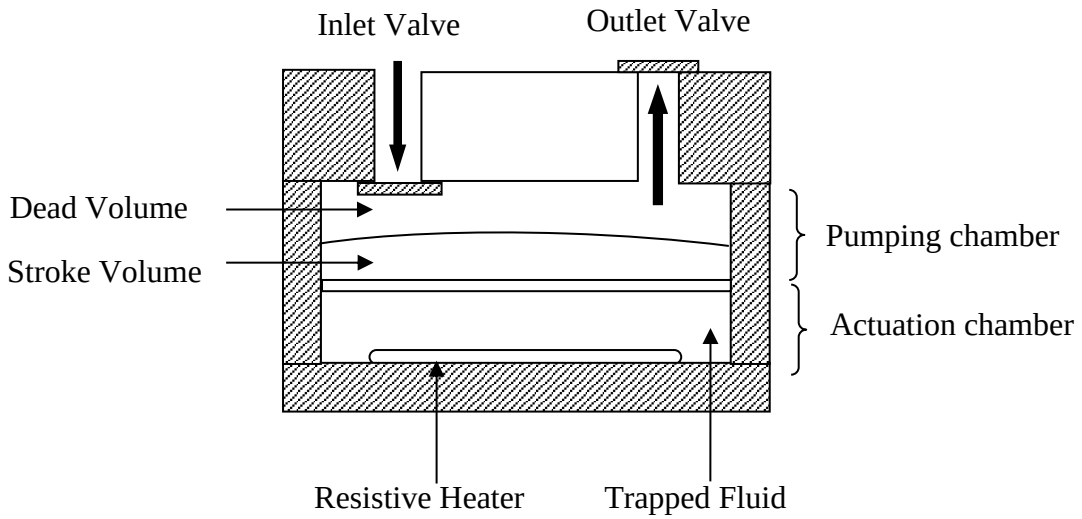

Figure 2.1.7.3: Thermo- pneumatic principle of actuation [28]

2.1.7.4 Electromagnetic Actuation

The electromagnetic actuation technique is in its grounding stage of development [2][28]. This micropump has a flexible membrane, a chamber including inlet and outlet valves, a permanent magnet and driving coils. This kind of actuation technique is shown in Figure 2.1.7.4 [2][3][19].

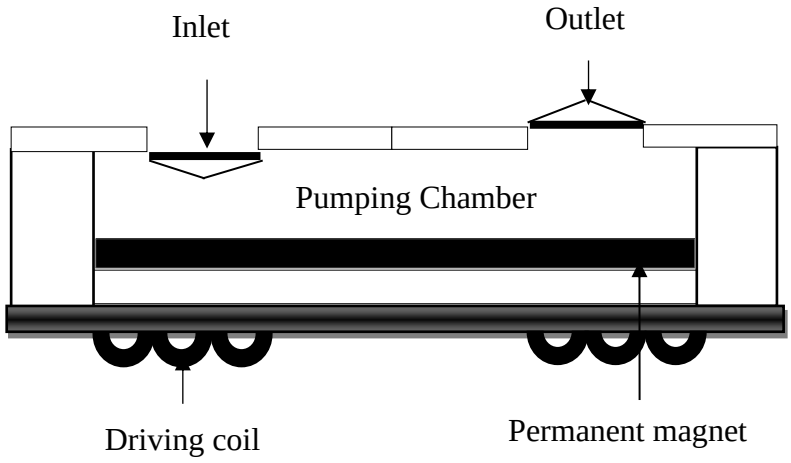

Figure 2.1.7.4: Electromagnetic principle of actuation [19]

In this principle, the membrane can be fixed with the set of coils or magnet. Here, the magnetic strength varies by varying the electric current in the coils and the electromagnetic actuation is realized by a solenoid plunger. Also, the force developed by this actuator is mainly based on the applied current and the number of turns.
However, this form of actuation requires relatively low voltages (~5V) where it has high power consumption and heat dissipation [2]. Further miniaturization is complicated due to required size of the solenoid coil. On the other hand, integration of the magnets, cores and the micro coils are also difficult [2][17].

2.1.7.5 Shape Memory Alloy (SMA) actuation

Shape memory alloy (SMA) actuation technique is mainly based on the shape memory effect. This effect is generated due to the phase transformation between two solid phases. The aforementioned two phases are austenite and martensite at high and low temperature respectively [2]. Here, Au/Cu, In/Ti, and Ni/Ti are used as shape memory alloys. In SMA materials, the martensite is much more ductile than austenite. Also, they might have significant deformation due to the selective migration of variant boundaries during the low temperature range. Then the material starts to form single variant austenite during the heating of austenite start temperature. The mechanical deformation for actuation occurs due to these phase transitions [2]. A schematic illustration of SMA micropump is shown in Figure 2.1.7.5.

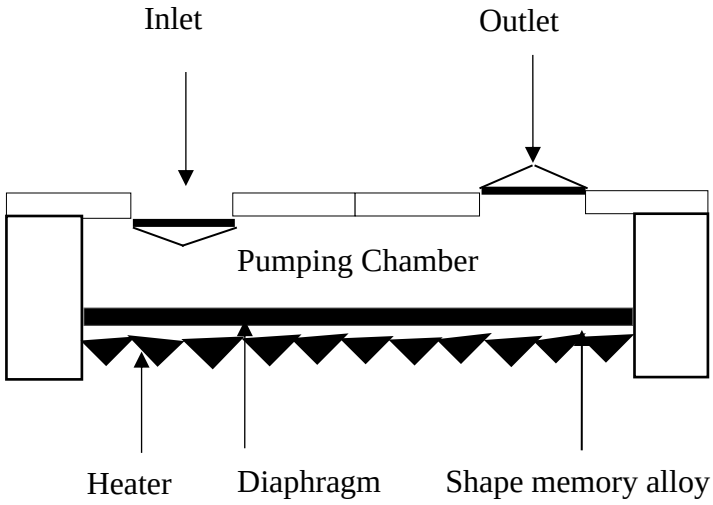

Figure 2.1.7.5: Schematic illustration of shape memory alloys [2].

In addition, SMA micropumps have high force-to-volume ratio and damping capacity. Also, they have the ability to recover large transformation stress and strain. In addition, these micropumps are biocompatible and chemical resistance. On the other hand, SMA micropumps need specific SMA materials and comparatively high power. Also the deformation is uncontrollable to temperature sensitivity [2][3][19][17].

2.1.7.6 Bimetallic Actuation

Bimetallic actuation is based on two different metals with different thermal expansion coefficients joined together. The deflection of a diaphragm is made of bimetallic materials induced against thermal alternation and thermal expansion factors. Implementing these techniques are simple with huge generation of forces because the diaphragm deflection is accomplished by thermal alternation only [2].

This kind of actuation technique is not suitable for high-frequency operation because this requires relatively low voltages than the other [2]. A schematic diagram of bimetallic actuation is shown in Figure 2.1.7.6.

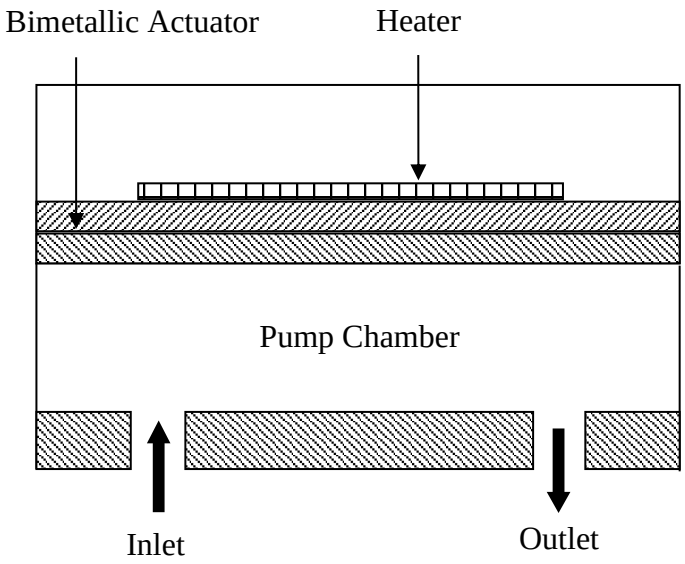

Figure 2.1.7.6: Schematic diagram of bimetallic Micropump[2]

2.1.8 Dynamic/Non-Mechanical Micropumps

Commonly, the operation of the non-mechanical micropumps are based on the direct conversion of mechanical or non-mechanical energy into a kinetic momentum. In this case, the flow is generally steady due to the continuous pumping. Hence, these pumps

do not have valves mechanism and they decide the flow direction according to the direction of the applied force [2][3][28]. These micropumps are developed with ultrasonic, magneto hydrodynamic (MHD), electro hydrodynamic (EHD), electro osmotic, or electrochemical methods. Here, the design principles are different according to the respective physical or chemical principle [2][28]. Though fabrications of these micropumps are moderately easy and simple, these can be used only for low conductivity fluids [2]. A detailed description of non-mechanical micropumps are presented accordingly.

2.1.8.1 Hydro Dynamic (MHD) Micropumps

These pumps are very useful for the flow of electrically conducting fluid in electric and magnetic fields. A typical MHD micropump contains microchannels, binary walls confined electrodes for the generation of electric-field and binary walls confined permanent magnets for the generation of opposite-polarity magnetic-field. The pressure and the flow rate of MHD micropump are given as [2]:

$$\Delta P = J_y B_x L \tag{2.1.8.1 a}$$

$$Q = \left| J_y B_x \right| \frac{\pi r_o^4}{8\eta} \tag{2.1.8.1 b}$$

Though these micropumps have the ability to pump high-conductivity fluids they are most suitable for medical/biological applications. In this micropumps, the flow rate is affected by the bubbles produced during ionization. But the bubble generation can be minimized by reversing the direction of applied voltage. Further, an ac driving mechanism will improve the performance of these micropumps[2].

2.1.8.2 Electro-Osmotic Micropumps (EO)

Electro Osmotic micropumps use the surface charge effects. These surface charges are developed artificially via electrodes or spontaneously during the contact of liquid with the wall of the channel. Further, the surface charge is protected by the oppositely charged ions produced in fluid. They can be manipulated by DC or AC electric fields [2].

In addition, this electro osmotic pumping mechanism needs any moving parts like check valves and they need high voltage as well as electrically conductive solution [2][3]. Figure 2.1.8 a shows the schematic illustration of such micropumps.

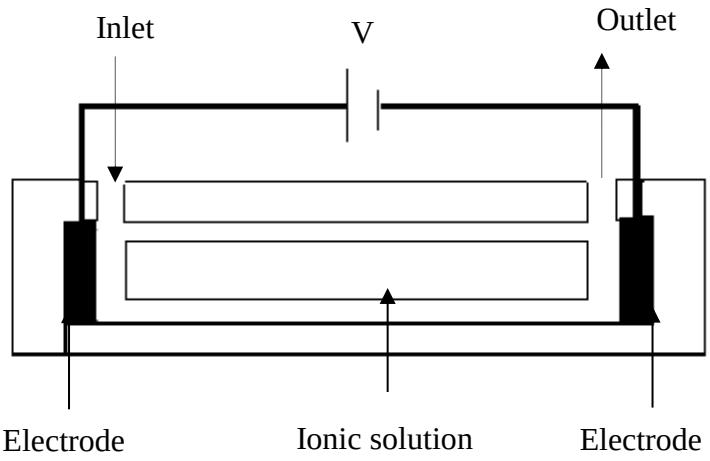

Figure 2.1.8.2: Schematic diagram of Electro-Osmotic Micropump[2]

2.1.8.3 Electro Wetting (EW) Micropumps

In electro wetting micropumps, fluid transport is done with the surface tension effect. As shown in Figure 2.1.8.3, when voltage is applied to the dielectric layer, the interfacial energy of the solid and liquid surfaces decreases and this causes the fluid to flow [2][3].

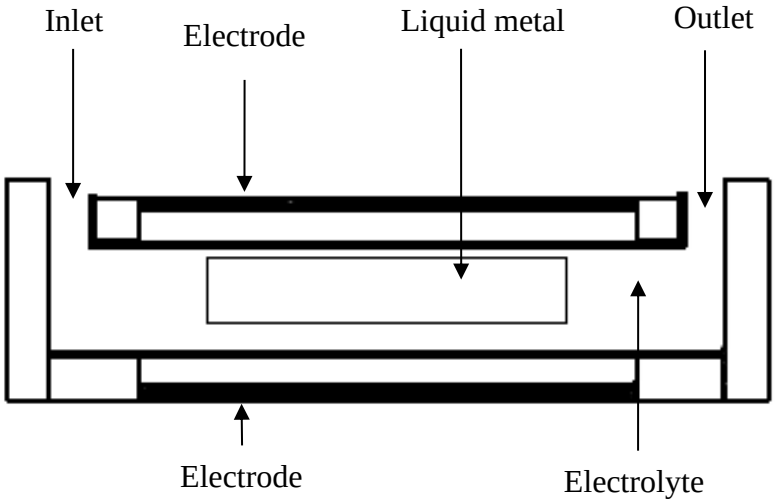

Figure 2.1.8.3: Schematic diagram of Electro Wetting (EW) Micropump[2].

Further, these micropumps have less power consumption with fast response. Since heating the liquid is not necessary, these techniques are used in lab-on-a-chip devices too [2].

2.1.8.4 Bubble-type Micropumps

Commonly, this pumping effect is based on the periodic expansion and collapse of the bubbles generated into the micro channels. The volume of the bubbles is collapsed and expanded in a periodic manner with controllable input voltage. The change in volume inside the chamber is obtained through a diffuser/nozzle mechanism which also defines the flow path [2].

This micropump is useful for possible mixing of two or more kinds of doses during the expanding/collapsing cycles [2]. A schematic illustration of bubble type micropump is shown in Figure 2.1.8.4.

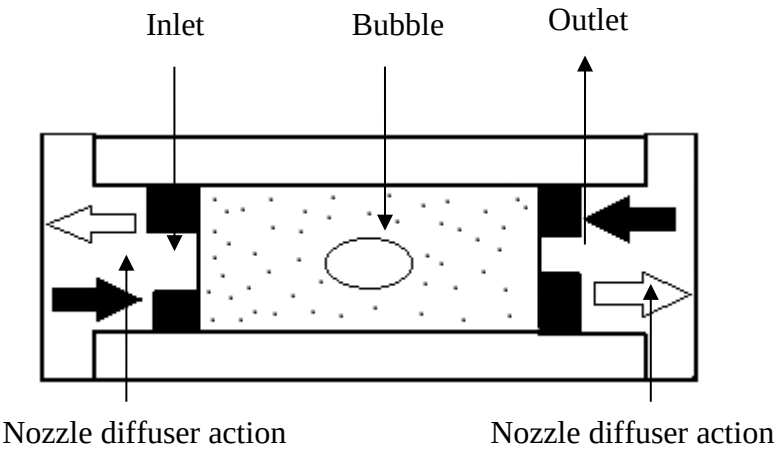

Figure 2.1.8.4: Schematic illustration of bubble type micropump[2]

2.1.8.5 Electrochemical Micropumps

In these kinds of micropumps, the actuation force uses bubble-generated due to electrochemical action. When applying DC current, water is electrolyzed between two platinum electrodes in a saline. Further, the generation of bubbles during the electrolysis process is the most important feature of these micropumps. This pump is more precise to pump solution in milliliter ranges. It also consumes less power [2][3]. The Figure 2.1.8.5 illustrates the schematic of this pump.

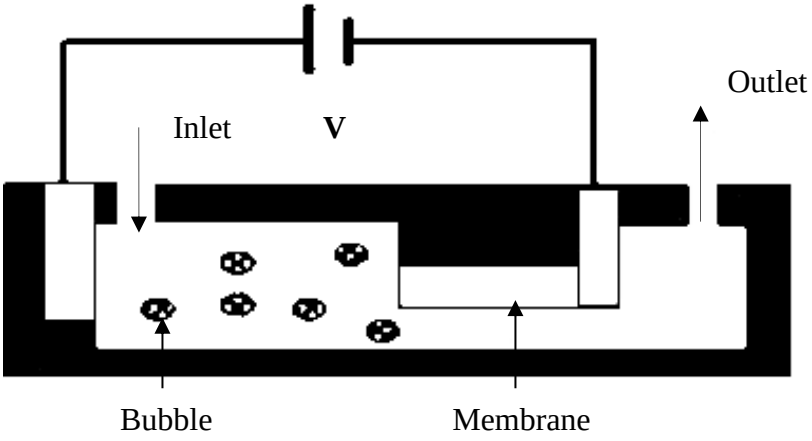

The Figure 2.1.8.5: Schematic illustration of electrochemical micropump[2]

2.1.9 Material selections and fabrication techniques of the micropump

The very first micropump was fabricated by C. Sun and Z.H. Yang in early 80's through conventional techniques [11]. Then, the first MEMS silicon micropump was fabricated using micro fabrication principles in 1984 [12]. Since that, it became very attractive and interesting area to improve the functionality and size of the micropumps. Van Lintel et al. fabricated the first silicon micropump with piezoelectric actuation in 1988 and soon, J.G. Smits published the results of his research in 1990 [13][14].

In addition, the most popular type of micropumps are piezoelectric diaphragm actuated micropumps and the first piezoelectrically actuated valveless micropump was fabricated by Stemme in 1993 through the microfabrication techniques [5].

2.1.9.1 Material selection

Due to the flexibility of shaping and machining, polymers are the good option during the selection of material. Machining from the bulk material, injection molding, and casting methods are the three identified possible processes to fabricate complex structures by using polymers.

Polydimethylsiloxane (PDMS) is an organic polymer contains silicon which is commonly used for fabrication due to its distinct characteristics. PDMS is transparent, inactive, non-toxic, and non-flammable material. Due to its special features, like transparency, bio- compatibility and cost effective, it is used in various microfluidic devices with no mechanical moving part for lab-on-a-chip applications [29].

In case of handling chemical components in micropumps, polyether–ether–ketone (PEEK) is most suitable for fabrication. Also, PEEK is a thermoplastic material which has a semi crystalline structure with valuable resistance properties. In addition to this, it is a suitable material for 3D printing techniques as well. Further, it is considered as a biomaterial for medical industry. Though PEEK is considerably expensive, the fabrication cost of micropump is cheap due to the less amount of materials required [30].

When considering diaphragm actuated micropump, stainless steel is one of the common material chosen for the metal diaphragm [30]. In this sense, special methanol-stable epoxy glue is used to bond metal diaphragm with plastic body [30].

A layer of Poly Dimethyl Siloxane (PDMS) elastomer is deposited on the metal diaphragm by using spin coating process for preventing leakages and improving sealings [30].

2.1.9.2 Manufacturing techniques of existing fabricated micropumps

Owing to the material cost and the difficulty in micro machining processes, usage of silicon in micropump fabrication is very much crucial. The use of plastic and other sub situational material establishes high potential in lowering fabrication cost. The most common popular solution is plastics which are disposable, inexpensive and assort to mass production manufacturing. There are various kind of micropumps that have been developed with these manufacturing methods [19].

In some researches, micropumps were designed to lie in the same plane. In this sense, micro fabrication techniques are very much useful to fabricate these features to avoid the additional expenses for prototyping. However, in some designs, the microchannels are placed in three-dimensional plane without lying in same plane. Besides the 3D geometry, it is a hard challenge to overcome the manufacturing of the minimum channel width and the vertical channels of large aspect ratio [31].

In complex micropump designs, separate machining approaches are needed for the channels and the additional assemblies of the chamber. Though during the production of low volume, this is not economically favorable due to the additional expense of injection molding die making process. In this case, 3D printing techniques are very much suitable because the molds can be categorized as permanent or fugitive. On the

other hand, shape deposition manufacturing is a manufacturing process which satisfies all the requirements to rapidly and directly create high performance metal parts. The basic steps of shape deposition manufacturing process are shown in Figure 2.1.9.2 a. In this sense, initially the material for each layer is deposited by using micro-casting techniques [32]. In order to make the net shape, the material is removed by using shaping technique. Then the component is exposed to the stress relief station to control and reduce the residual stresses [11]. Finally, the component is moved back to the deposition point where supplementary material is placed. Thickness of the layer and the sequence for depositing the primary and support materials depends upon the local surface geometry.

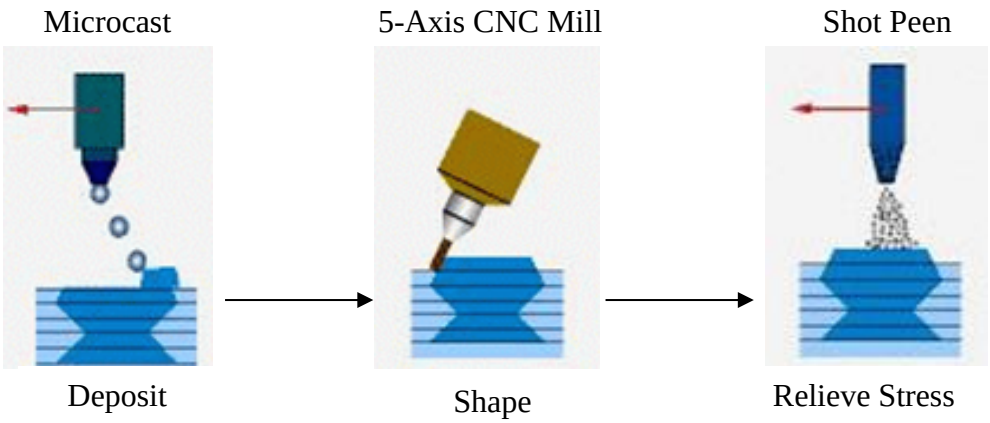

Figure 2.1.9.2 a: The basic steps of Shape Deposition manufacturing process [32]

In addition, a 3D-printing technique called stereolithography (SL) is used as an alternative to soft lithography and plastic molding techniques in case of rapid prototyping technique. This technique is essential for commercializing biomedical devices.

For a short overview of material selection and fabrication techniques of a mechanical micropumps, the Table 2.1.9 summarizes their construction, fabrication details, key features and performance characteristics as well [3][1].

Table 2.1.9: Details of the developed micropump [3][1]

Reference	Actuation principles	Size	Valve Type	Voltage/(V)	Frequency /(Hz)	Pressure/ (kPa)	Flow rate/ (µl/min)	Structure Fabrication	Application reported
Judy et al., 1991	Electrostatic	-	active valve	50	-	-	-	Selective etching deposition	-
Zengerle et al., 1992		-	Passive	170	1-100	25	70	Isotropic etching technique using lithography	-
Zengerle et al., 1995		-	passive	200	-	31	850	Bi directional silicon	-
Bourouinay et al., 1997		-	-	10	-	-	0.01-0.1	-	Drug delivery
Cabuz et al. 2001		-	-	160	30	-	30	Injection molding	Chemical & biological sensing
Yu Sun et al., 2002		-	-	10.7 in X & 70.1 in Y	-	-	-	Deep Reactive ion Etching (DRIE)	Micro manipulation and micro assembly

Table 2.1.9: Details of the developed micropump [3][1] Contd.

Reference	Actuation principles	Size	Valve Type	Voltage/(V)	Frequency /(Hz)	Pressure/ (kPa)	Flow rate/ (µl/min)	Structure Fabrication	Application reported
Teymoori and Sani, 2005	Electrostatic	7mmx4mmx1mm	-	-	-	-	9.1	-	medical applications
Machauf et al., 2005		-	-	50	-	-	1	flip chip bonding	-
Podder et.al, 2011		1mmx1mmx50µm	Nozzle/ Diffuser	-	-	-	0.167	-	Biomedical applications
Rosmani and Alabqari, 2013		-	-	0-20	-	-	-	-	-
Koch et al.,1998	Piezoelectric	8mmx4mmx70µm	-	600	200	2	120	-	Drug delivery of insulin
Cao et al., 2001		70 mm x 35 mm x 1 mm	Active	-	-	-	-	MEMS technology	-

Table 2.1.9: Details of the developed micropump [3][1] Contd.

Reference	Actuation principles	Size	Valve Type	Voltage /(V)	Frequency /(Hz)	Pressure/ (kPa)	Flow rate/ (µl/min)	Structure Fabrication	Application reported
Schabmueller et al., 2002	Piezoelectric	12mm x 12mm x 0.85mm	Passive	-	-	-	-	Bulk KOH etching	-
Junwu et al., 2005		-	-	-	-	27	-	-	Drug delivery
Feng and Kim, 2005		10mm x 10mm x 1.6 mm	-	80	-	0.12	3.2	fabrication with biocompatible materials	ideal for implantable micropump
Geipel et al., 2006		-	Active	-	-	-	-	Bulk silicon process	Drug delivery
Suzuki et al., 2007		-	-	-	-	-	336	-	-
Pham et al., 2007		20mm x 16mm x 4mm	-	-	-	1.8	900	fabrication with polydimethyl siloxane	-

Table 2.1.9: Details of the developed micropump [3][1] Contd.

Reference	Actuation principles	Size	Valve Type	Voltage /(V)	Frequency /(Hz)	Pressure/ (kPa)	Flow rate/ (µl/min)	Structure Fabrication	Application reported
Podder et al., 2012	Piezoelectric	5mm x 5mm x 0.2mm	Nozzle /Diffuser	-	169.8	-	375	-	-
Yoshida et al., 2012		20mmx13mmx 18.5mm	-	-	-	-	-	-	-
Ganesan and Palanisamy, 2012		-	-	-	-	-	100	MEMS fabrication	-
Shukur et al., 2013		4mm x 4mm x 0.5mm	-	-	-	30	191.635	-	-
Zdelblick and Angell, 1987	Thermo-pneumatic	-	Passive	6	-	5	34	-	-
Jeong and Yang, 2000		-	Nozzle /Diffuser	8	4	2.5	14	n-type Si wafer	-

Table 2.1.9: Details of the developed micropump [3][1] Contd.

Reference	Actuation principles	Size	Valve Type	Voltage/ (V)	Frequency /(Hz)	Pressure / (kPa)	Flow rate/ (µl/min)	Structure Fabrication	Application reported
Zimmerman et al., 2004	Thermo-pneumatic	-	-	-	-	16	9	-	-
Hwang et al., 2005		13mm x 9mm x 0.9mm	-	15/20	-	-	2/3.33	-	Transdermal drug delivery
Kim et al., 2005		-	nozzle/ diffuser	20	2	-	21.6	-	Micro total analysis systems
Jeong et al., 2005		-	-	-	-	-	-	PDMS elastomer	-
Baruah et al., 2012		-	-	-	-	-	60	-	Micro/ nano liter level fluid control systems
OU et al., 2012		-	-	10	1	-	0.1	-	-

Table 2.1.9: Details of the developed micropump [3][1] Contd.

Reference	Actuation principles	Size	Valve Type	Voltage/ (V)	Frequency /(Hz)	Pressure/ (kPa)	Flow rate/ (µl/min)	Structure Fabrication	Application reported
Bohm et al., 1999	Electromagnetic actuation	10mm x 10mm x 8mm	-	-	-	-	-	-	-
Geong et al., 2000		-	-	-	125	-	70	-	-
Yamahata et al., 2005		-	Valveless	-	12 & 200	12	400	-	disposable lab on chip systems
Yamahata et al., 2005		-	-	-	-	2.5	30	-	micromachining techniques
Pan et al., 2005		-	Ball check valves	0.013	-	-	774	-	-
Feldmann et al., 2007		10mm x 6mm x 3mm	-	-	-	-	-	-	-

Table 2.1.9: Details of the developed micropump [3][1] Contd.

Reference	Actuation principles	Size	Valve Type	Voltage /(V)	Frequency /(Hz)	Pressure / (kPa)	Flow rate/ (µl/min)	Structure Fabrication	Application reported
Shen et al., 2007	Electromagnetic actuation	-	ball valve	-	20	35	6000	-	Micro machining techniques
Zordan et al., 2009		-	Nozzle /diffuser	-	45	-	119100	-	drug delivery
Chang et al., 2013		-	valveless	-	-	-	470	-	-
Benard et al., 1997	Shape memory alloy actuation	-	-	-	0.9	4.23	49	-	-
Xu et al., 2001		6mm x 5mm x 1.5mm	-	-	-	100	340	-	-
Shuxiang and Fukuda, 2004		-	-	-	-	-	500-700	-	biomedical applications

Table 2.1.9: Details of the developed micropump [3][1] Contd.

Reference	Actuation principles	Size	Valve Type	Voltage /(V)	Frequency /(Hz)	Pressure/ (kPa)	Flow rate/ (µl/min)	Structure Fabrication	Application reported
Zhang and Qiu, 2006	Shape memory alloy actuation	8mm x 8mm x 1.8mm	-	-	80	-	235	-	-
Xia et al., 2007		-	valveless	-	-	-	-	-	-
Pierce, 2011		-	-	-	-	-	66000	-	-
Zhan et al., 1996	Bimetallic actuation	6mm x 6mm x 1mm	-	5.5	0.5	12	45	-	-
Zou et al., 1997		13mm x 7mm x 2mm	check valves	-	-	0.5	336	-	-

2.1.10 Thermo-Elastic Damping Effect in PZT Actuators

Thermo-elastic damping is a kind of internal friction that may take place in any substance which is exposed to cyclic stress. In thermo elastic substance, the material thermal expansion coefficient is directly linked with strain and temperature. This linking expels energy dissipation in order to permit the substance to move to equilibrium and this leads to the irreversible heat flow across the material [33][34].

The effect of thermo-elastic damping (TED) in microscale PZT actuators is a serious issue. This is because when piezoelectric actuators are under cyclic stress, piezoelectric elements are heated up and this causes temperature rise. Hence the operation of piezoelectric actuators is inaccurate due to thermal expansion in piezoelectric elements. Also the characteristics of the piezoelectric element vary with temperature and this causes complete obliteration of the PZT actuation effect [35].

The thermo elastic damping effect is simply explained through quality factor. Zener was the first person who explained an analytical approximation for the quality factor in 1930s [33][36][37][38] [39][40]. The effect of quality factor Q is explained as [33]:

$$Q = 2\pi\left(\frac{Energystored}{Energydissipatedpercycle}\right) \qquad (2.1.10)$$

According to the expression of the quality factor, if the heat dissipation is high, then the quality factor will be less. Further, if heat dissipation is higher than the heat generation, there will be no effect in PZT actuators due to thermo elastic damping. In addition, this effect can be addressed in various temperatures which are less than the Curie temperature of the PZT material in order to identify the operational temperature range of PZT actuator. Hence analyzing the thermo elastic damping effect theoretically is very much useful.

2.2 MEMS based Pressure Sensors

With emerging technologies around the world, monitoring pressure and getting response is vital in biomedical devices. At present, developing micro pressure sensors is a challenge and Micro Electro Mechanical System (MEMS) is the one and only

technique to fabricate these pressure sensors. Further Micro Electro Mechanical Systems (MEMS) technologies are the good option to fabricate minuscule high performance biomedical devices [2][41].

Micro Electro Mechanical Systems (MEMS) is a technology defined as miniaturized mechanical and electro-mechanical elements which are made using the microfabrication techniques [1][2][41]. Also, the most notable elements of MEMS are micro sensors and microactuators [2][41][42]. Due to the diversity and demand in wide range of requirements, MEMS market is growing. The design and manufacturing technologies are motivating the extensive usage and prompt development of these devices [2]. In 1984, Howe and Muller developed the first polysilicon surface micromachined device [1][42].

According to previous research findings and demand, MEMS devices have advanced performances than macro devices. In addition, pressure sensors are the one of the prominent MEMS device in various industries as well as in biomedicine [3][43][44][45].

There are number of researches that have been carried out on the pressure feedback mechanism in wide range of applications. But only few of them have gone up to the level of publication. In 2014, insulin micropump was developed with embedded pressure sensors [46]. Further, modelling of a piezoelectric MEMS micropump for insulin delivery and validating with integrated pressure sensors was presented in 2017 [47]. The cost effective feedback controlled syringe pumps for microfluidics was also developed in 2017 [48].

2.2.1 Applications of MEMS Pressure Sensors

MEMS pressure sensors are widely used in various kinds of applications in the fields of automatic safety application, navigation and environment sensing as well as biomedical applications. Some of the specific applications are listed below.

- Automotive tire pressure
- Pneumatic controls
- Pressure switches and controllers
- Portable gauges and manometers

- Catheter pressure
- Respiratory applications
- Sleep apnea
- Anesthesia
- Ventilation
- Disposable blood pressure

2.2.2 Sensing Principles and Existing Pressure Sensors

There are various kinds of sensing principles of pressure sensors which are presented in literature as follows [49][50].

- Capacitive
- Piezoelectric
- Electromagnetic
- Optical potentiometric
- Piezoresistive

In the aforementioned sensing principles, some of them are widely used in pressure sensors. Commonly, pressure sensors are designed according to the range of pressure to be operated and the type of pressure to be measured [3]. The Table 2.2.2 shows some of the developed sensors which is incorporated with various kinds of sensing principles.

Table 2.2.2: Developed pressure sensors incorporated with various kinds of sensing principles

Sensing Techniques	**Reference**	**Materials used for sensing**	**Applications**
Piezoelectric	M. Asadnia et al. [43]	Liquid crystal polymer	Underwater sensing
Piezoelectric	A. P. Dabrowski et al. [44]	LTTC (Low temperature co-fired ceramics and PZT (Lead zirconate titanate) transducer	High pressure up to 10 MPa sensing applications
Piezoelectric	E. Teomete et al. [45]	Reinforced cement-based matrix composite	Measurement of crack length sensitivity
Piezoelectric	J.Wang et al. [49]	Quartz	Application in automotive, petroleum, meteorological, aerospace and spacecraft field
Piezoelectric	H.Schmid-Engel et al.	Pt-SiO_2	High temperature pressure measurement
Capacitive	J. Cheng et al. [51]	Textile based surface	Activity recognition
Capacitive	A.Arogbonlo et al. [52]	Neoprene and SAC plated nylon fabric	Applications across industries associated to sports performance, ergonomics, rehabilitation
Capacitive	Lee et al. [53]	Polymer	Artificial robotic limbs
Capacitive	Rey et al. [54]	Silicon	Fingerprint recognition
Piezoresistive	X. Huang et al. [55]	Peninsula-structured diaphragm	Low pressure sensing applications
Piezoresistive	Aqilah et al. [56]	Conductive rubber	Robotic hand
Piezoresistive	Noda et al. [57]	Silicon rubber	Dexterous manipulation (Robotic application)

2.2.3 Available Materials and Fabrication techniques of pressure sensors

MEMS pressure sensors are fabricated through massive batch fabrication techniques in micromachining. Though several kinds of materials like polymers, alloys, metals, ceramics, glass and others are used in this micromachining process, silicon is commonly used for making pressure sensors. This is because silicon has good elastic property, lighter weight than aluminium and comparably identical modulus of elasticity with stainless steel [3][41][58]. Also, preparing single crystal substrates of silicon is economic and easy. Due to this positive mechanical properties, silicon pressure sensors are commonly available in product market [41].

Bulk micromachining is the prevalent and oldest technology which is extensively used in fabrication of pressure sensors [41]. The bulk micromachining is carried out through the selective exclusion of substrates. Wet and dry etching and substrate bonding are the important micro fabrication techniques used in bulk micromachining [41][58][59][60].

In this sense, silicon in wet etch and wafer bonding are removed by using anisotropic wet etchants. As an initial step, a specified thickness of respective wafer is produced by etching. Hence well-regulated thicknesses of required structures are created [3]. But this method has weaknesses for producing thin features of thickness less than 20μm.

The Figure 2.2.3 a and Figure 2.2.3 b illustrate the sectional view for piezoresistive pressure sensors made using electrochemical and boron doping etch-stop methods. The boron doping method needs the growth of a lightly doped region on top of a boron doping etch-stop layer. Thus this coating is used for locating piezoresistors [41][58][61].

Further, bulk micromachining using dry etching are very much useful for anisotropic dry silicon etching process. Deep Reactive Ion Etching (DRIE) and the accessibility of Silicon on Insulation (SOI) wafers with a thick layer of silicon are the most preferable things to use in this technique [3].In addition, these techniques are necessary for fabricating high-aspect-ratio vertical structures. The Figure 2.2.3 c expresses the Deep Reactive Ion Etching Process [41][61].

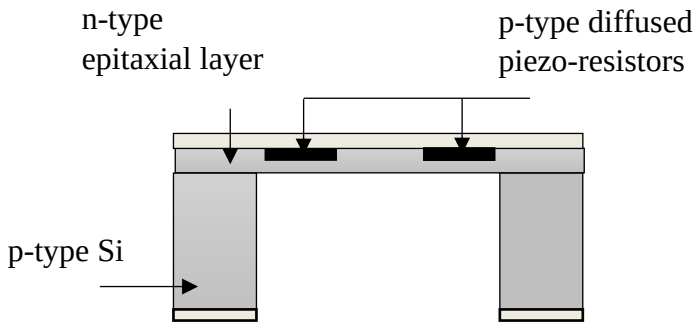

Figure 2.2.3 a: Piezoresistive pressure sensor fabrication with electrochemical technique – sectional view [41][62][63]

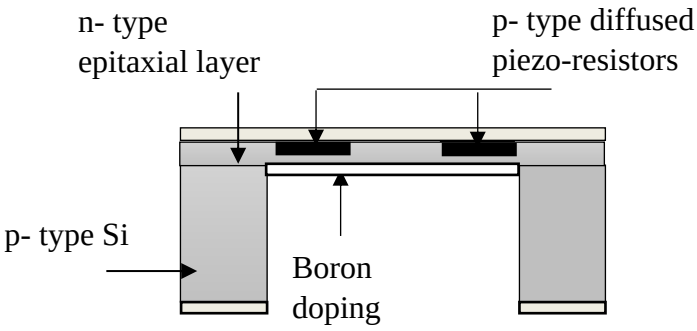

Figure 2.2.3 b: Piezo-resistive pressure sensor made by using Boron doping etch-stop technique- sectional view of [41][63] [64]

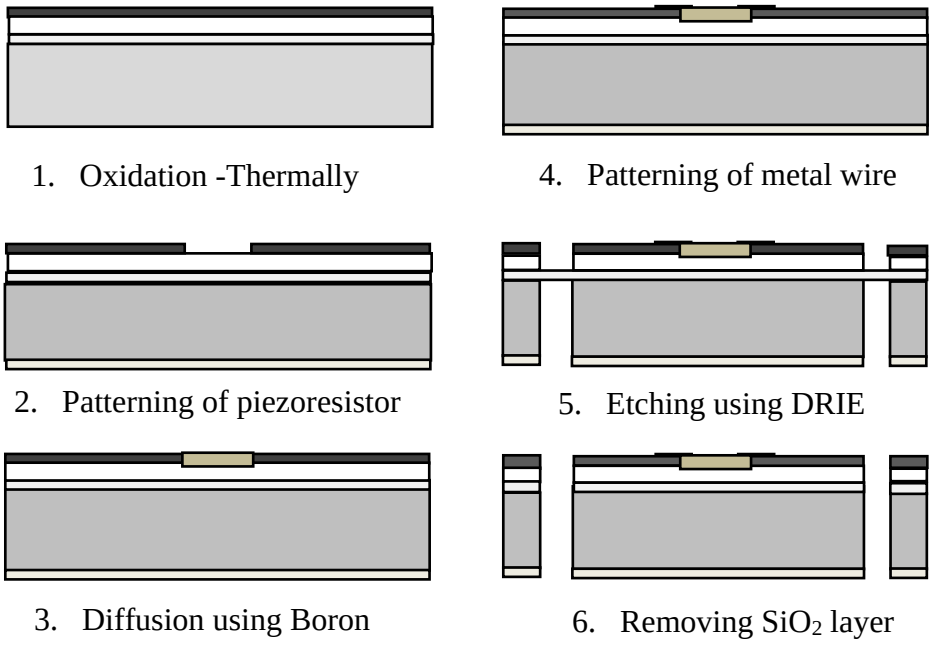

Figure 2.2.3 c: Deep Reactive Ion Etching Process[41][63]

2.2.4 Thermo-mechanical behaviour of pressure sensors

Silicon based piezoresistive pressure sensors always grieve from the temperature drift characteristics [65]. Hence, it is very much essential to consider the thermo-mechanical behavior of these kind of pressure sensors.

In 1980s, Kanda presented a theoretical model for the relationship between piezoresistive coefficients, dopant concentration and temperature. According to his model, for an arbitrary dopant concentration and temperature the piezoresistive coefficient is expressed as [5][62][66][67]

$$\pi(N, T) = P(N, T) * \pi_{ref} \qquad (2.2.4\ a)$$

Where π_{ref} is the value of the piezoresistive coefficient of interest for lightly doped silicon (10^{16} cm^{-3}) at 300 K. Here all of the piezoresistive coefficients (π_{11}, π_{12}, π_{44}, π_l, and π_t) are scaled linearly using the piezo resistance factor P,[5]

Also, according to Kanda's model, the piezo resistance factor *P* is calculated in the following manner [62].

$$P = \frac{300}{T}\frac{F'_{s+(1/2)}}{F_{s+(1/2)}} \qquad (2.2.4\ b)$$

Where F_s and F'_s are the Fermi integral and its derivative with respect to the Fermi energy, E_F.

To account for the density of states available for conduction, the Fermi level is determined as follows [5][62]:

$$\frac{E_F}{k_b T} = \frac{\ln(u)}{1-u^2} + \upsilon - \frac{\upsilon}{1+(0.24+1.08\upsilon)^2} \qquad (2.2.4\ c)$$

Where,

$$u = \frac{\pi^2 N_d}{\upsilon\sqrt{2}}\left(\frac{m_d^* k_b T}{h}\right)^{-3/2}$$

$$\upsilon = \left(\frac{3u\sqrt{\pi}}{4}\right)^{2/3}$$

Here, h - Planck's constant, m^*_d - density of states effective mass, n - carrier concentration, K_b - Boltzmann constant, v - number of carrier valleys, N_d - doping concentration.

Also there are 6 valleys for n-type and p-type silicon and m^*_d is 1.08 for n-type and 0.49 for p-type respectively [5][68][69].

In 2000, an empirical model for the piezoresistance factor is developed by Harley [62]. In his model, P is calculated as follows:

$$p = \log_{10}\left(\left[\frac{b}{n}\right]^a\right) \qquad (2.2.4\ \text{d})$$

Where $a = 0.2014$, $b = 1.53 \times 10^{22}$ cm^{-3}, and n is the dopant concentration.

Nevertheless, Harley's model is perfect for dopant concentrations level beyond 1×10^{18} cm^{-3} and over forecasts P for lower concentrations. Moreover, this model is only for *P(N)* and not suitable for *P(N,T)*. Hence, this is not suitable for devices operating at temperatures above or below 300K. Also, this model does not have any information for temperature coefficient of sensitivity.

Later an updated model is presented in 2008 by Richter et al. In his model, the piezoresistance factor of p-type silicon is in a function of dopant concentration and temperature. This model is developed based on the first principles including both phonon and ionized impurity scattering [5]. But in Kanda's model, phonon scattering is only included. The Richter's complete model is reduced to an analytical formula given as [5][62][70].

$$p = \frac{T_n^{-\theta}}{1 + \left(\frac{N}{N_b}\right)^{\alpha} T_n^{-\beta} + \left(\frac{N}{N_c}\right)^{\gamma} T_n^{-\eta}} \qquad (2.2.4\ \text{e})$$

Where Tn = T/300 is the normalized temperature. The fitting coefficients θ, Nb, Nc, α, β, γ and η are presented in Table 2.2.4.

Also comparing with other models, Richter's model is admirable at high concentrations and P tends to 1 at low concentrations. Though the model is developed specifically for p-type silicon but it fits for n-type silicon as well. In contrast with Harley's fit, Richter's model is temperature dependent [5]. Also, the piezoresistance factor predicted by Richter's model is accurate over the entire temperature range as well as for dopant concentrations less than 10^{16} cm^{-3}. This model is extensively improved at low temperature as well as in higher temperatures.

Table 2.2.4: The Fitting Coefficients of Ritcher Model [5]

Parameter	Ritcher model [J. Ritcher]	Modified Ritcher Model
θ	0.9	0.95
N_b	$6x10^{19}$	$4.9x10^{19}$
N_C	$7x10^{20}$	$2.6x10^{20}$
α	0.43	0.39
β	1.6	1.35
γ	0.1	0.94
η	3	4.55

2.4 Conclusion- Literature Review

The inventive efforts initiated in developing micropump started 1975. Nevertheless the development stage were carried out in 1980s with microfabrication technology [4][28]. From this point onwards, advancement of technologies have succeeded according to the necessities of biomedical industry to develop micropumps for various onsite applications.

In literature, it is observed that various micropump with different materials have been used for biomedical applications. However, Si has been typically used in fabrication of microfluidic devices. On the other hand, Si is brittle and has risk for human health care. Presently there is tendency to move towards organic polymers because biocompatibility is a considerable factor for human health. Polymers, such as PDMS, PGA, PLA and PMMA are considered appropriate for biomedical devices because of their virtuous biocompatible effect, economic, ease of fabrication as well as excellent chemical and mechanical properties [2].

In addition, thermal effects in micro structures are very crucial for the enhancement of those devices. Hence the temperature effects on actuators and pressure sensors has also been reviewed under the literature.

Based on the history of micropumps, the commercialization is still in the ground level. Since nowadays there is a huge demand for the onsite analysis, it is necessary to

fabricate micropumps for such applications. In addition, discharge pressure feedback and monitoring are essential in these kinds of micropumps. Since then, few researches have been carried out on pressure monitoring and feedback in these micropumps [46] [47][71]. Therefore, developing a micropump integrated with discharge pressure feedback mechanism is highly encouraged in microfluidic applications. However, developing proper micropumps for specific requirements is a great achievement and this will motivate further research studies in developing micropumps for microfluidic applications.

CHAPTER 3.0 DESIGN AND SIMULATION OF MICROPUMP

3.1 Introduction

As per conclusion of literature review relevant to this research, it is recognized that it is necessary to develop a micropump with better performance. Based on the literature, it is also found that the valveless micropumps are very simple and useful for miniaturization. Also, these kind of micropumps have high durability than the micropumps with active type valves. One of the principle objectives of this study is to design and simulate a micropump with novel mechanisms and applications. Hence it is proposed to design and simulate a nozzle jet valveless micropump with the available resources. In this sense, the fluid flow rectification was done due to the flow resistance exerted on the fluid by fixed geometry of the nozzle jet element.

The three important features namely nozzle jet, microstructure and actuation principles were considered during the design and simulation of this micropump. The 3D model of the micropump with significant features is shown in Figure 3.1. Hence, as an initial step, this study is focused on designing a PZT actuated membrane micropump with nozzle jet.

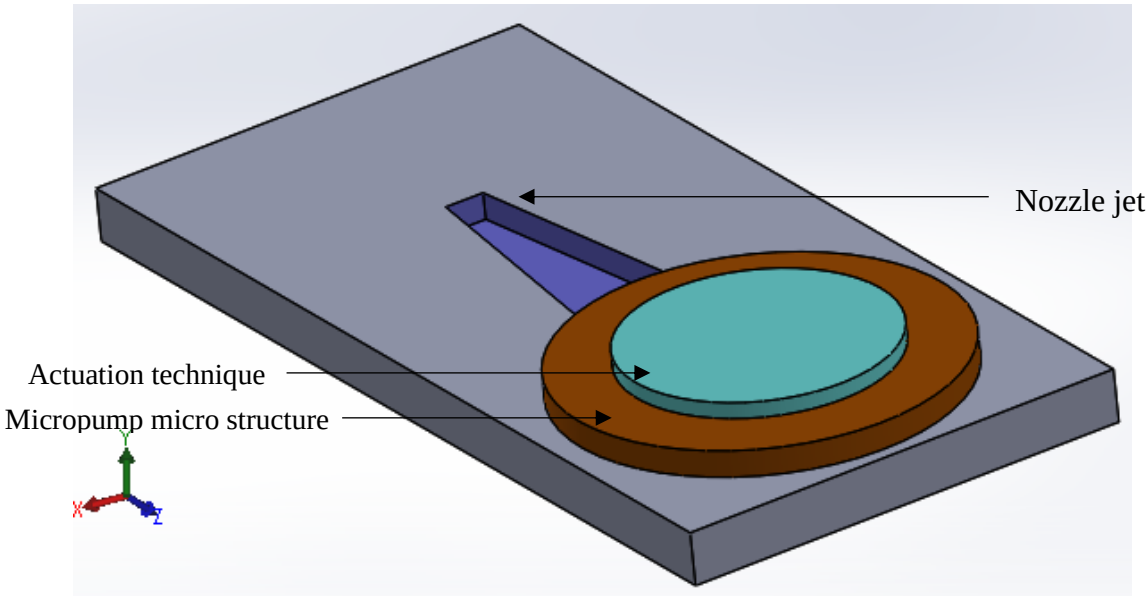

Figure 3.1: The 3D model of the micropump with significant features

3.2 Design of nozzle jet

As a first core feature, designing a nozzle jet as expressed in Figure 3.2 a is very much useful for the betterment of the fluidic network. This would also provide good performance during the operation.

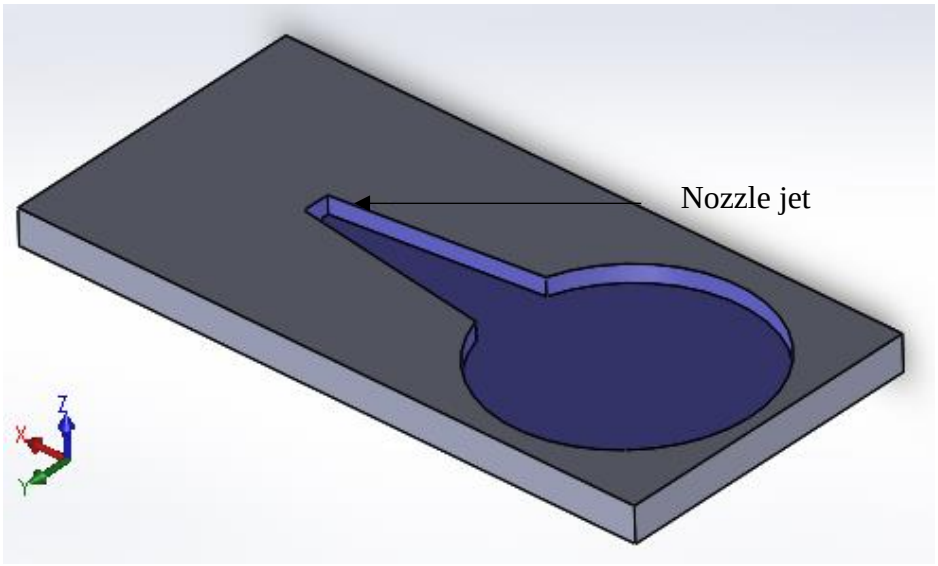

Figure 3.2 a: Three-dimensional model of the nozzle jet

In this sense, the geometrical cross sections of the diffuser/nozzles are the dominant parameter of the performance and this would be a crucial factor during the design. Hence, based on the geometrical cross-sections, diffuser/nozzles are classified as flat-walled and conical diffusers which are represented in Figure 3.2 b and Figure 3.2 c respectively.

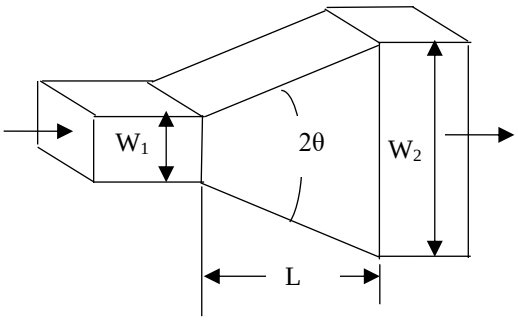

Figure 3.2 b: Flat walled diffuser [72]

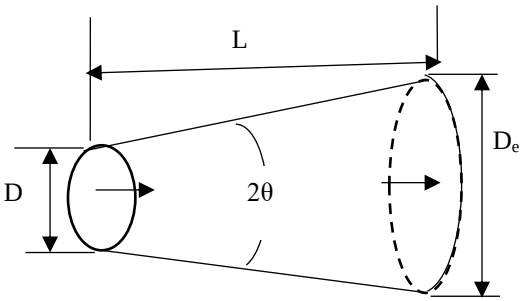

Figure 3.2 c: Conical diffuser [72]

Commonly, the best conical diffuser is 10% to 80% lengthier than the paramount flat walled one [72]. Since the overall dimension is considerable due to the portability, the flat walled design is most preferable and the flat wall of rectangular cross section with two parallel flat walls and two convergent flat walls are chosen for this nozzle design. In addition, the nature of flow in a nozzle/diffuser is demonstrated by the 'stability map' and the 'performance map', as shown in Figure 3.2 d and Figure 3.2 e respectively. According to this map, nozzle/diffusers with higher pressure recovery coefficient C_p will give better performance and it will be achieved in the transitory stall region. The dimensions of the diffuser element are the divergence angle 2θ, the diffuser length L and the width of the narrowest part W. Further, the diffuser performance depends on the boundary conditions at the inlet and is given as the pressure recovery, C_p.

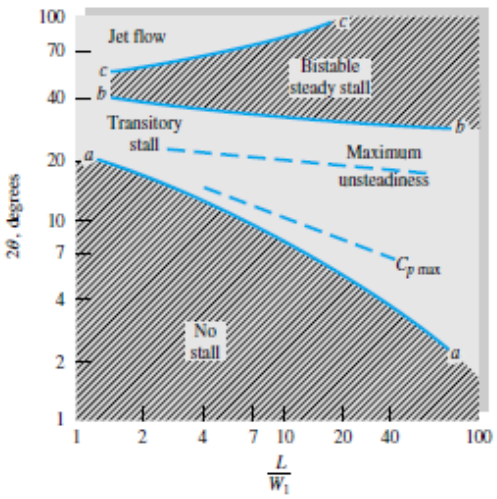

Figure 3.2 d: Stability map of a Flat diffuser[72] [73]

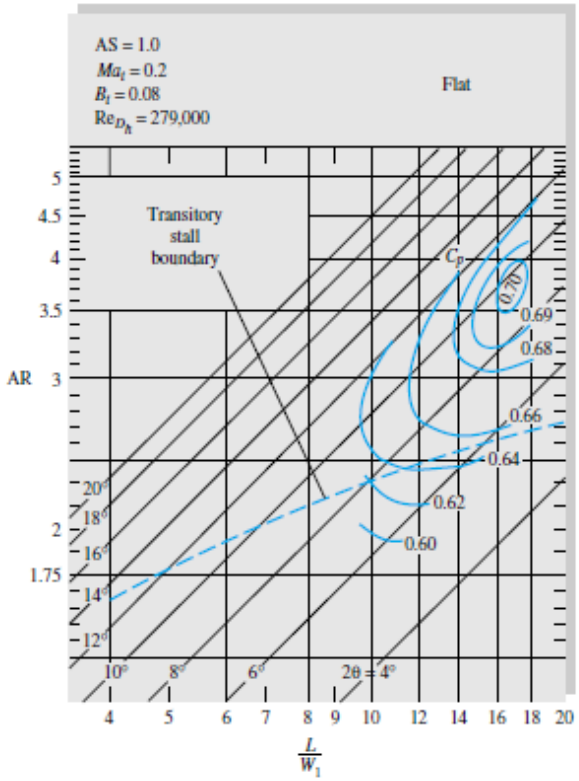

Figure 3.2 e: Performance map for a typical flat walled diffuser [72] [73]

In this research, initially there are three different nozzle parameters as given in Table 3.2 that are studied to investigate the impact of nozzle parameters on the flow rate.

Table 3.2 Three kind of nozzle parameters

Description	Type 1	Type 2	Type 3
Divergence Angle (2θ)	10˚	7˚	10˚
Slenderness (L/W)	11.7	11.7	17.9

3.3 Design and Simulation of PZT Actuated Diaphragms

Though PZT actuated membrane is a second core feature of this micropump, designing this in a precise manner is beneficial. Here the PZT disk is fixed on top of the membrane as shown in Figure 3.3 and the analysis are persisted.

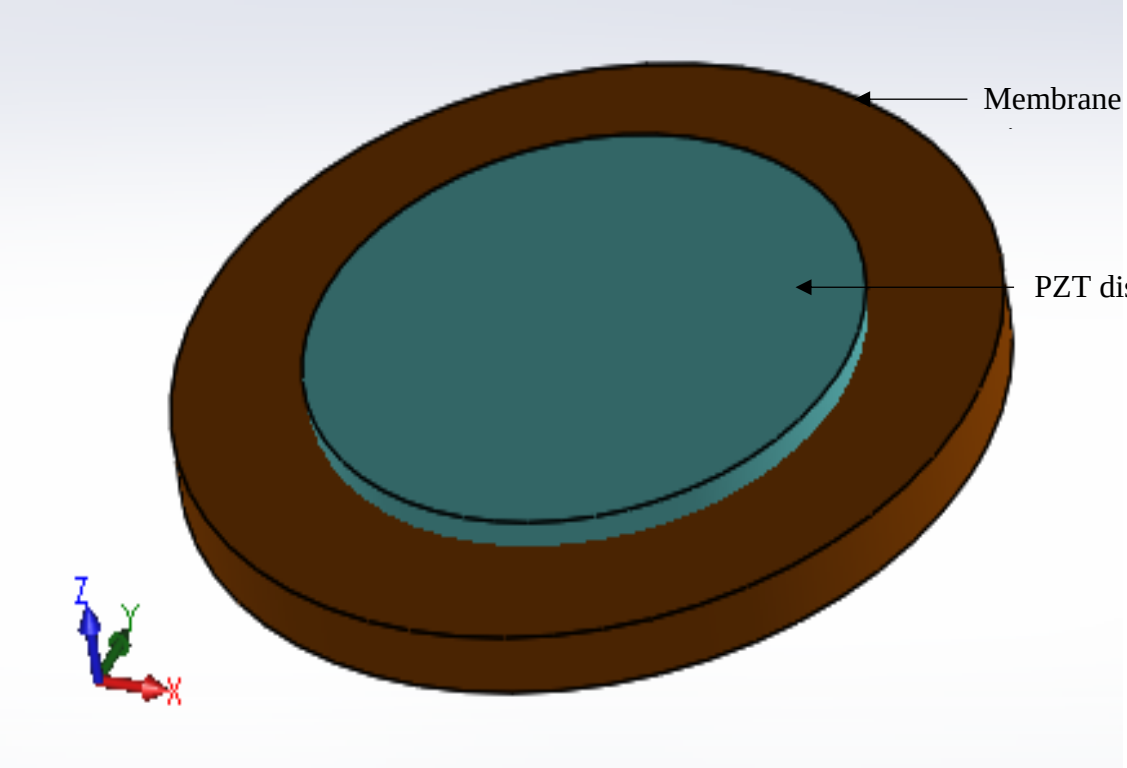

Figure 3.3: PZT actuated membrane

3.3.1 Effect of Piezoelectric (PZT) Actuation in PZT Actuators

Nowadays the application of piezoelectric materials in energy harvesting is very much popular due to the favorable environmental characteristics of piezoelectric materials [74][75][76][77][78]. Owing to the virtuous piezoelectric effect (PZT), piezo-electric actuators are widely used in many kinds of applications from industries to biomedicine. Though some of the applications are limited because of their brittleness, less impact resistance, inflexibility, processing difficulties as well as the higher natural frequencies [79][80][81].

In order to attain different vibration modes, piezoelectric crystals can be made into various forms. There are several frequency modes that have been developed with various kinds of PZT ceramics to achieve small, cost effective, and performance enhanced products. There are PZT-5H and PZT-5A which are most commercially available piezoelectric ceramics [18]. In this sense, PZT-5H can produce highest first resonance frequency than PZT-5A.

Also, this will provide lowest potential than PZT-5A and it is an excellent material for actuators. Hence commercially available PZT-5H is selected for the proposed design. When a piezoelectric material is exposed to an electric field, the mechanical strain is produced. In addition, the piezoelectric constitutive strain–charge relationship with isothermal is explained by the following expressions [1][82]:

$$S_{ij} = S_{jk}^{E} T_k + d_{kj} E_k \tag{3.3.1 a}$$

$$D_i = d_{ij} T_j + \in_{ij}^{T} E_j \tag{3.3.1 b}$$

Where, S is the mechanical strain, S^E is the elastic compliance coefficient at constant electric field, T is the mechanical stress, d is the piezoelectric strain coefficient, D is the electric displacement, E is the electrical field, ϵ^T is the permittivity at constant stress, and i, j and k are vector notations along x, y, z directions respectively[1].
In addition, the piezoelectric strain coefficient for PZT-5H is expressed by:

$$\left[d_{ij}\right] = \begin{matrix} 0 & 0 & d_{31} \\ 0 & 0 & d_{31} \\ 0 & 0 & d_{33} \\ 0 & d_{15} & 0 \\ d_{15} & 0 & 0 \\ 0 & 0 & 0 \end{matrix} \tag{3.3.1 c}$$

$d_{31} = -274 \times 10^{-12}$ C/N, $d_{33} = 593 \times 10^{-12}$ C/N, $d_{15} = 741 \times 10^{-12}$ C/N.

Since, the residual stress is insignificant and $S_{jk}^{E} T_k$ on the right side of equation (3.3.1 a) is also trivial. Also assuming that the strain produced in a thin circular membrane is only in a radial direction, the expression is simplified as[1]:

$$S_1 = d_{31} E_3 \tag{3.3.1 d}$$

In this sense, the piezoelectric structural and electrical simulation was executed in COMSOL Multiphysics 5.3 to simplify the theoretical analysis. This analysis was performed on eigenfrequency study setup under piezoelectric stress/strain mode. Here, the brass diaphragm with circular cross section was glued around its boundary. The PZT 5H disk was merged on top of the diaphragm. The dimensions of the diaphragm and the characteristics of brass are articulated in Table 3.3.1. Then the model was meshed with the physics controlled mesh. The designed model and the meshed model are shown in Figure 3.3.1 a.and Figure 3.3.1 b respectively. Hence, the micropump diaphragm was deflected owing to the PZT effect when a 20 V of alternating electrical signal of was applied.

Table 3.3.1. Dimensions of the diaphragm and the material properties of brass

Description	Value
Diameter of the diaphragm (mm)	35
Thickness of the diaphragm (mm)	0.3
Thickness of the PZT-5H disk (mm)	0.22
Density (kg/m^3)	8360
Young's modulus (GPa)	125
Poisson's ratio	0.33

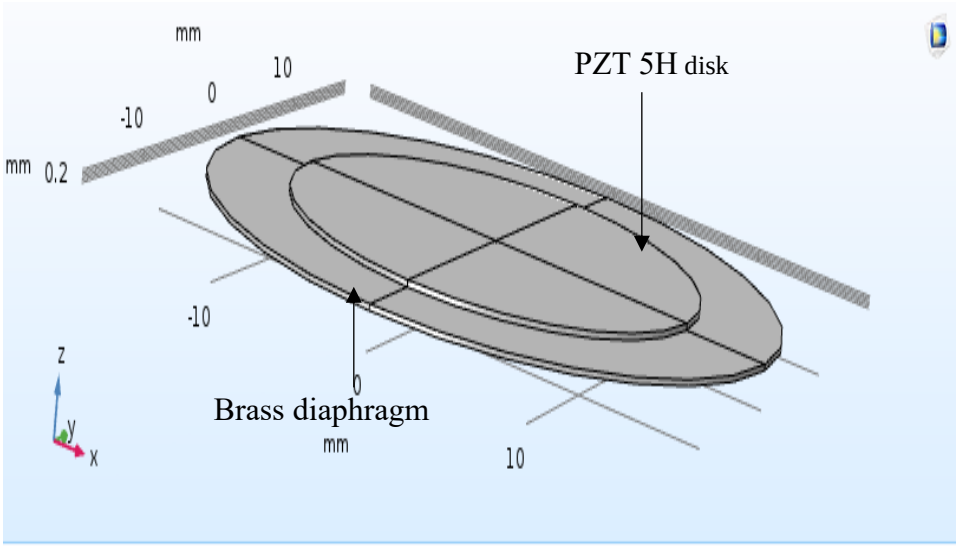

Figure 3.3.1 a**:** Designed model of the PZT actuated diaphragm

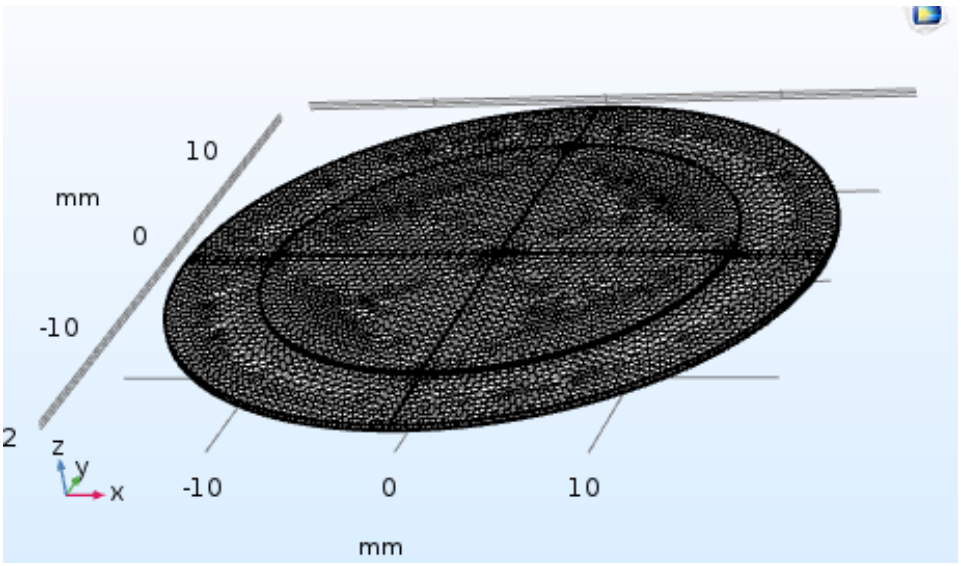

Figure 3.3.1 b**:** Meshed model of the PZT actuated diaphragm

At the supplied voltages of different eigen-frequencies, the deflection analysis of the PZT 5H disc is shown in Figure 3.3.1 c and Figure 3.3.1 d accordingly. These outputs are very much helpful to identify the frequency at which the maximum displacement was achieved.

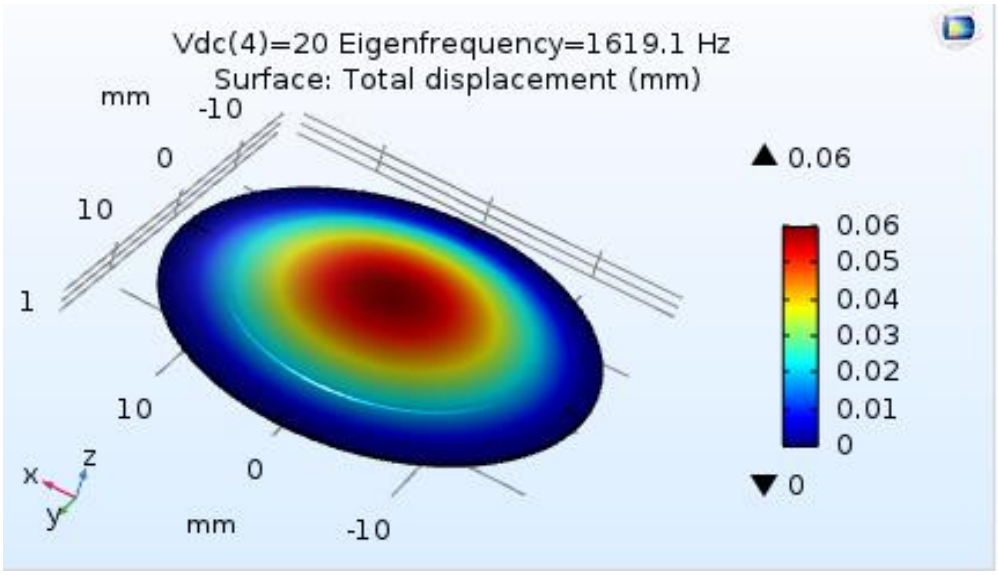

Figure 3.3.1 c: Deflection analysis for first mode of PZT 5H diaphragm

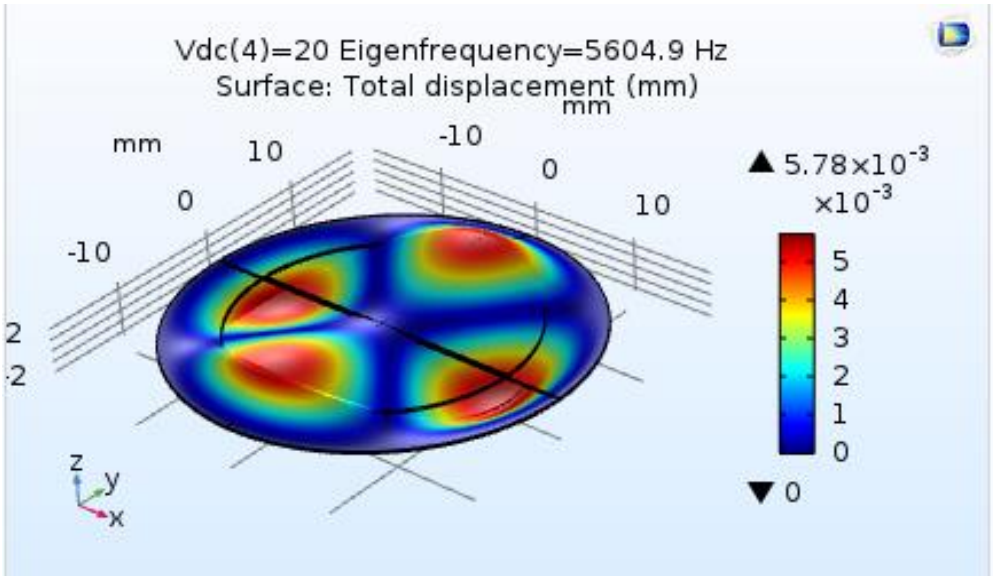

Figure 3.3.1 d: Deflection analysis for fourth mode of PZT 5H diaphragm

According to this analysis, 0.06 mm of maximum center displacement was achieved at the 1619 Hz of first mode eigenfrequency. This frequency is not only the maximum displacement occurring mode but also the maximum change of volumetric volume occurring frequency too. In order to vary the frequency to be applied to the piezoelectric diaphragms within the prescribed range, these data are very advantageous. Hence, the control system of the pump is designed for an electric signal in which the frequency varies from 1 Hz to 1619 Hz.

On the other hand, the eigenfrequency values may vary from the theoretical value when fixing piezoelectric disc with the micropump.

3.4 Design and model development of micropump

Initially, there are two kinds of designs with various nozzle parameters are considered. As per the literature, there are cross junction micropumps with one PZT actuated diaphragm developed for compressible fluid flow applications. But in this research, the analysis was carried out by varying the divergence angle and slenderness of the nozzle to reach maximum flow rate. In order to identify the applicability of the device, single diaphragm micropump was analyzed for three various kinds of nozzle jet parameters. Further the dual diaphragm micropump with optimal nozzle jet parameter was designed with feasible dimensions. Hence, this is a novel concept to enhance the flow rate during incompressible fluid flow applications. The schematic illustration of the design process is shown in Figure 3.4.

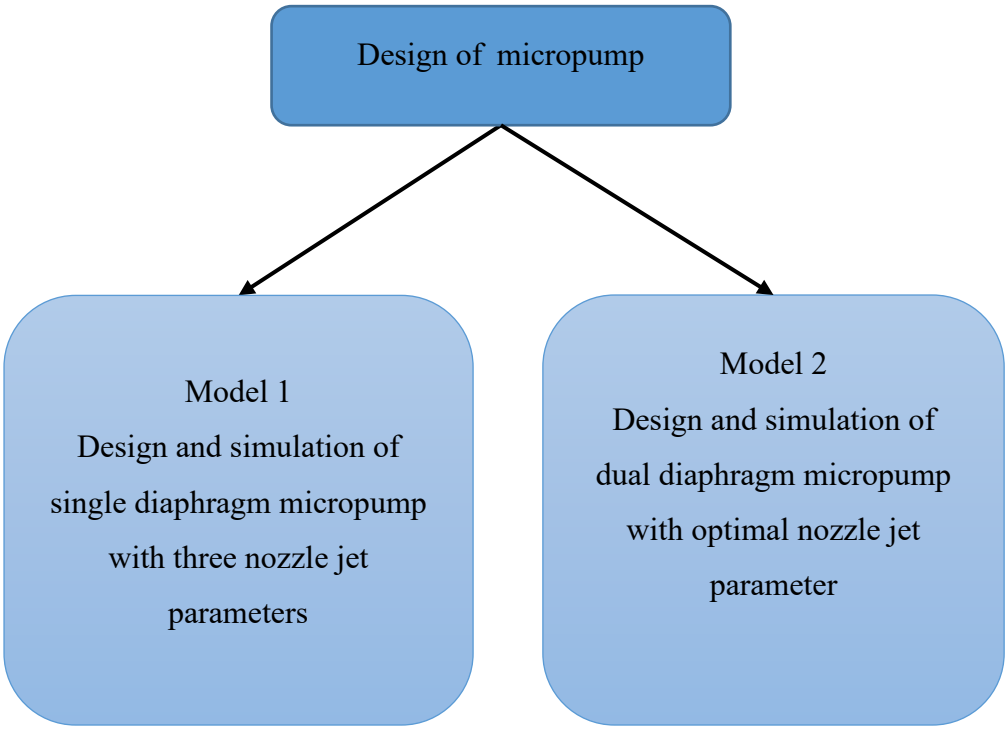

Figure 3.4: Design of micropumps - two kinds of designs

3.4.1 Design and model setup of single diaphragm micropump (Model 1)

The model 1 of the proposed design system contains a 0.3 mm thick and 35 mm diameter circular PZT actuated metal diaphragm as actuator. The thickness of the PZT disk is 0.22 mm. The fluidic network comprises a circular pump chamber of 30 mm diameter with one nozzle element enclosed by a PZT actuated membrane on bottom as well as two inlet and an outlet channels. The details of these microfluidic channels are expressed in Figure 3.4.1 a. In this sense, the circular shaped design is most preferable to permit smooth fluid flow through the channels by diminishing leakages and bubbles at the edges and walls. In addition, circular membranes deliver better displacement comparing with the other shapes of the membrane, for the same applied load [1][11][82] [83]. On the top side of the micropump, the inlet and outlet ports are placed for easy handling.

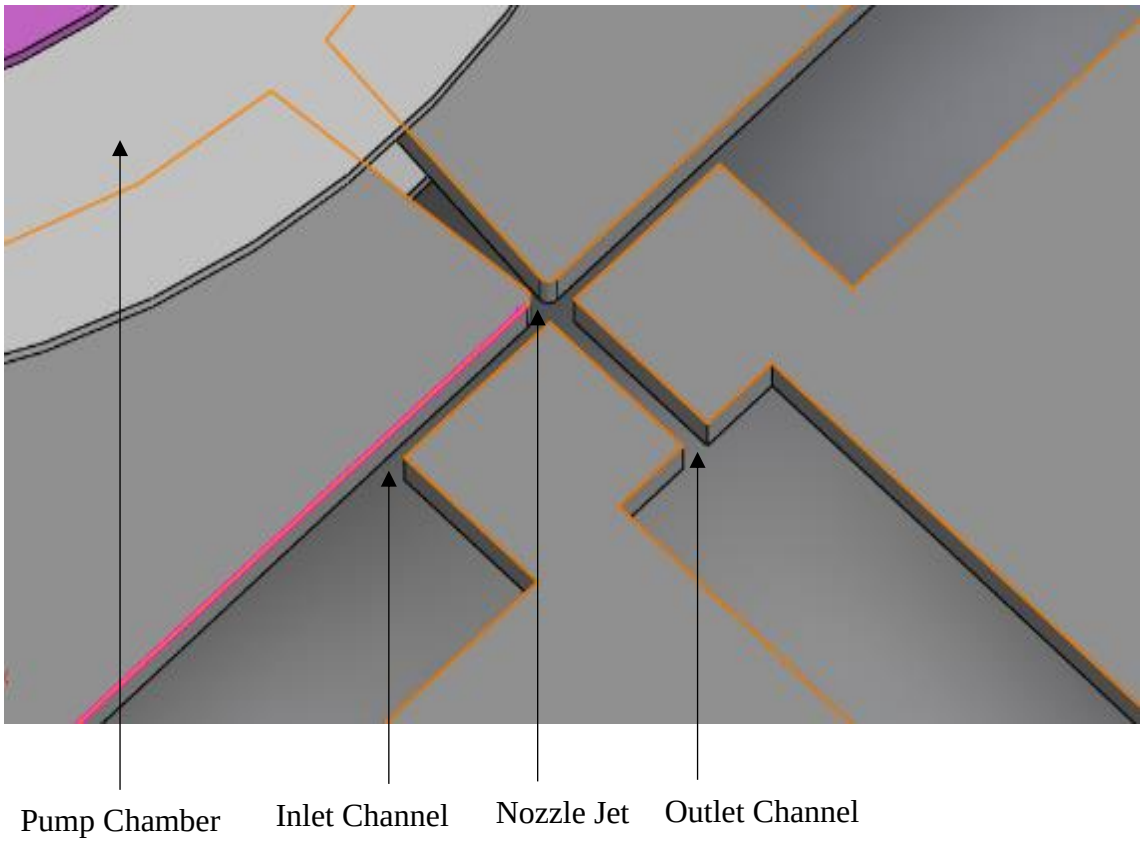

Figure 3.4.1 a: Details of the microfluidic channel

As a rule of thumb, cross sections of the inlets must be greater than the outlet at the cross junction to reduce fluidic resistances [84][85][86][87][88]. Thus, the cross sections of the inlet and outlet channels are designed accordingly and the dimensions of them are 0.5 × 1.5 (mm^2) and 0.6 × 0.5 (mm^2) respectively.

The entire micropump structure is designed as thin layers of polymethyl methacrylate (PMMA) sheets and packed to establish the required fluidic network. The top and bottom views of the designed model are expressed in Figure 3.4.1 b and Figure 3.4.1 c respectively. The dimensions of the proposed device are 100 mm × 60 mm × 5.5 mm respectively.

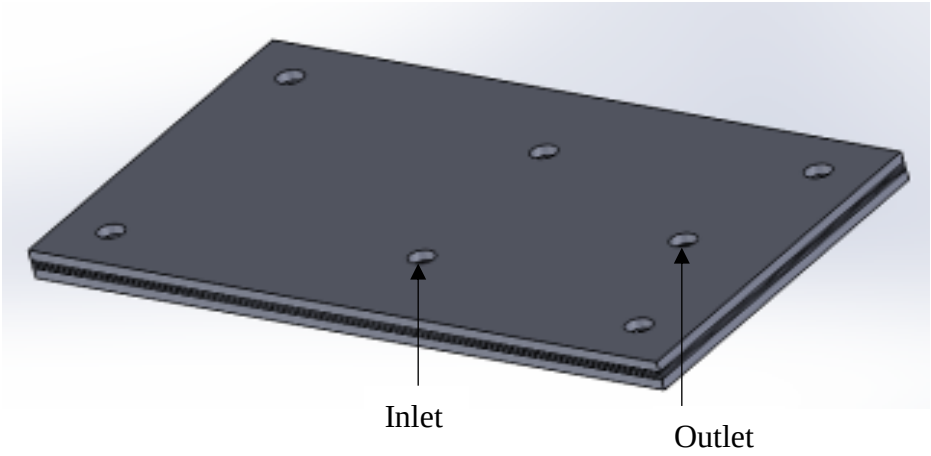

Figure 3.4.1 b: The designed model of the single diaphragm micropump– Top view

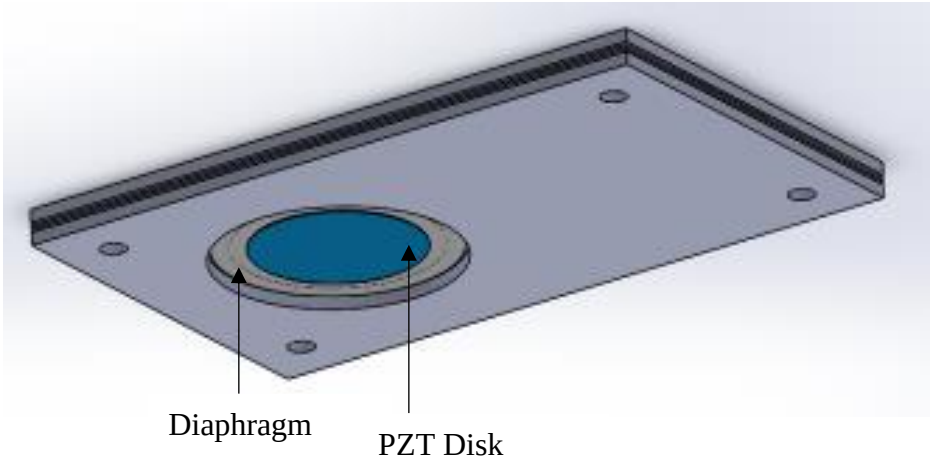

Figure 3.4.1 c: The designed model of the single diaphragm micropump – Bottom view

3.4.2 Design and model setup of dual diaphragm micropump (Model 2)

The second proposed design of the micropump system contains 0.3 mm thick and 35 mm diameter of two identical circular PZT actuated metal diaphragms as actuators. The thickness of PZT disk is 0.22 mm. In this sense, the entire fluidic network is designed with a circular pump chamber of 30 mm diameter including one nozzle element enclosed with two PZT actuated membranes on the top and bottom as well as two inlet and an outlet channels. The cross sections of the inlet and outlet channels and nozzle jet are designed as 0.5 × 1.5 (mm^2), 0.6 × 0.5 (mm^2) and 0.3 × 0.5 (mm^2) respectively. The entire micropump assembly is designed as thin layers of polymethyl methacrylate (PMMA) sheets and completely packed. The size of the whole packed device is 100 mm × 60 mm × 5.5 mm respectively. The whole packed design of model 2 and its exploded view are shown in Figure 3.4.2 a and Figure 3.4.2 b respectively.

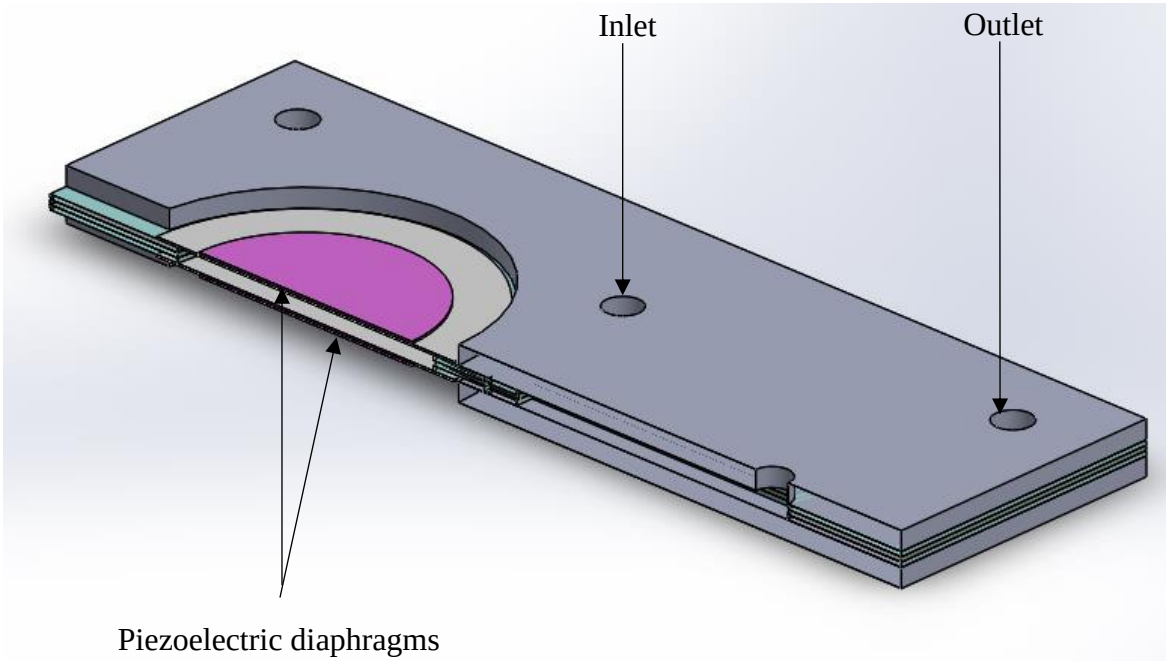

Figure 3.4.2 a: The whole packed model

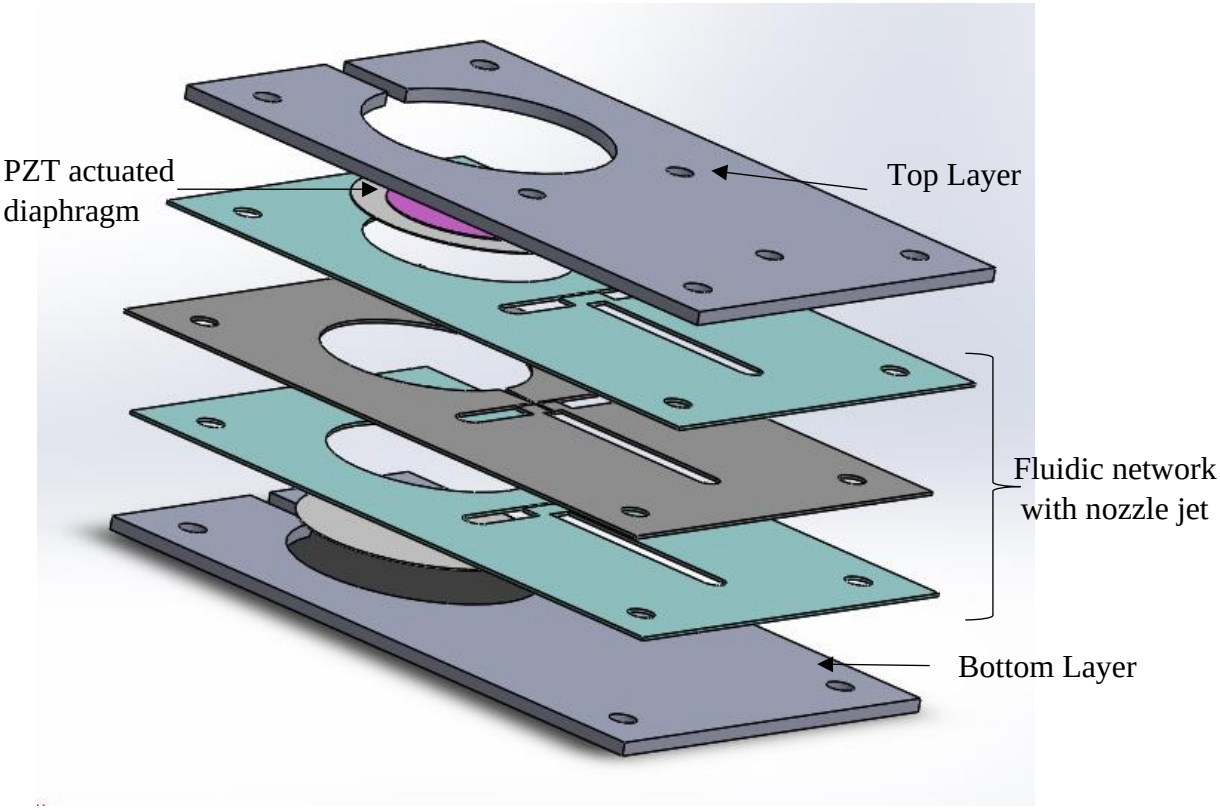

Figure 3.4.2 b: The exploded view of the model

3.4.3 Working principles of micropump

According to the deformations of the PZT actuated diaphragms, the pumping action of the micropump is divided into two parts namely suction and compression strokes. When PZT actuators are actuated by an alternating voltage, PZT diaphragms periodically deform in a convex and concave pattern. Hence, the chamber volume would vary accordingly. Basically, PZT membranes are bent in a convex manner during the pumping stroke (Figure 3.4.3 a). Thus, more fluid is straightly ejected out through the outlet channel because the inlet and outlet channels are perpendicular to each other (Figure 3.4.3 b).

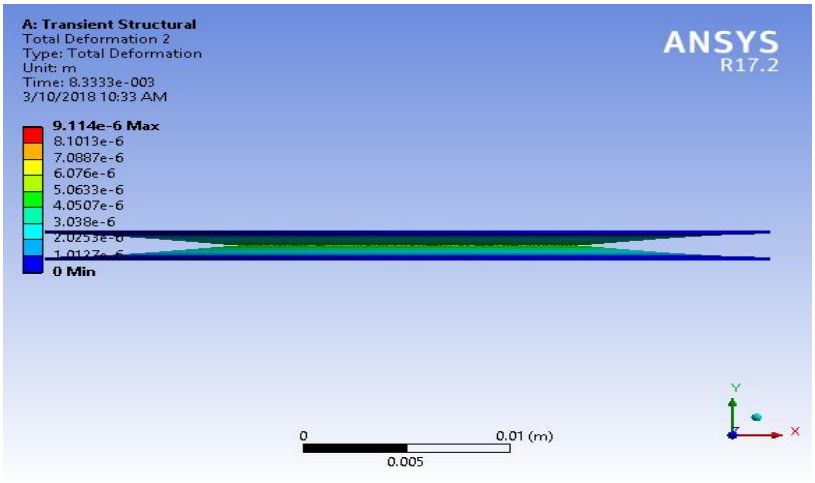

Figure 3.4.3 a: Deformation pattern during compression stroke

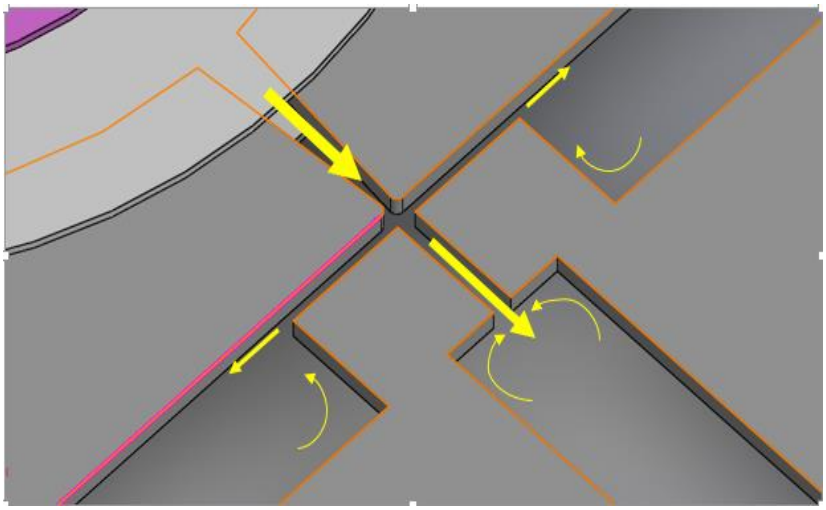

Figure 3.4.3 b: Fluid flow motion during compression stroke[89]

On the other hand, PZT membranes are deflected in a concave manner during the suction stroke (Figure 3.4.3 c). Then, the fluid is sucked into the chamber due to the low pressure. (Figure 3.4.3 d). At this moment, more fluid will flow through the inlet channels than the outlet due to the difference between forward momentum and fluid flow resistances along the channels at inlet/outlet (Figure 3.4.3 e).

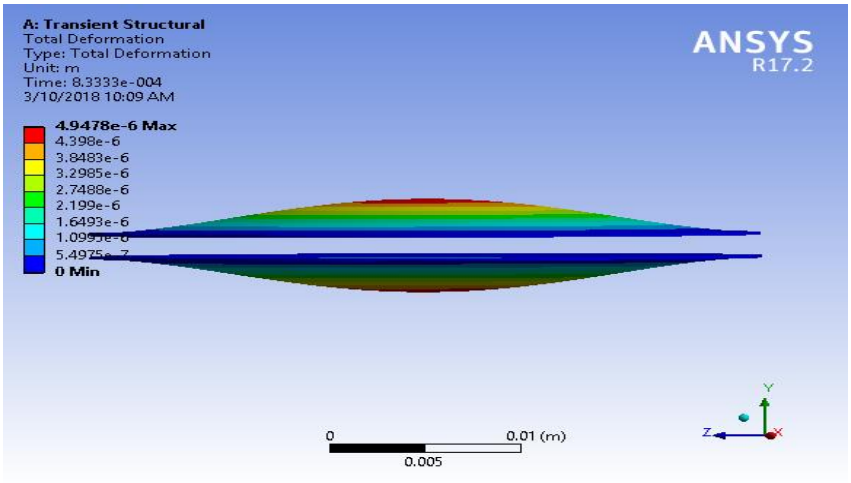

Figure 3.4.3 c: Deformation pattern during suction stroke

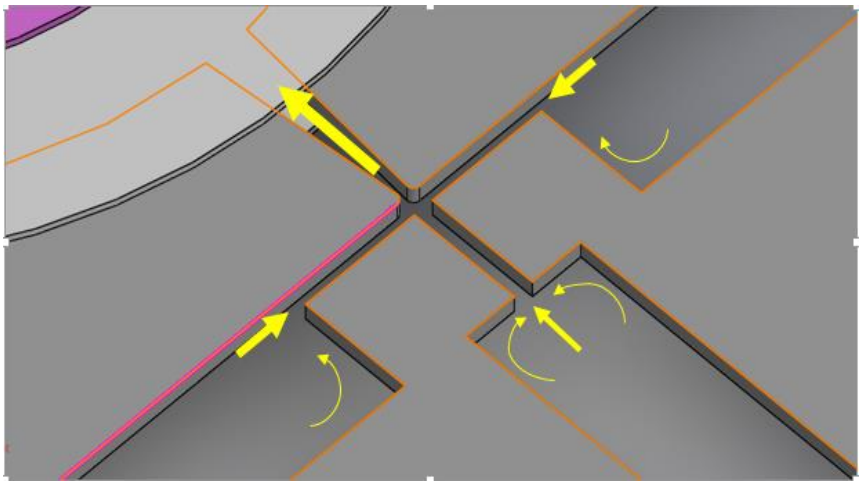

Figure 3.4.3 d: Fluid flow motion during suction stroke[89]

3.4.4 Simulation analysis of micropump

The incompressible Navier–Stokes equations describes the solutions for fluid flow within the micropump. The mass and momentum conservation for the motion of the fluid are explained by the following equations with given notations [7][82][83]84] [85][86][87][88] [99][100].

$$\nabla \cdot \vec{u} = 0 \qquad (3.4.4\ a)$$

$$\rho \frac{\partial \vec{u}}{\partial t} + (\vec{u} \cdot \nabla)\rho\vec{u} = -\nabla p + \nabla \cdot (\eta \nabla \vec{u}) \qquad (3.4.4\ b)$$

Where p - pressure of the flow; ρ density of the fluid; η - dynamic viscosity of the fluid; $\vec{u}$ - velocity vector.

When a constant force is applied to the PZT actuated diaphragms of the micropump, the deflections of the diaphragms is described by the first symmetric motion mode of the thin circular plates fixed along its perimeter [1][82][86][87]:

$$\varphi(r,t) = \Theta_0 \sin(2\pi ft)\left[1-\left(\frac{r}{R}\right)^2\right]^2 \qquad (3.4.4\ c)$$

Where *r*- defined radius from the center; *R* – radius of the diaphragm; *f* – applied frequency to the load; Θ_0 - amplitude at the center.

Assume that there is no preliminary pressure gradient during the working stage of the micropump and there is no pressure imposed at the inlet and outlet. Non-slip conditions are also assumed at the walls. Therefore, the time derivative of deflection motions of PZT diaphragms are conveyed to the inlet velocities and it is expresses as follows [82][83][91] [92]:

$$v(r,t) = (2\pi f\Theta_0)\cos(2\pi ft)\left[1-\left(\frac{r}{R}\right)^2\right]^2 \qquad (3.4.4\ d)$$

During the transient structural simulation, the time step Δt was selected as $\Delta t = 1/(fN)$. Here, N was 12 to replicate the flow behavior throughout a single cycle of fluctuation in PZT diaphragm.

The aforementioned solutions of the Navier–Stokes equations were accomplished by carrying out coupled field analysis in ANSYS-Fluent. In this sense, the spatial derivatives and time advance approximations were done by using second-order accuracy scheme. The fluidic simulation was done based on the k-ε realizable model with pressure-based transient solver method. The velocity–pressure coupling algorithm was defined with SIMPLE scheme and the working fluid was liquid water with ambient temperature. After that, the fluidic part was meshed with dynamic mesh with smoothing. Then the solution was initialized with hybrid initialization.

From the coupled field analysis, volumetric plots and the net flow rates were obtained at different frequencies. The Figure 3.4.4 a show the volumetric plots of velocity profile at compression phase of PZT actuated single diaphragm micropump.

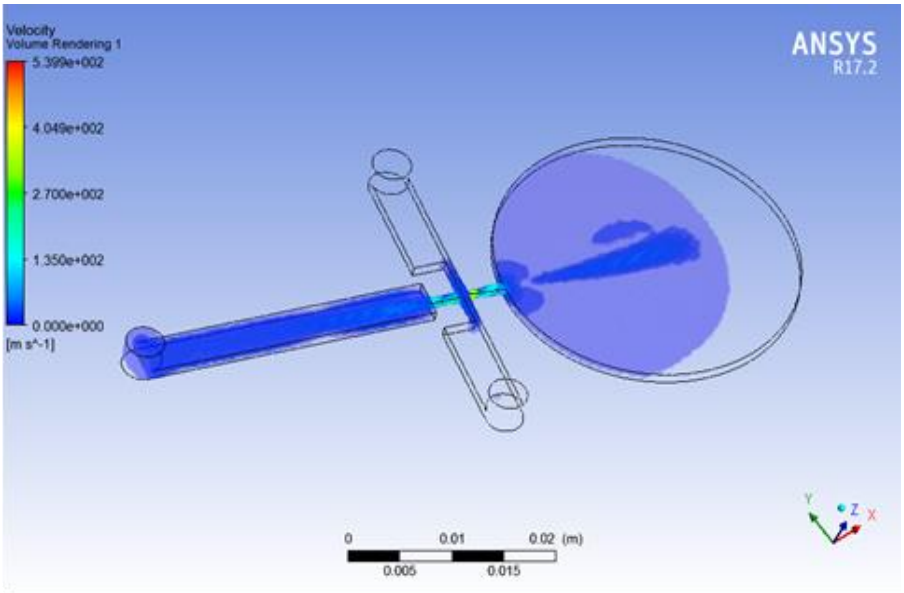

Figure 3.4.4 a: Volumetric plot of velocity profile for single diaphragm micropump

The variation of net flow rates with frequency were plotted by using the volumetric plots at different frequencies for all three kind of nozzle designs in model 1. The Table 3.4.4 a and the Figure 3.4.4 b reveal the simulation results of net flow rates with frequency for model 1 and variation of net flow rates over the range of frequency for all three kinds of nozzles in model 1.

Table 3.4.4 a. Simulation results of net flow rates with frequency for Model 1

Frequency/(Hz)	Flow rates/(ml/s)		
	Type1	Type 2	Type 3
1	0	0	0
50	0.8	0	0
100	1.9	0	0.0054
500	12.68	0.54	0
1000	22	5.14	0
1500	0	0	0

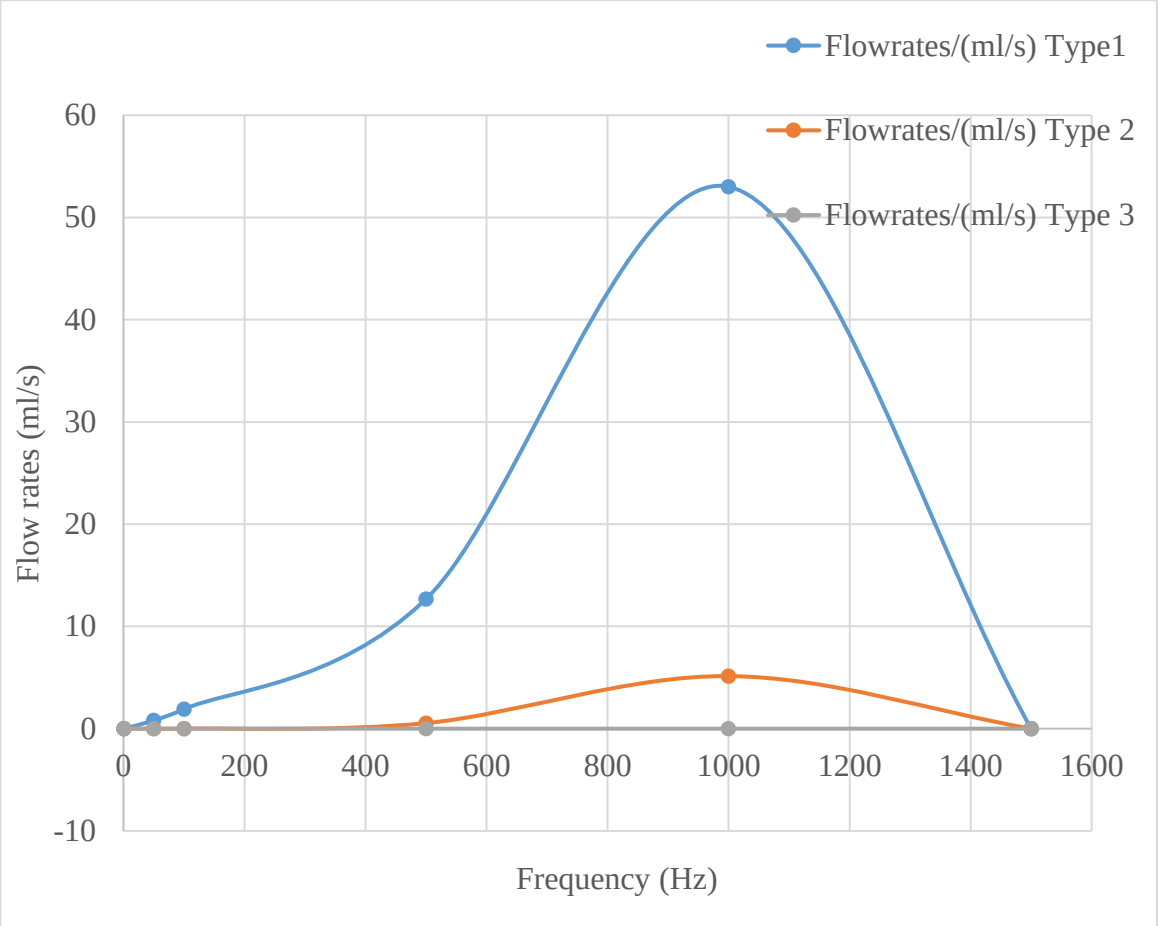

Figure 3.4.4 b: Variation of net flow rates with frequency for model 1

Further, the coupled field analysis was carried for model 2 as described in the Model 1 with the optimal nozzle parameters. Figure 3.4.4 c shows the volumetric plots of velocity profile at the compression phase for model 2 (PZT actuated dual diaphragm micropump). Then the simulation results of net flow rates were also tabulated and it is illustrated in Table 3.4.4 b. By using this data, variation of net flow rates with frequency were plotted and it is expressed in Figure 3.4.4 d.

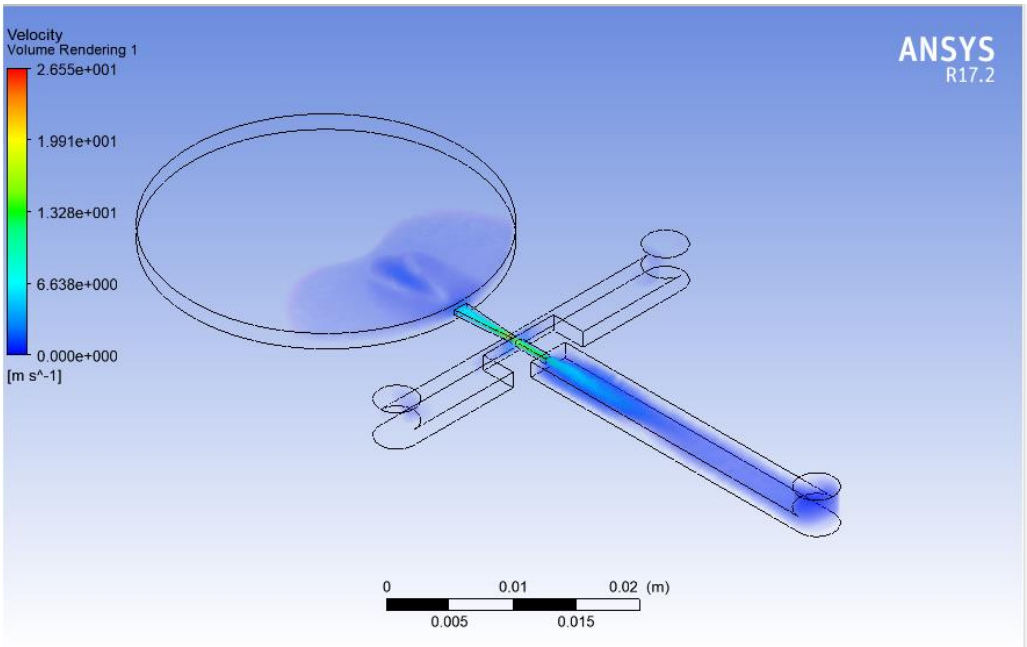

Figure 3.4.4 c: Volumetric plot of velocity profile for Model 2

Table 3.4.4 b. Simulation results of net flow rates with frequency for Model 2

Frequency(Hz)	Flow rate(ml/s)
1	0.00
50	1.52
100	9.37
500	2.17
1000	0.03
1500	0.00

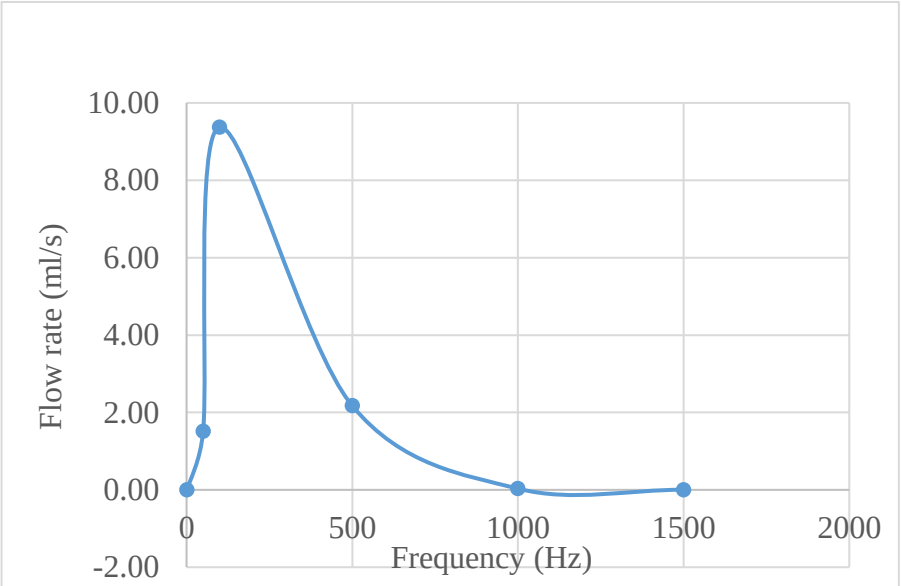

Figure 3.4.4 d: Variation of net flow rates with the frequency for Model 2

CHAPTER 4.0 FABRICATION OF MICROPUMP

4.1 Material selection and Laser fabrication

Micropumps are fabricated through various kinds of materials as discussed in literature. PDMS and PMMA are the two organic polymers widely used for fabricating microfluidic devices with less weight. The micropump device in this research is to be developed for onsite microfluidic applications, with weight is a considerable factor. Though the aforesaid materials are suitable for this fabrication, PMMA is very much preferable due to its adverse features such as transparent, cost effective, high modulus of elasticity and ease of fabrication. In addition, owing to the rigidity of PMMA, thin layers of PMMA will not have any impact due to pressure developed during the flow. In addition, thin layers of PMMA can be fabricated through laser fabrication by using laser cutters as well.

Laser cutting technique is very much popular for fabricating thin layers of microfluidic devices using polymers. As it is proposed in design stage, each and every thin layer of PMMA is designed in AutoCAD and exported to a software that comes with laser cutters. According to the design requirements, the settings of the laser is changed and the thin layers of polymethyl methacrylate (PMMA) plates are fabricated as specified in the design stage.

In order to reach the required micropump, it is necessary to bond all the thin layers by using proper bonding techniques. Thermal bonding or adhesives are the good options for this bonding as mentioned in literature, [93]. But thermal bonding technique is most preferable to avoid blockages in microfluidic channels. Also, this is a leak proof technique and good option for micropumps used in microfluidic applications [94].

4.2 Fabrication of single diaphragm micropump

As the preliminary stage, the single diaphragm micropump was fabricated according to the Model 1 developed at the design stage. In order to reach clear picture about single diaphragm micropump, the position of diaphragm and the states of that during suction and compression are expressed in Figure 4.2 a. In this sense, initially the thin layers of PMMA sheets were prepared by using laser cutters as described in the design stage and the PZT actuator was chosen from the commercially available PZT brass

diaphragm attached with PZT 5H material (http://www.murata.com). The fabricated thin layers of micropump is shown in Figure 4.2 b.

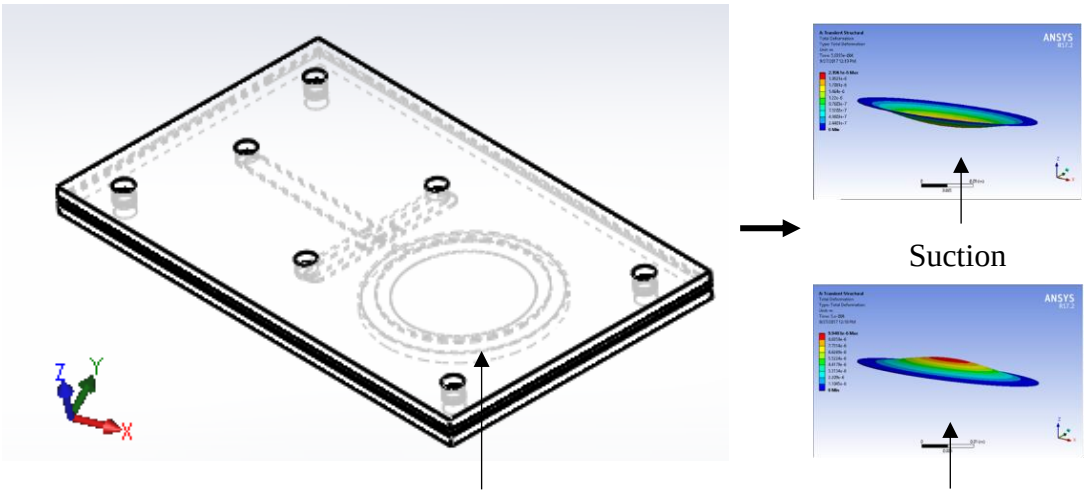

Figure 4.2 a: Position of diaphragm with states during suction and compression

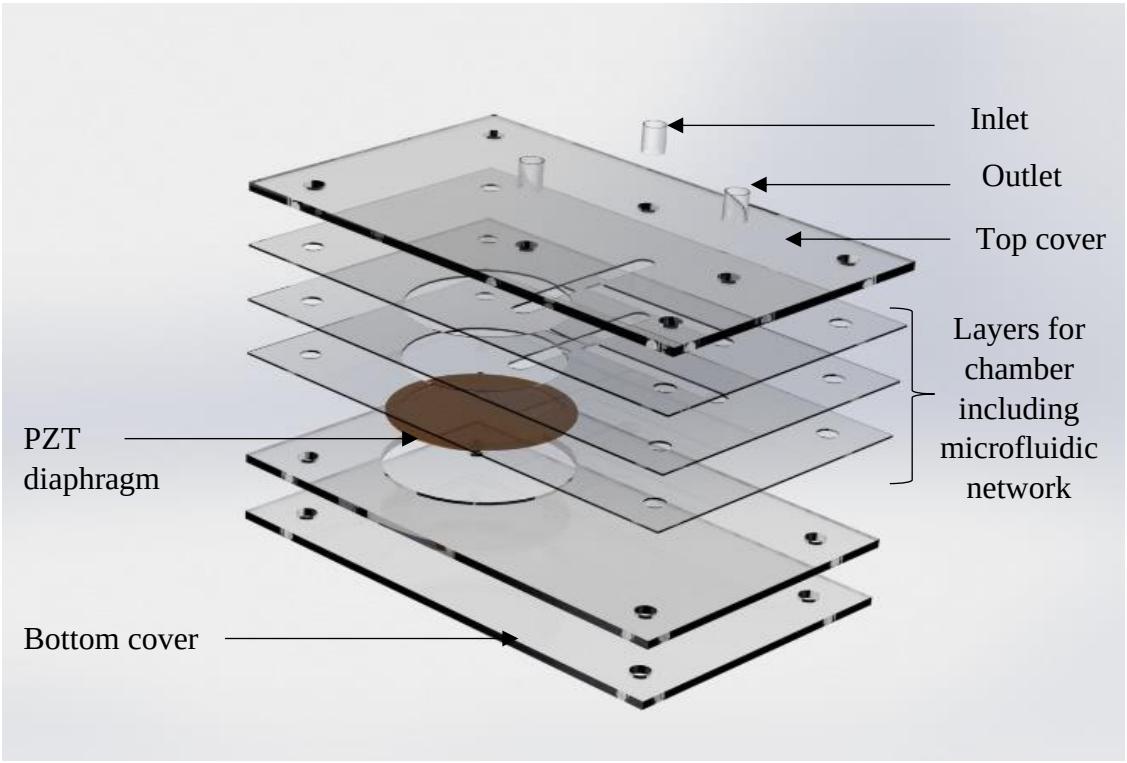

Figure 4.2 b: Fabricated thin layers of micropump[89]

These fabricated thin layers were cleaned by using detergents to remove dusts on the surfaces. After that, they were washed by using deionized (DI) water and dried properly. These layers were assembled one by one by applying “isopropyl alcohol” (surgical spirit) on each layer using syringe. This prepared structure was fastened by using paper fasteners.

Finally, this was kept inside the preheated oven (68 ^{0}C) for ten minutes [94]. Further, this thermally treated structure was taken out from the oven and slowly cooled at room temperature for five minutes. Then the paper fasteners were removed and the required single diaphragm micropump was fabricated as a sample. The fabricated micropump is presented in Figure 4.2 c.

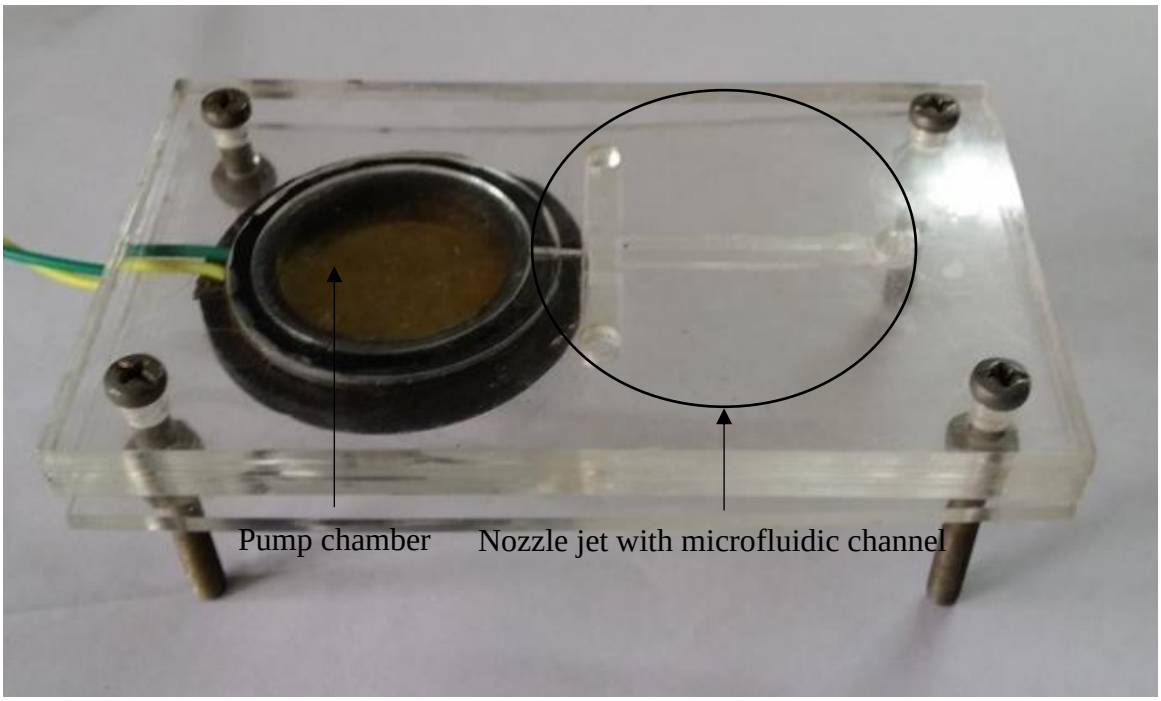

Figure 4.2 c: Single diaphragm micropump[89]

4.3 Fabrication of dual diaphragm micropump

As the improvement of the single diaphragm micropump, introducing dual diaphragms on top and bottom will be more advantageous and precise. The Figure 4.3 a illustrates the position of two diaphragms and the states of them during suction and compression. Hence the dual diaphragm micropump was also fabricated using the same fabrication techniques described in single diaphragm micropump.

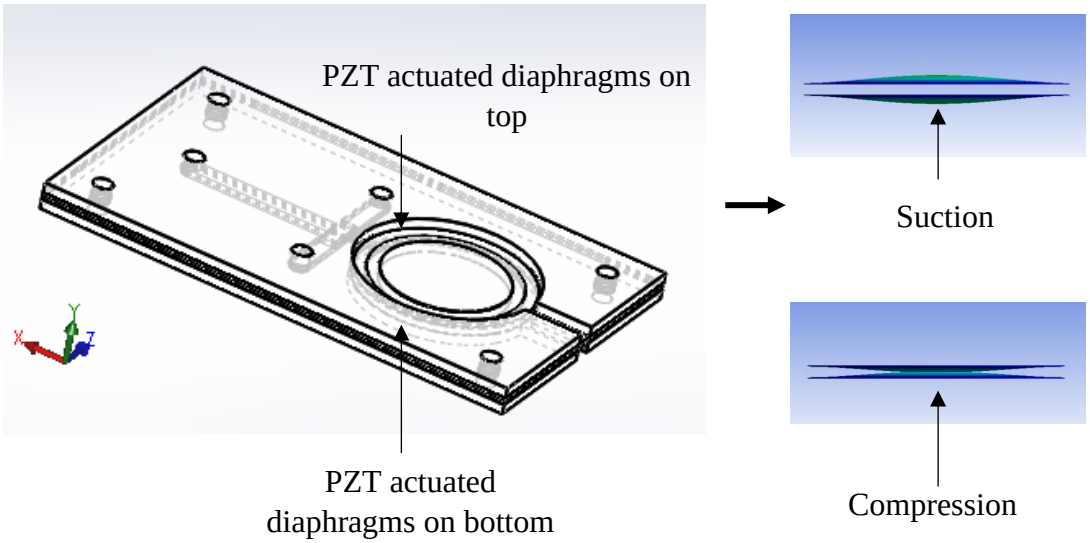

Figure 4.3 a: Position of diaphragm with states during suction and compression

As discussed in the single diaphragm, here also the PZT actuators were obtained from the commercially available brass diaphragms attached with circular PZT-5H material (http://www.murata.com). This fabricated dual diaphragm micropump contained a pump chamber, reservoir, and testing plate.

The pump chamber was developed with three PMMA sheets of thickness 1 mm. Then two piezoelectric transducers were fixed on top and bottom sides of the pump chamber to reach the enclosed chamber. The reservoir and the testing plates were fabricated with the remaining PMMA sheets. The measured reservoir capacity was 10 ml. The components and the assembled view of the fabricated dual diaphragm micropump are illustrated in Figure 4.3 b and Figure 4.3 c respectively.

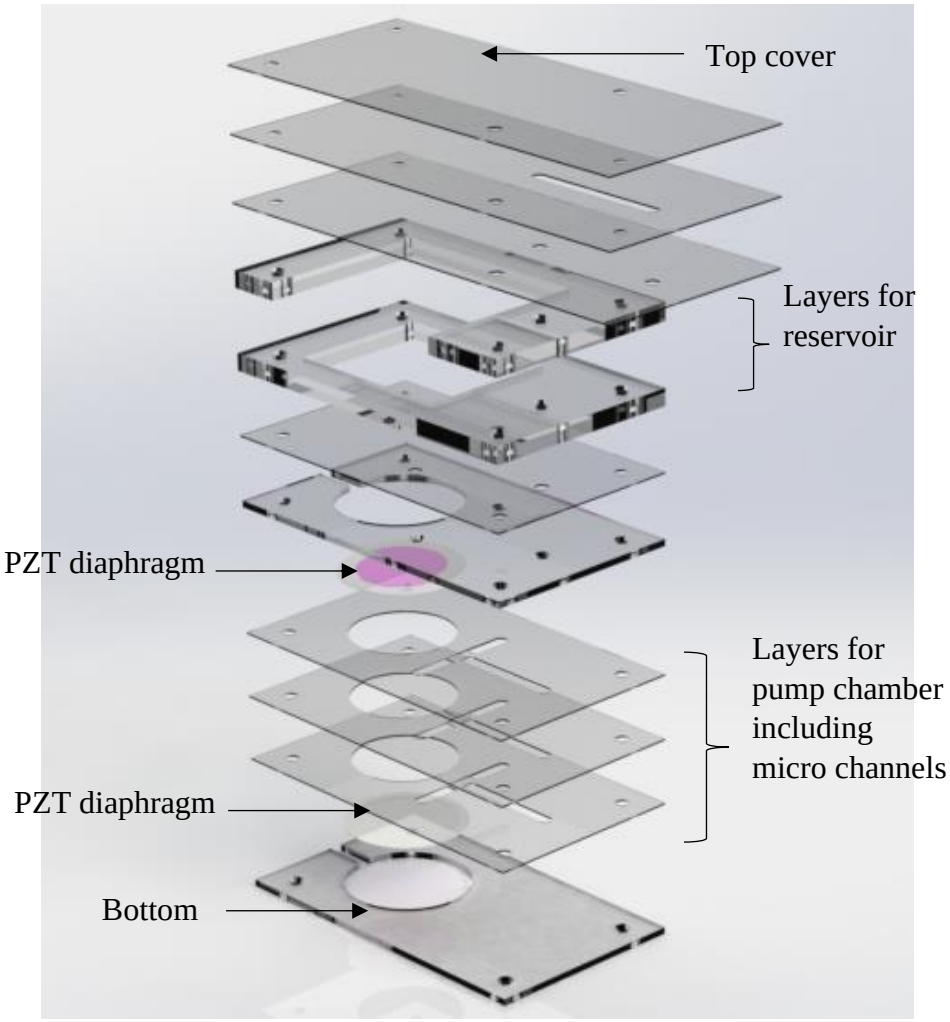

Figure 4.3 b: Components of the dual diaphragm micropump[89]

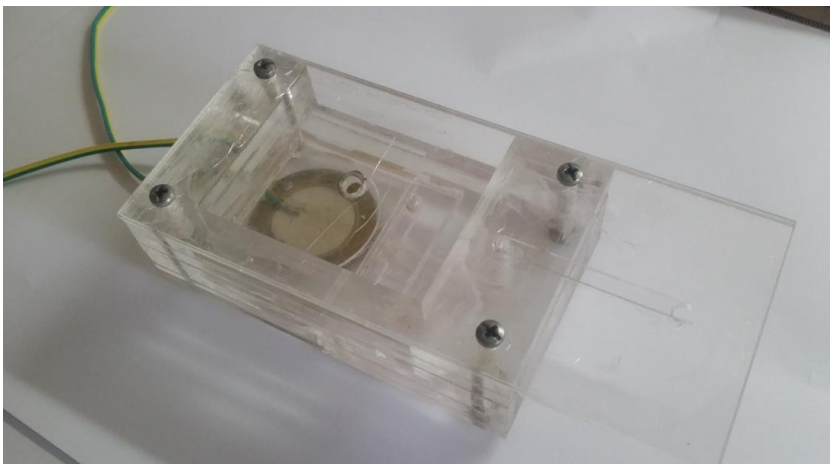

Figure 4.3 c: Assembled view of fabricated dual diaphragm micropump[89]

CHAPTER 5.0 ELECTRICAL CIRCUITRY AND SIGNAL CONDITIONING

Signal conditioning and electrical circuitry is a basic necessity for the easy operation and control of the fabricated micropump. In order to test and validate the fabricated micropump within the prescribed ranges, it is vital to setup an experimental layout with a simple electrical circuit as described in the Figure 5.0.

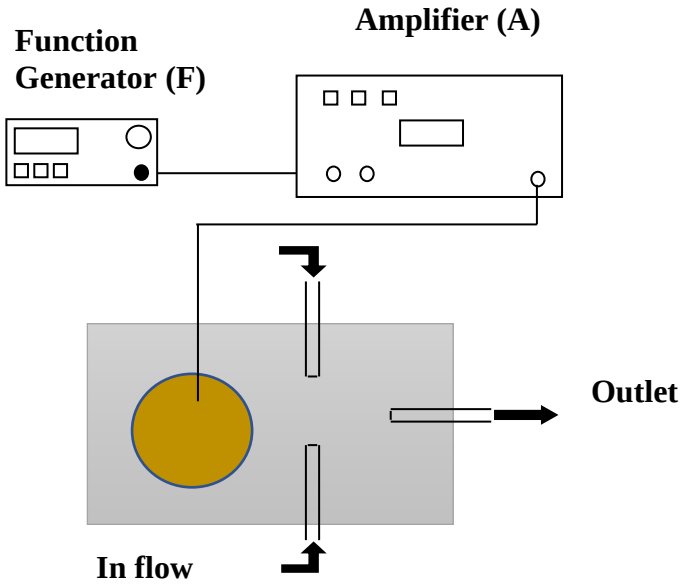

Figure 5.0: Experimental Layout

According to this experimental layout, initially the dual diaphragm micropump was controlled by using a signal generator which uses square wave signals. The frequency of this signal generator was controlled by Arduino Mega 256 micro controller. On the other hand, it was noted in most of the researches based on piezoelectric diaphragm micropumps, the optimum condition of a pump would be achieved when the diaphragm vibrate in its resonant frequency. As per the FEM analyses, the resonant frequency of the PZT actuated diaphragm was 1619 Hz. In this case, when the supply frequency exceeds 1100Hz (under -10V to +10V peak to peak amplitude), the PZT diaphragm started to deteriorate and short circuit.

Further it was found that the sin waves were the best signal condition to control the PZT diaphragm. Hence AD9850 Signal Generator Module with a basic circuit design

was used and this design can create a pure frequency and phase programmable, analog sine waves relative to time. Though operational amplifiers are stable and easy to handle, the AC sine wave was amplified using an LM741 operational amplifier in the first stage of the amplifier circuit. Finally, the dual diaphragm micropump was tested to validate the test results with the simulated outcomes.

CHAPTER 6.0 TESTING AND VALIDATION

According to developed experimental setup, the micropump was operated and controlled as described in Chapter 5. Henceforward the time taken was determined to collect 5 ml of water along the outlet. During the operation, the states at every five seconds throughout one minute is presented in Figure 6.0 a to Figure 6.0 l respectively. This process was initiated by varying the frequency at the discharge head of 0 mm and was performed for three different trials for accuracy. The outcomes of this test are tabulated in Table 6.0 a.

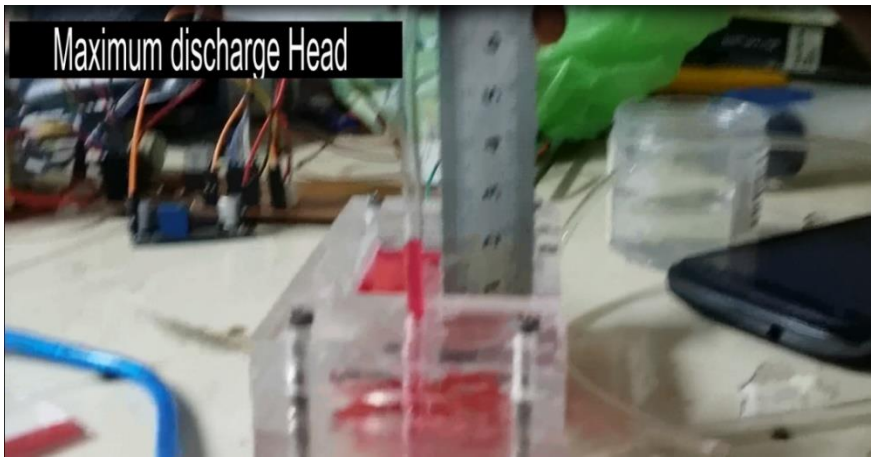

Figure 6.0 a: Flow rate at 5 s

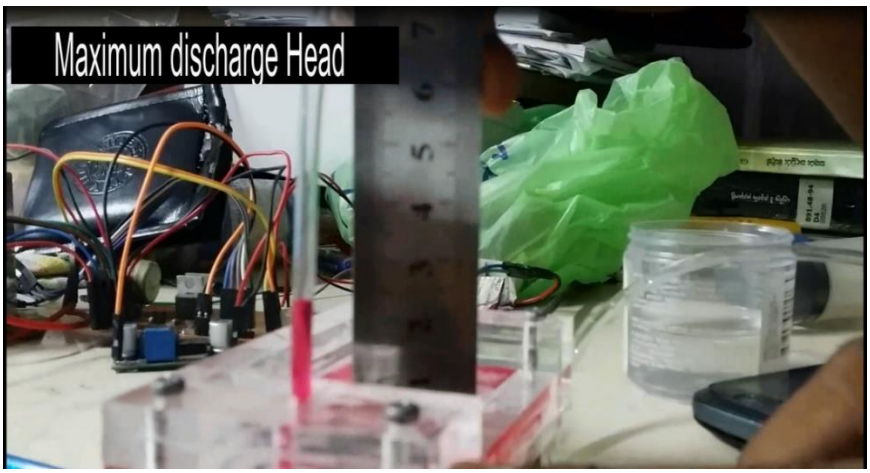

Figure 6.0 b: Flow rate at 10 s

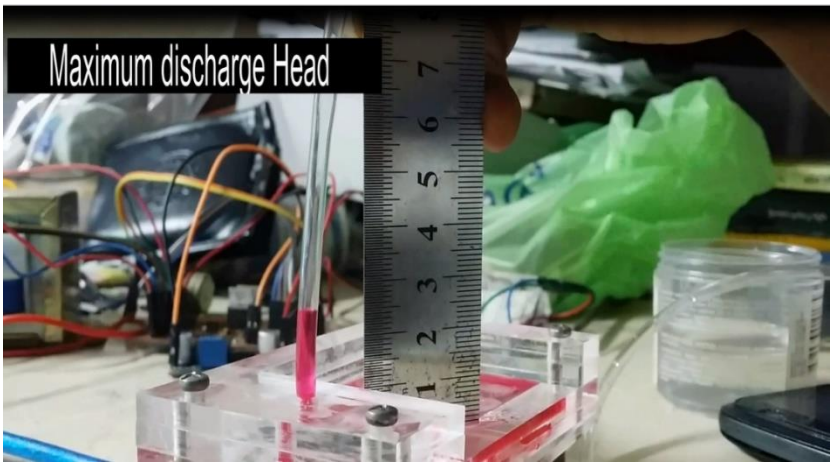

Figure 6.0 c: Flow rate at 15 s

Figure 6.0 d: Flow rate at 20 s

Figure 6.0 e: Flow rate at 25 s

Figure 6.0 f: Flow rate at 30 s

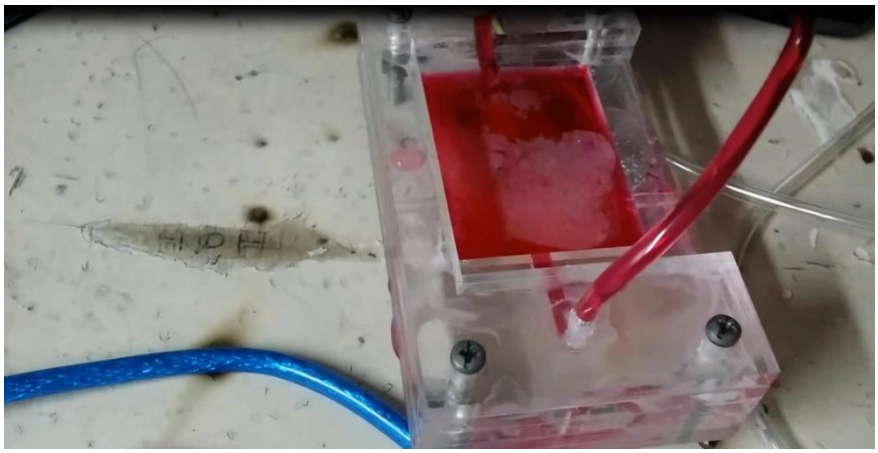

Figure 6.0 g: Flow rate at 35 s

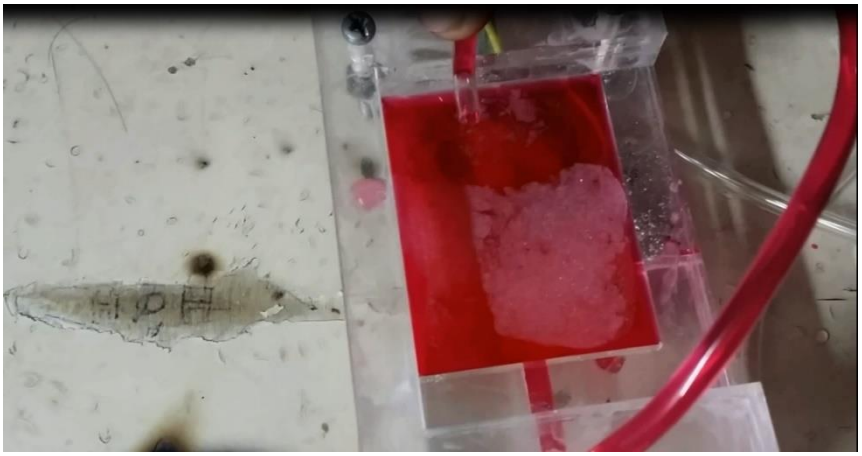

Figure 6.0 h: Flow rate at 40 s

Figure 6.0 i: Flow rate at 45 s

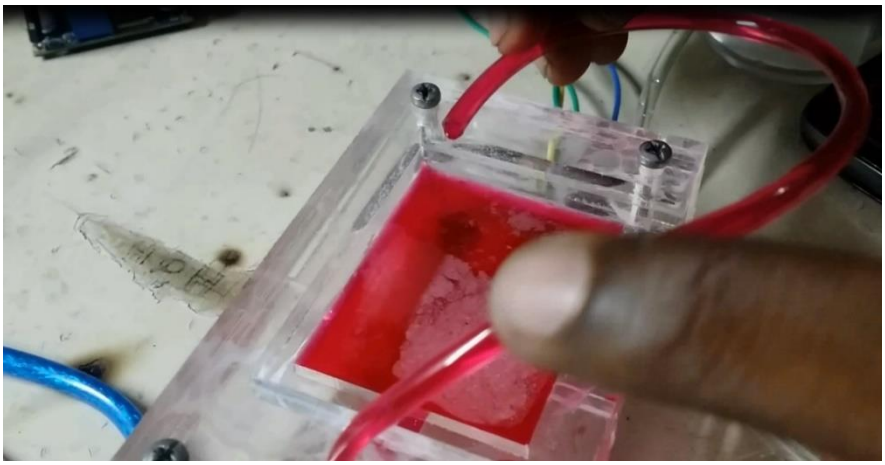

Figure 6.0 j: Flow rate at 50 s

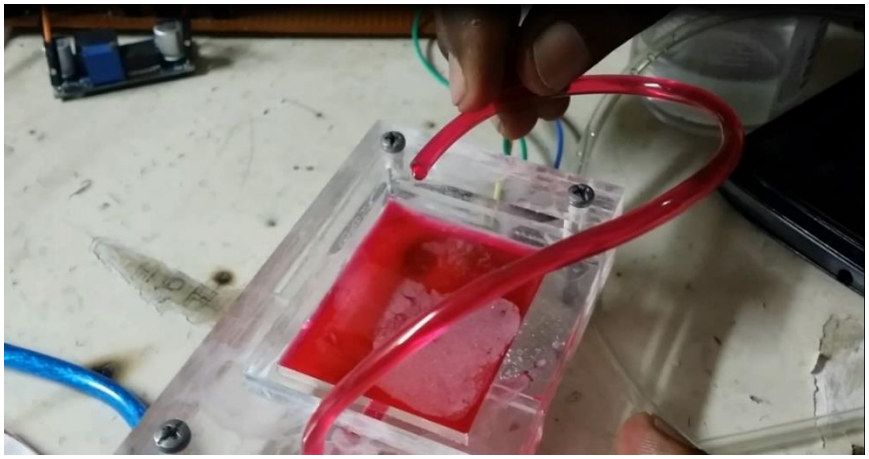

Figure 6.0 k: Flow rate at 55 s

Figure 6.0 l: Flow rate at 60 s

Table 6.0 a: Collected data for different frequency at 0 mm discharged head

Frequency (Hz)	Test A Time (s)	Test B Time (s)	Test C Time (s)	Average Time (s)	Flow Rate(ml/s)
5	-	-	-	-	0
50	11.91	12.43	12.04	12.12667	0.412314458
100	10.04	9.56	9.29	9.63	0.5192108
500	23.84	24.56	24.91	24.43667	0.204610558
1000	80.84	79.92	80.41	80.39	0.062196791

Further, the average net flow rates were calculated at different frequencies and tabulated in Table 6.0 b. According to this respective tabulated data, the variation net flow rates with applied frequency is plotted as shown in Figure 6.0 m.

Table 6.0 b: Experimental results for the average net flow rate with frequency

Frequency (Hz)	Flow Rate(ml/s)
5	0
50	0.412314458
100	0.5192108
500	0.204610558
1000	0.062196791

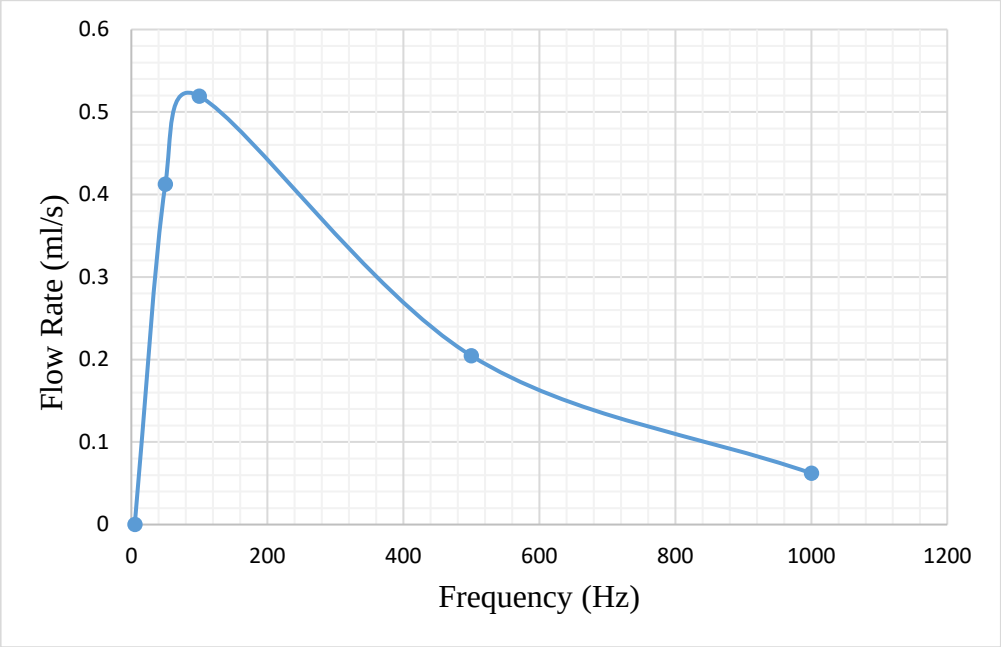

Figure 6.0 m: Variation of net flow rates with frequency

In order to succeed number of experimental data sets at different discharged heads, PMMA plates with the thickness of 5 mm were added as a plate-by-plate element to the fabricated micropump. Then, the time taken was determined to reach 5 ml of volume at the frequency of 50 Hz for different discharged heads and the outcomes are presented in Table 6.0 c

Table 6.0 c: Data sets for different discharged head at 50Hz

Head (mm)	Volume (ml)	Test 1 Time (s)	Test 2 Time (s)	Test 3 Time (s)	Average Time (s)
0	5	11.91	12.43	12.04	12.13
5	5	18.34	17.89	18.26	18.16
10	5	24.52	24.31	24.79	24.54
15	5	35.48	34.98	35.81	35.42
20	5	47.38	46.97	47.11	47.15
24	5	-	-	-	-

By using these data, flow rates at different discharged heads were calculated and tabulated in Table 6.0 d. Finally, the variation of net flow rates with discharged heads are plotted as shown in Figure 6.0 n.

Table 6.0 d: Calculated experimental flow rates at different discharged head

Head (mm)	Flow Rate (ul/s)
0	412.3
5	275.3
10	203.7
15	141.2
20	106.0
24	0

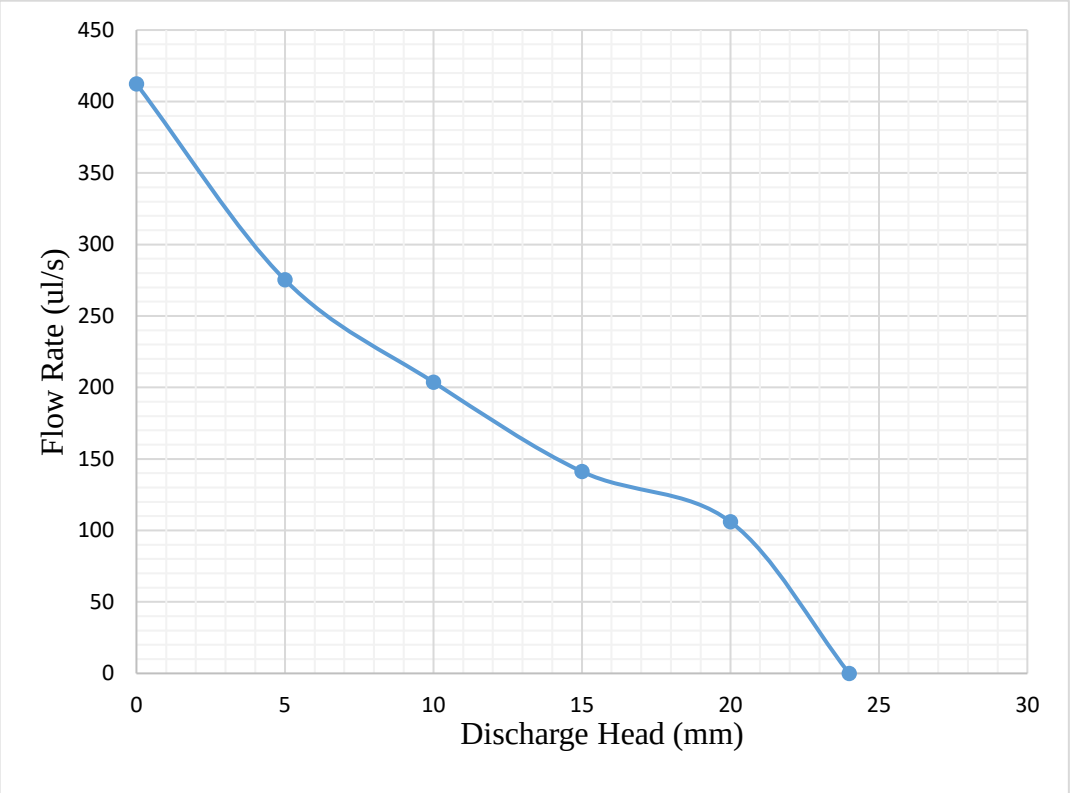

Figure 6.0 n: Variation of net flow rates with discharged head at constant frequency

CHAPTER 7.0 PERFORMANCE ENHANCEMENT OF MICROPUMPS

7.1 Thin film deposition techniques on PZT actuators

Generally, the thin film depositions techniques have the ability improve the mechanical properties of microstructures. Compared with the pure PZT actuators, PZT actuators with thin film deposition have many features such as better displacement for a particular force, better flexibility, stronger plasticity, easier performance improvement, less natural frequency and so on. In order to enhance the micropump performance, analyzing thin film deposition techniques on PZT actuators are also worthwhile in this study. Hence design and simulation analysis were performed for thin film deposited PZT actuators.

Basically, thin film deposition techniques are introduced through various kinds of organic polymers with different thin film fabrication techniques. In this sense, the two kinds of polymers namely, Poly Methyl Methacrylate (PMMA) and Poly Dimethyl Siloxane (PDMS) are chosen due to their adverse mechanical and chemical characteristics. In addition, PMMA and PDMS are transparent, light weight and low cost [1][95]. They are highly compliant and suitable for thin film applications as well [96].

Though there are several thin film fabrication techniques such as evaporation, sputtering, chemical vapor deposition, spin on deposition and others are available in literature, spin on deposition technique is selected to prepare the PMMA and PDMS thin films. Because these can allow fast and reproducible production [97][98][99]. The resulting film thickness mainly depends on the polymer molecular weight, concentration of the polymer in solution, spinning velocity and spinning time [100][101][102][103].

In order to analyze this effect theoretically, the piezoelectric structural and electrical simulation analysis were performed using COMSOL Multiphysics. This analysis was carried out on eigen frequency study setup under piezoelectric stress/strain mode. Initially, two kinds of models with PMMA and PDMS thin films at different thicknesses varying from 100 um to 220 um were developed. As a reference, the designed models of PMMA thin film deposited PZT diaphragm as well as the PDMS

thin film deposited PZT diaphragm are shown in Figure 7.1 a and, Figure 7.1 b respectively.

An alternating electrical signal was applied to the PZT actuator at varying thin film of PMMA with the same voltage of 20 V as described previously. The deformation and the stress analysis are plotted as shown in Figure 7.1 c, Figure 7.1 d, Figure 7.1 e and Figure 7.1 f respectively.

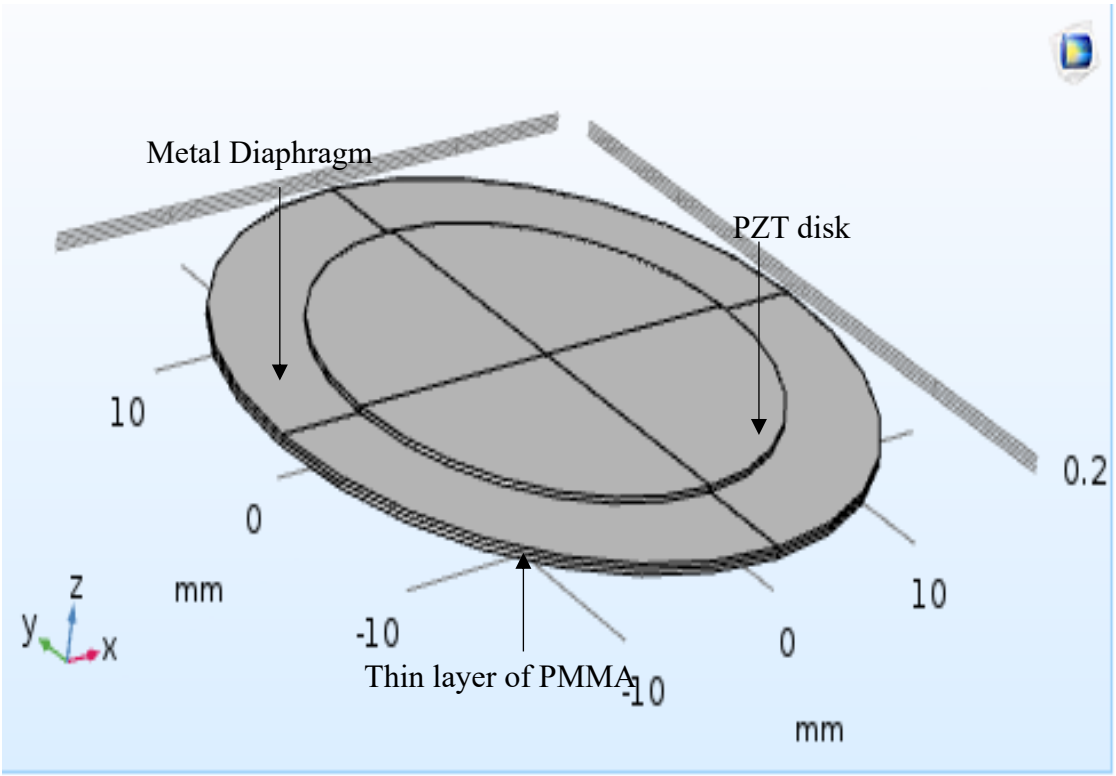

Figure 7.1 a: Designed model of the PZT brass diaphragm with thin layer deposition of PMMA

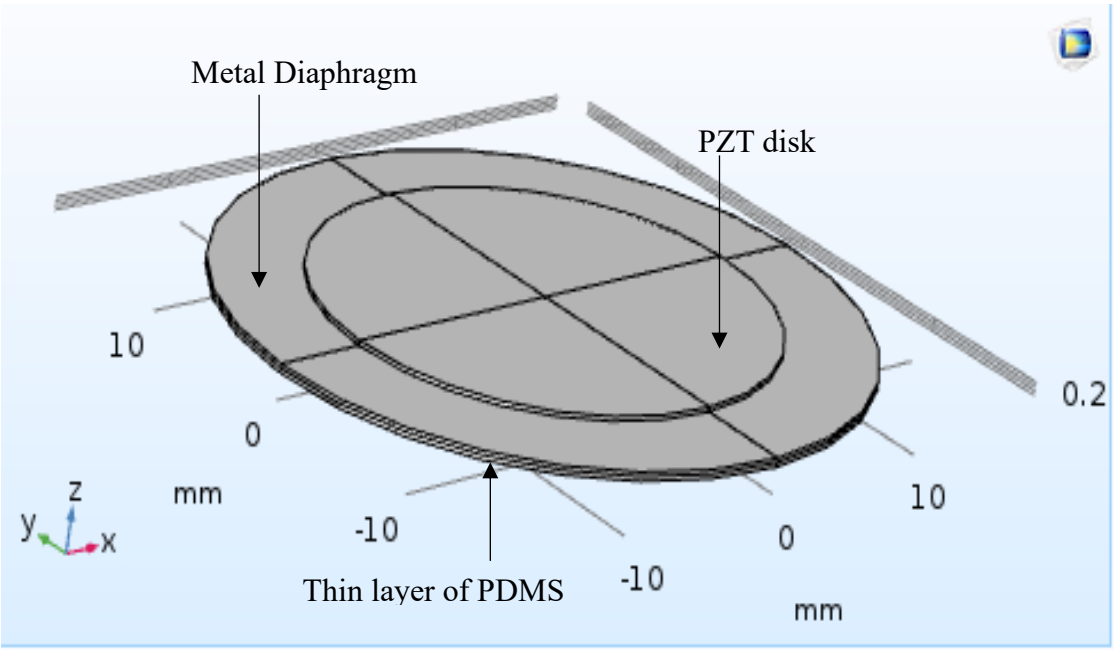

Figure 7.1 b: Designed model of the PZT brass diaphragm with thin layer deposition of PDMS

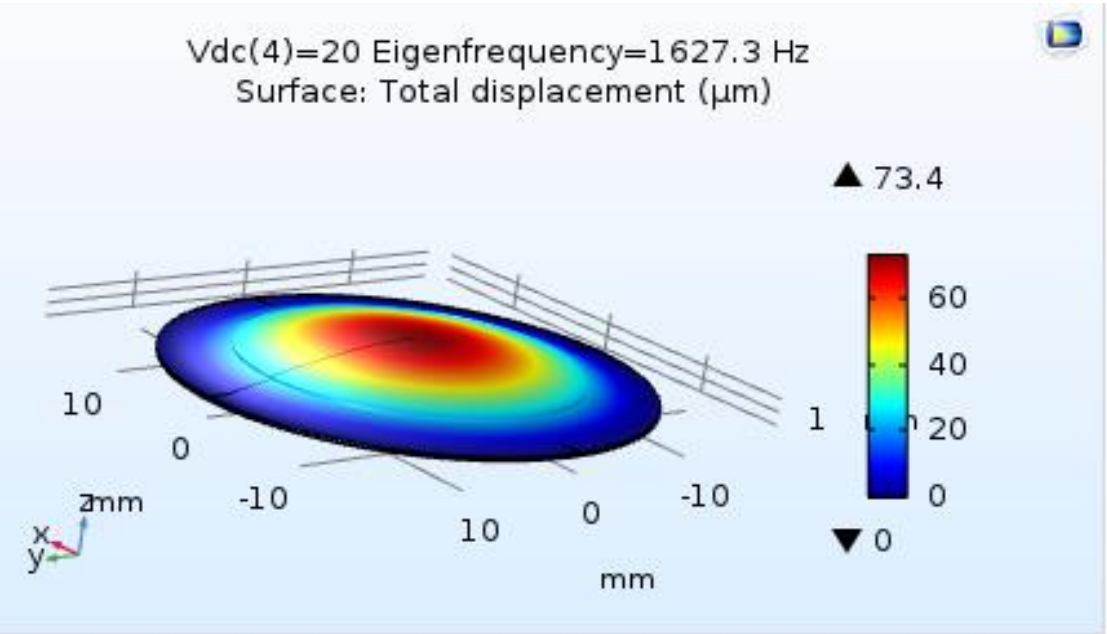

Figure 7.1 c: Deflection analysis of the PZT brass diaphragm with thin film deposition of 100 um PMMA

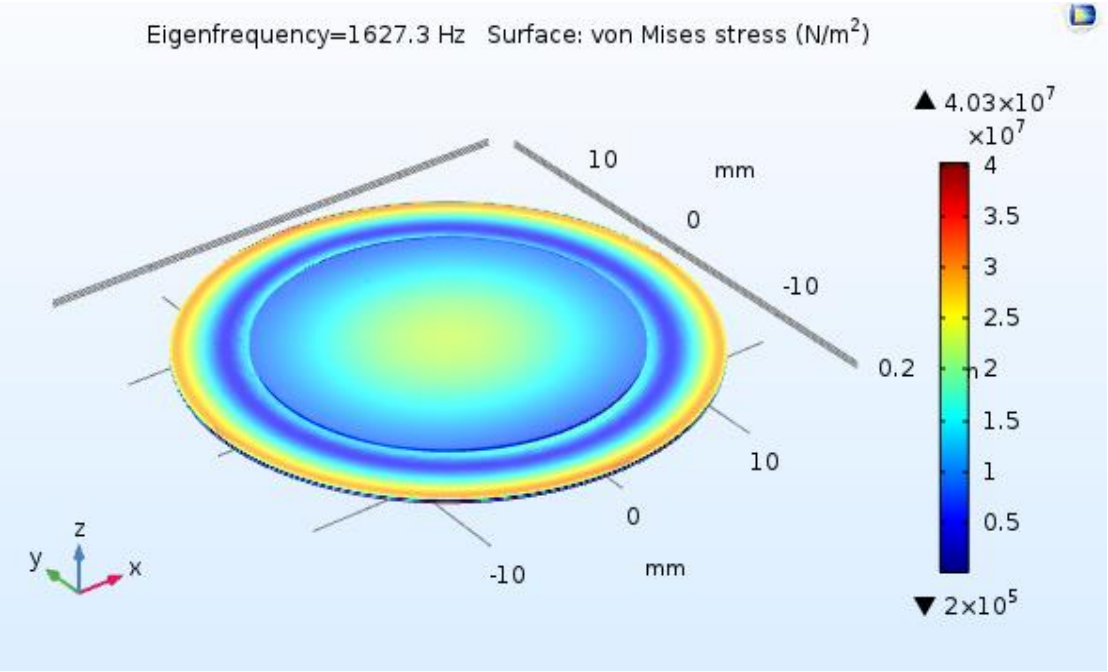

Figure 7.1 d: Von misses stress analysis of the PZT brass diaphragm with thin film deposition of 100 um PMMA

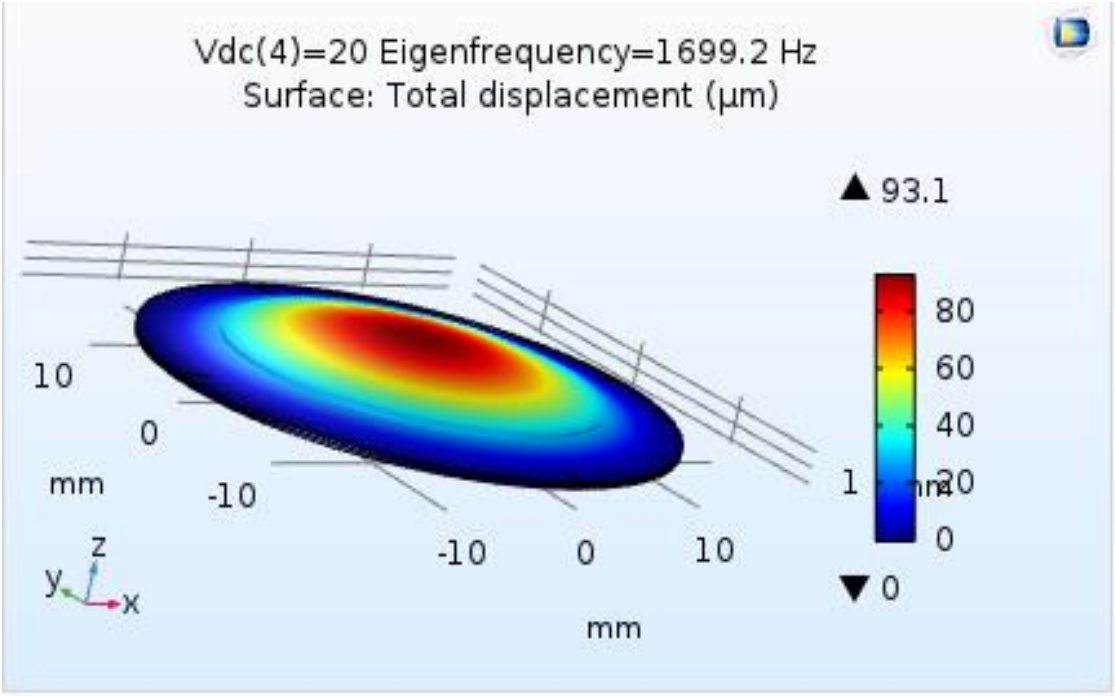

Figure 7.1 e: Deflection analysis of the PZT brass diaphragm with thin film deposition of 220 um PMMA

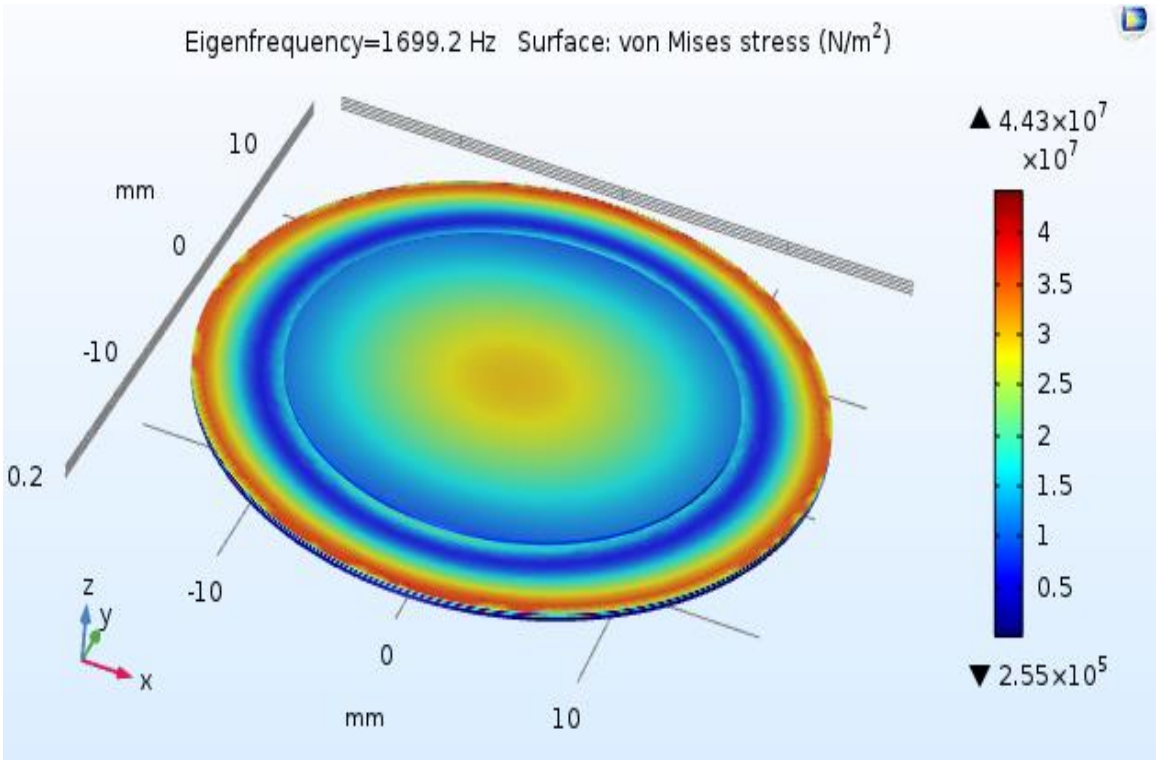

Figure 7.1 f: Von misses stress analysis of the PZT brass diaphragm with thin film deposition of 220 um PMMA

Then the thicknesses of thin film deposition varying from 100 um to 220 um of PDMS were also analyzed in the same manner which explained for the PMMA thin film. The outcomes of this analysis are plotted as illustrated in Figure 7.1 g, Figure 7.1 h, Figure 7.1 i and Figure 7.1 j respectively.

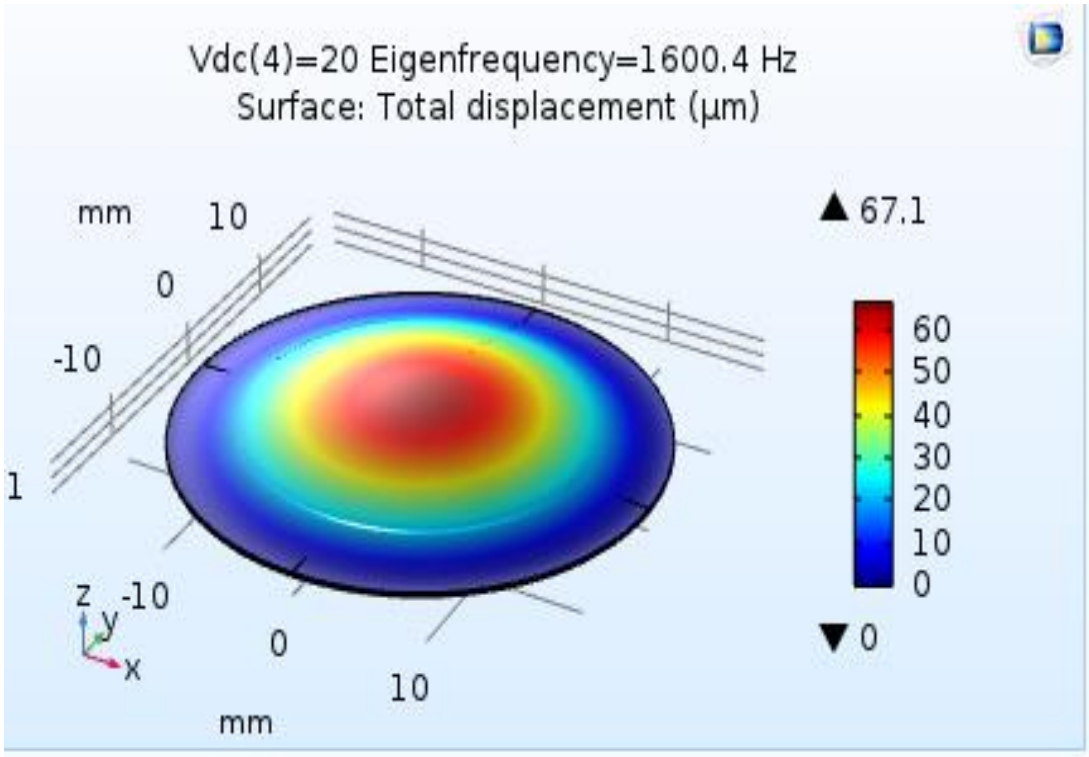

Figure 7.1 g: Deflection analysis of the PZT brass diaphragm with thin film deposition of 100um PDMS

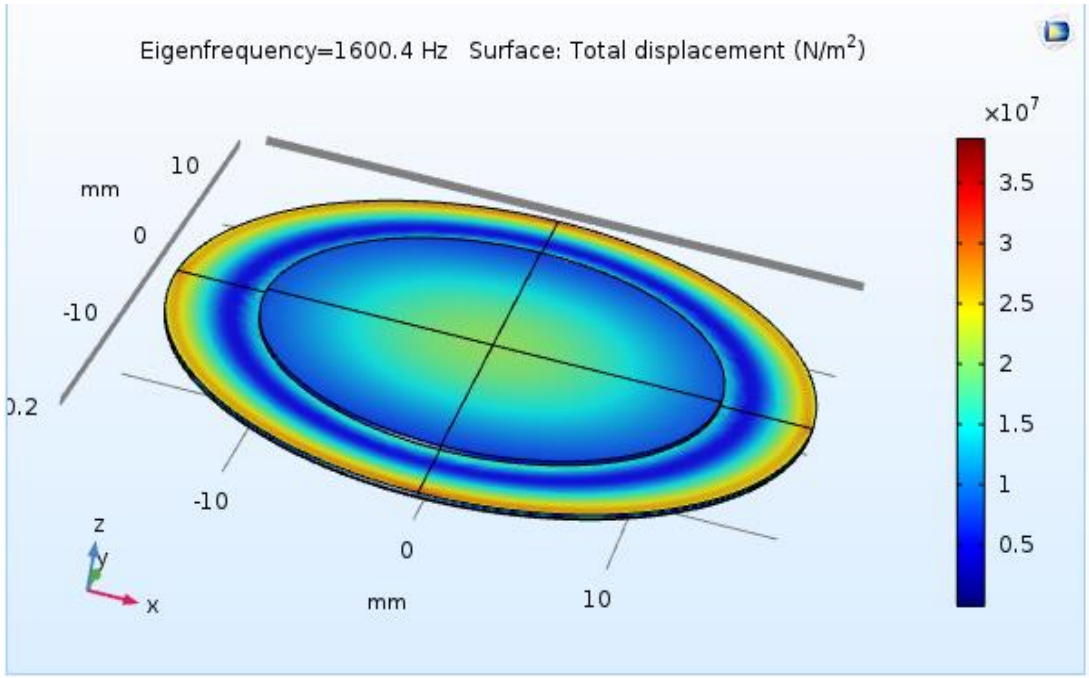

Figure 7.1 h: Von misses stress analysis of the PZT brass diaphragm with thin film deposition of 100um PDMS

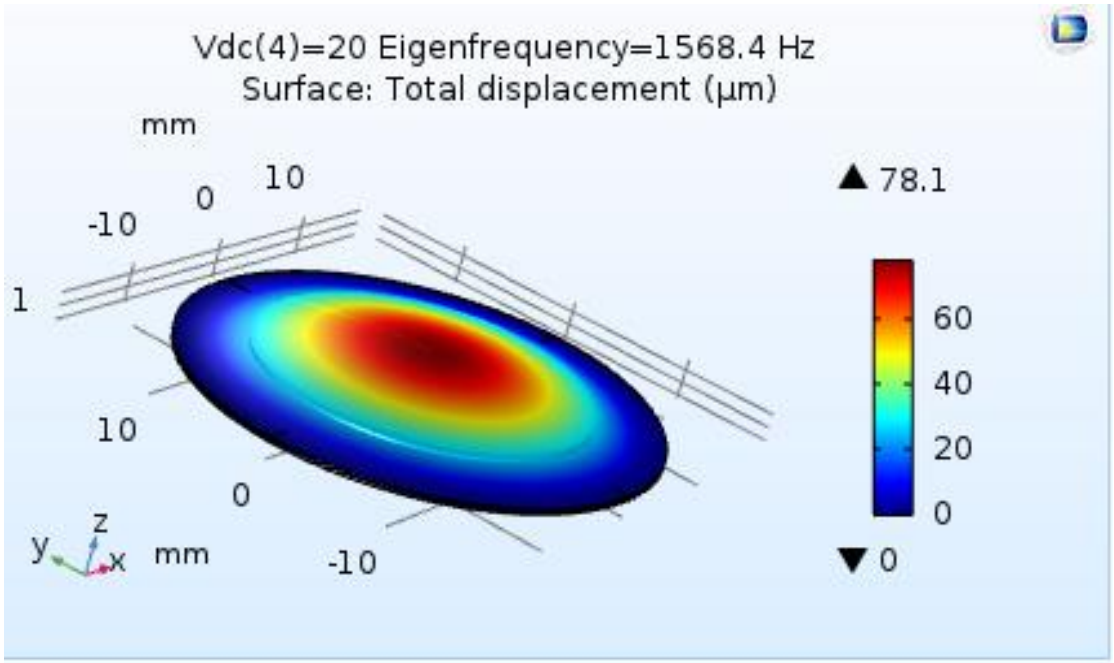

Figure 7.1 i: Deflection analysis of the PZT brass diaphragm with thin film deposition of 220um PDMS

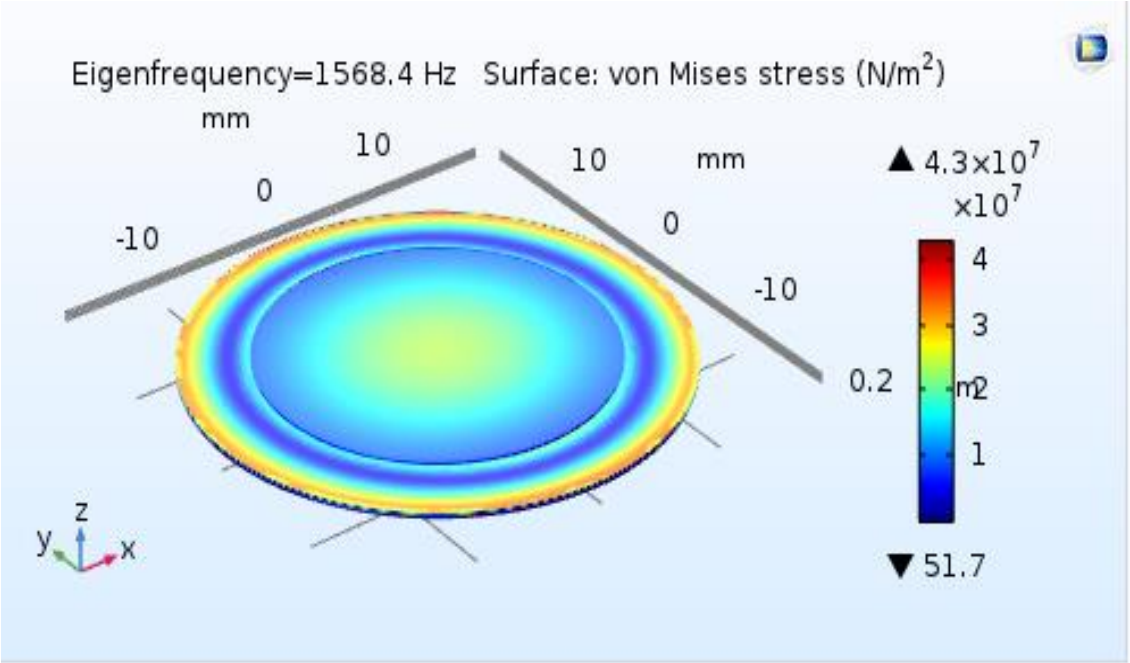

Figure 7.1 j: Von misses stress analysis of the PZT brass diaphragm with thin film deposition of 220um PDMS

7.2 Thermo Elastic Damping Analysis in PZT Actuator

Commonly, a micro-scale PZT actuators have major impact on the performance of the micropump due to thermo-elastic damping effect in PZT actuators. But it was very much difficult to analyze this effect using theoretical equations explained in literature. Hence the model was analyzed using COMSOL Multiphysics under the Thermo-elasticity physics tree with Eigen frequency study setup.

This analysis was initiated with the temperature of 300K at different eigen frequencies for simple PZT actuators and PDMS/PMMA polymer thin film deposited PZT actuators. The outcomes are plotted as shown in Figure 7.2 a, Figure 7.2 b, Figure 7.2 c and Figure 7.2 d respectively.

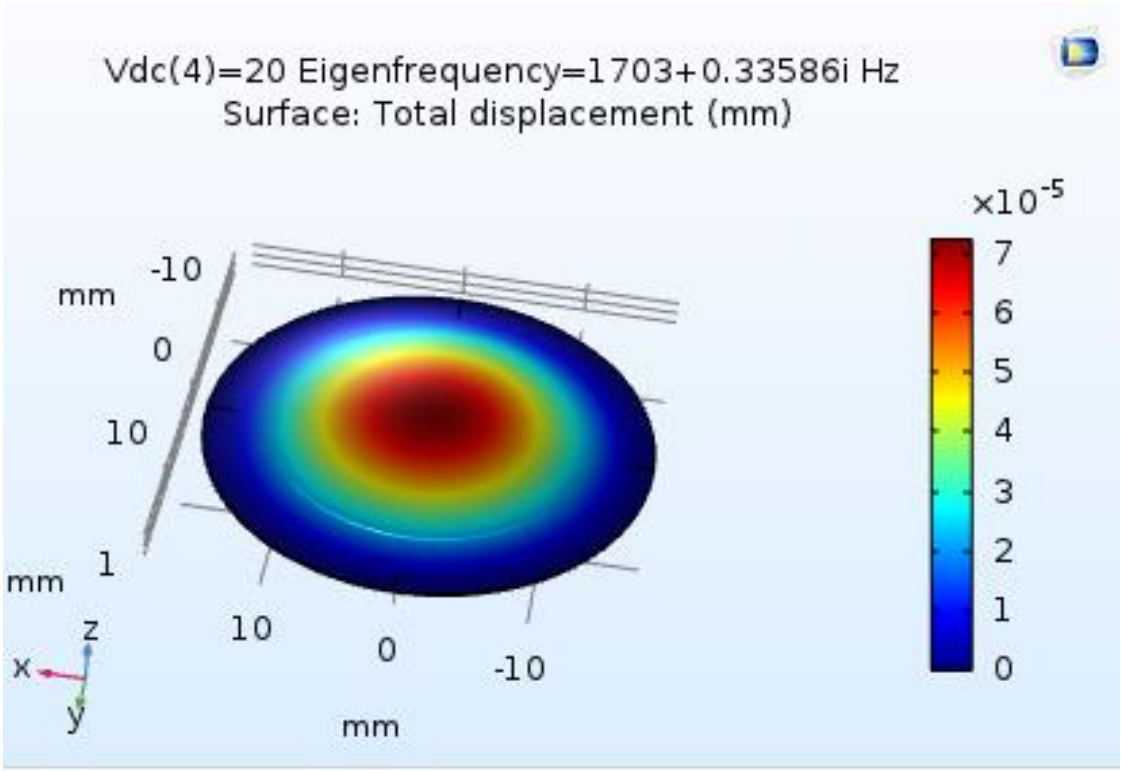

Figure 7.2 a: Displacement profile of a simple PZT actuator at first mode frequency

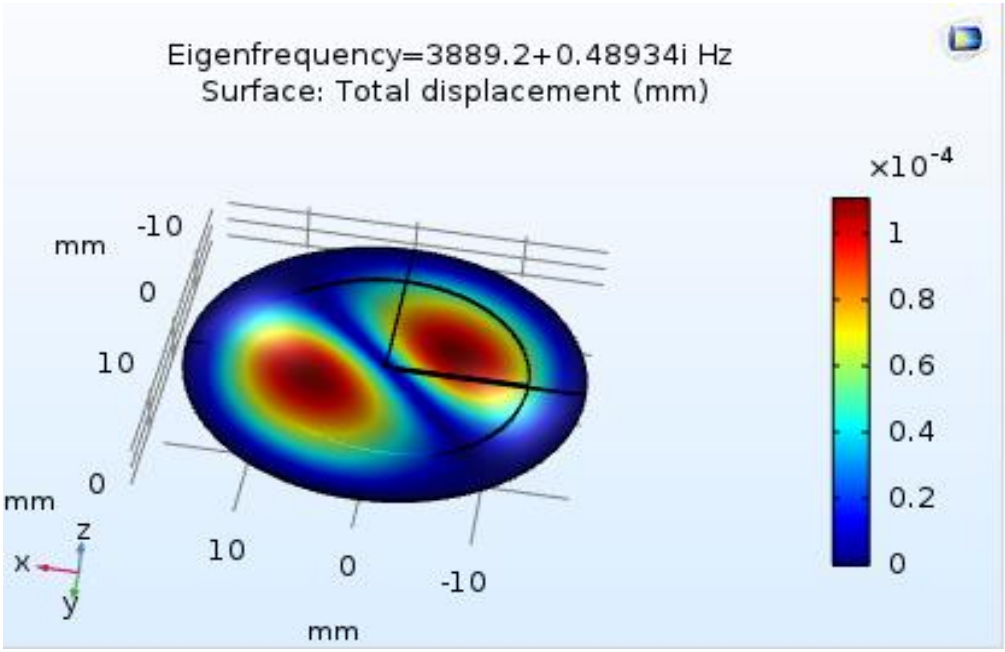

Figure 7.2 b: Displacement profile of a simple PZT actuator at second mode frequency

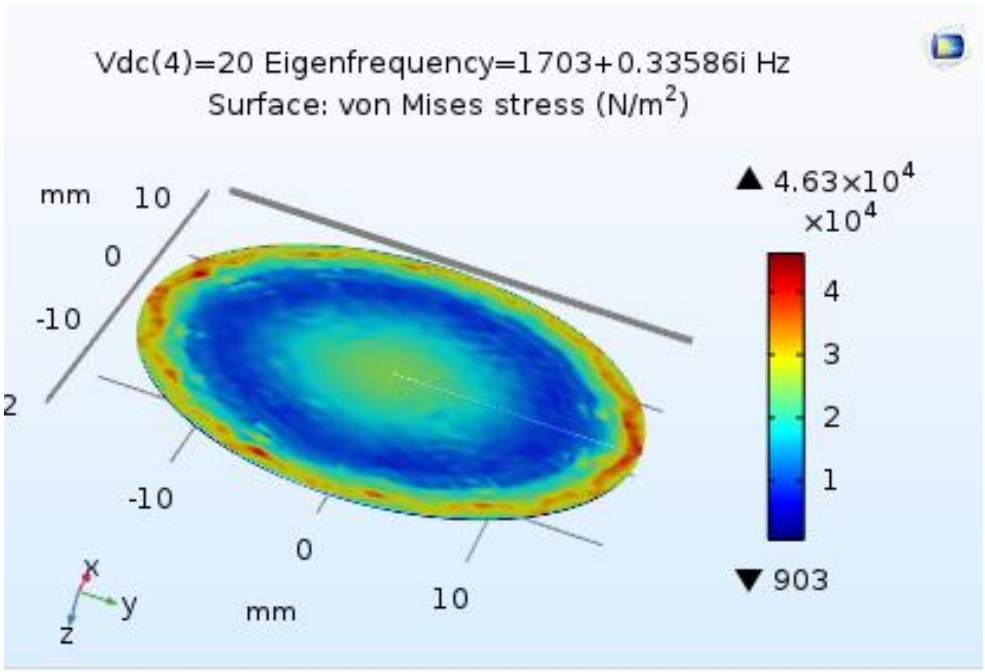

Figure 7.2 c: Stress profile of a simple PZT actuator at first mode frequency

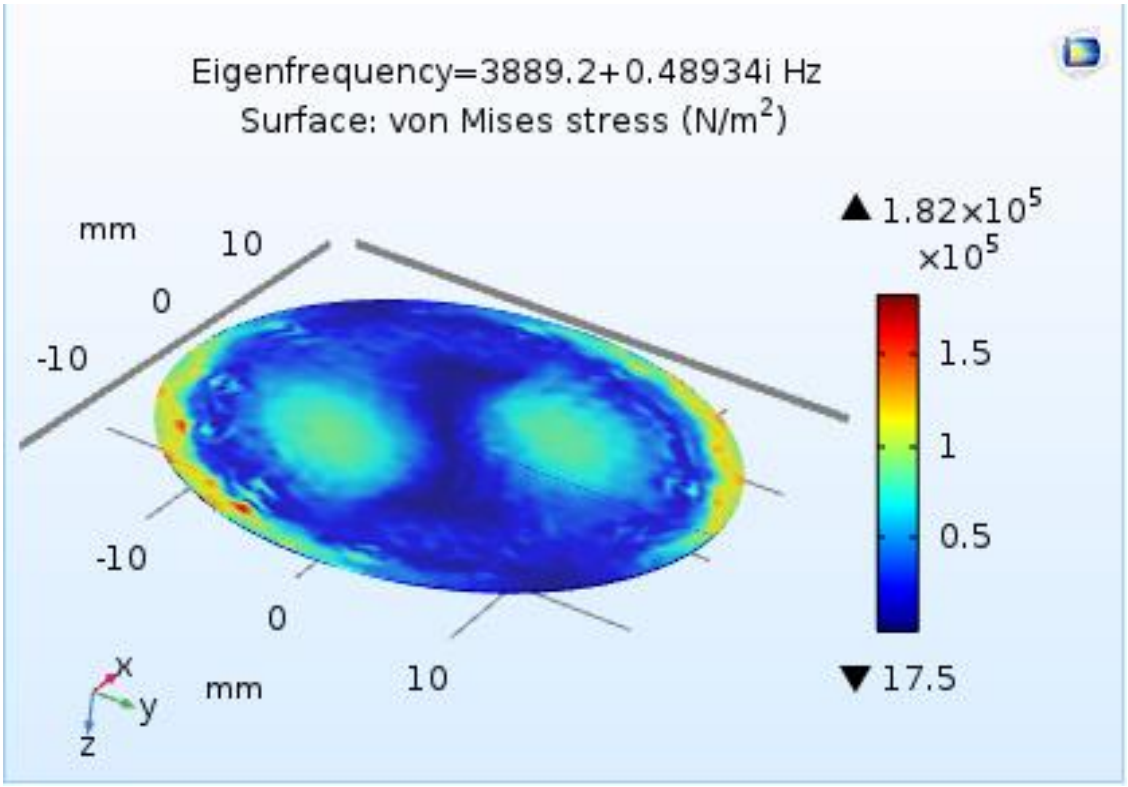

Figure 7.2 d: Stress profile of a simple PZT actuator at second mode frequency

In addition, the variation of Q factor with different mode frequencies were also obtained in all three aforementioned PZT actuators as illustrated in Figure 7.2 e, Figure 7.2 f and Figure 7.2 g respectively. As per the definition of Q factor given in literature, the variation of Q factor would give the sufficient information about the heat dissipation from the structure.

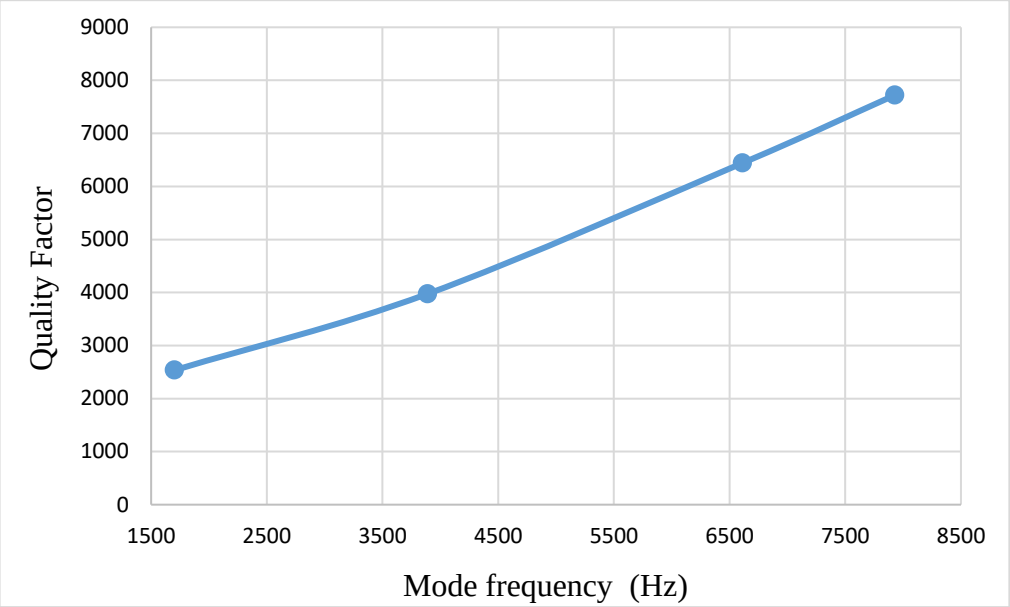

Figure 7.2 e: Variation of Q factor with mode frequencies for simple PZT actuator at 300 K

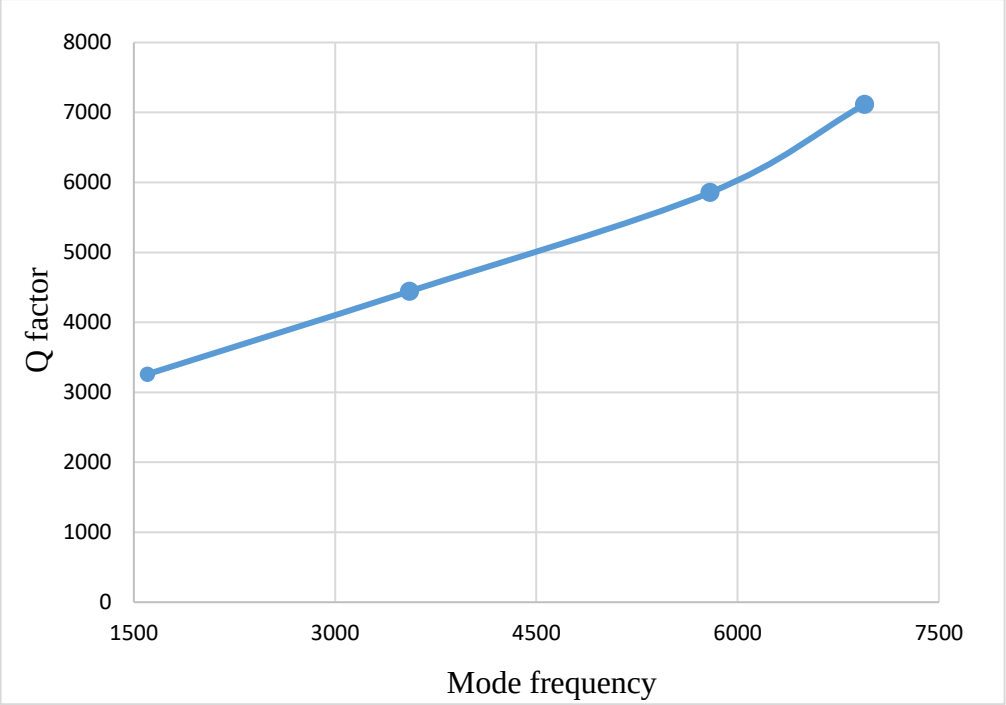

Figure 7.2 f: Variation of Q factor with mode frequencies for PDMS thin film deposited PZT actuator at 300 K

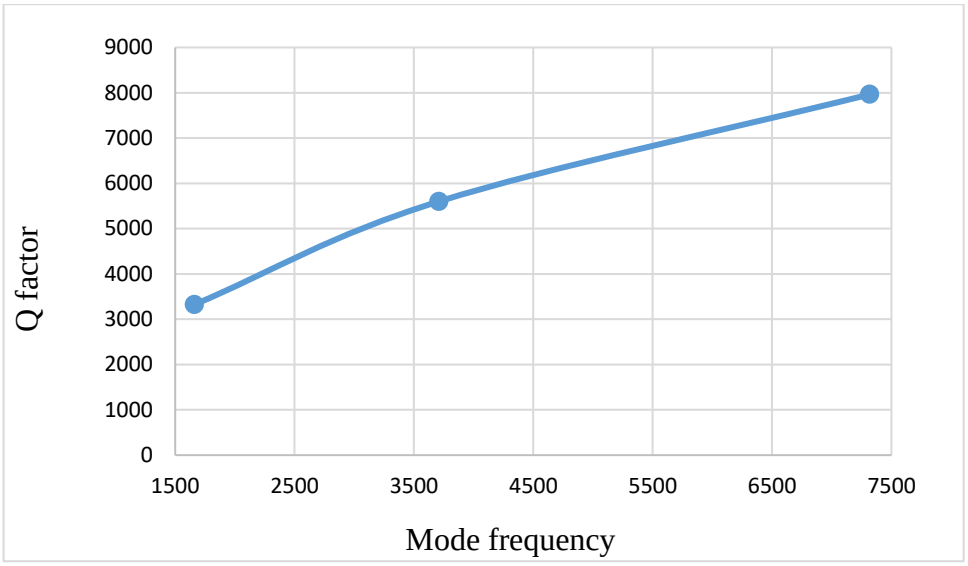

Figure 7.2 g: Variation of Q factor with mode frequencies for PMMA thin film deposited PZT actuator at 300K

According to the respective plots, the first mode frequency which is closer to piezoelectric mode frequency has the maximum volumetric change. The heat dissipation effect is also high in this frequency. Hence the first mode frequencies are selected to analyze for the temperatures varying from 200 K to 300 K at 25 K intervals. Then the variations of heat generation and heat dissipation effects with temperature are plotted as expressed in Figure 7.2 h, Figure 7.2 i and Figure 7.2 j respectively.

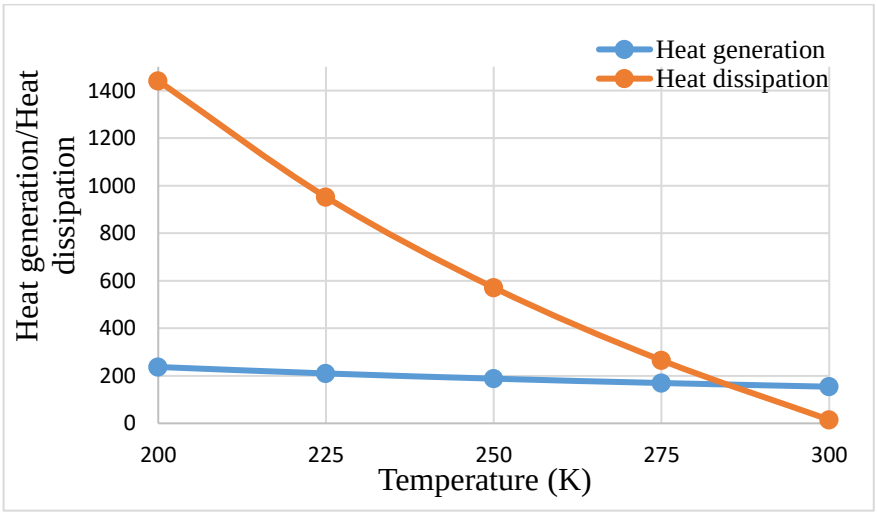

Figure 7.2 h: Variation of heat generation and heat dissipation with temperature for simple PZT actuator at first mode frequency of 1703 Hz

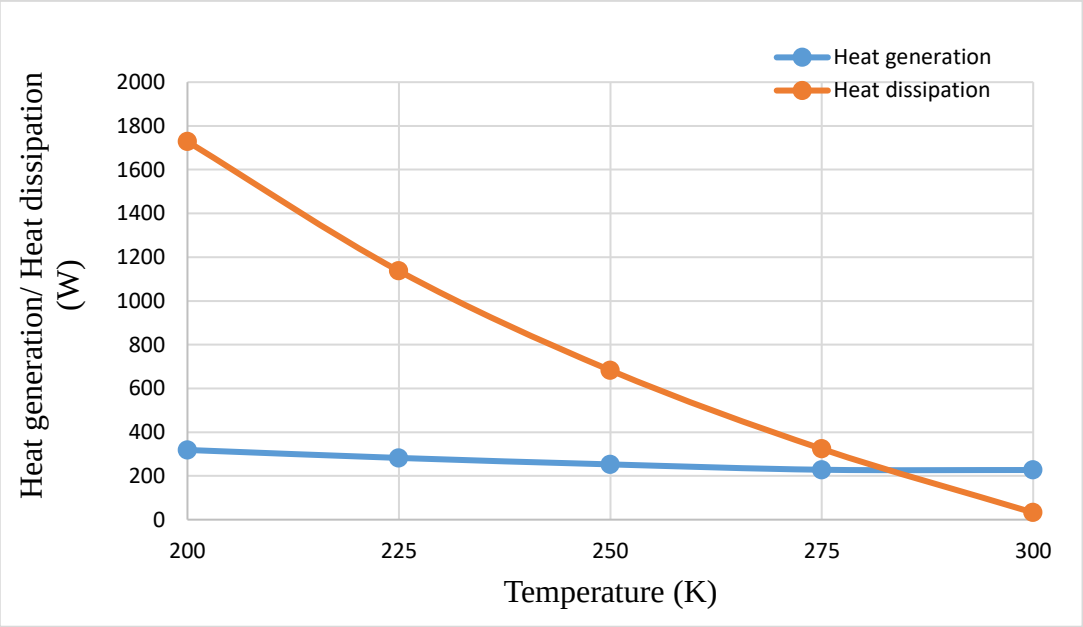

Figure 7.2 i: Variation of heat generation and heat dissipation with temperature for PDMS thin film deposited PZT actuator at first mode frequency of 1600.4 Hz

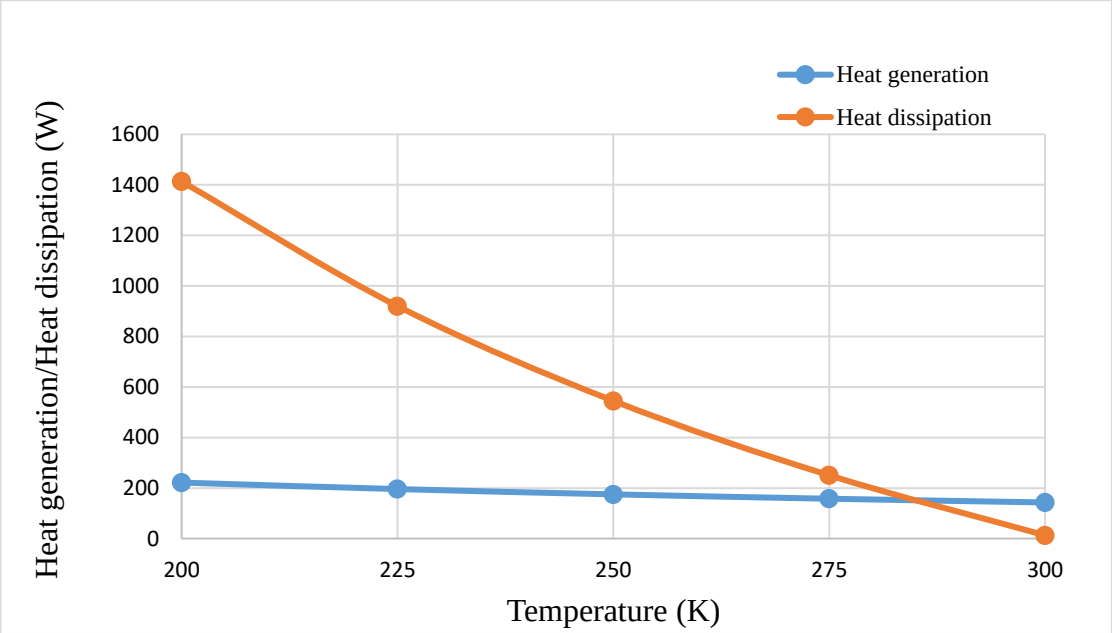

Figure 7.2 j: Variation of heat generation and heat dissipation with temperature for PMMA thin film deposited PZT actuator at first mode frequency of 1662.3 Hz

According to this analysis, the dissipation is decaying with temperature varying from 200 K to 300K. Comparing with energy generation, the PZT actuator doesn't have any thermal effects due to high thermal dissipation until 275 K. But the thermal energy generation is higher than the thermal energy dissipation when temperature reached beyond 275 K. Hence air-cooling calculations were done beyond this temperature.

7.2.1 Cooling air flow calculation of PZT actuators

Commonly, the required cooling air flow rate is expressed as,

$$Q=3160*KW/\Delta t \quad (7.2.1)$$

Where, Q is the air flow required in cubic feet /min, KW is the power dissipation in the equipment measured in kW and Δt is the rise of temperature across the equipment in ˚ F. According to the given expression, the required cooling air flow rate was calculated and tabulated in Table 7.2.1.

Table 7.2.1: The required cooling air flow

Description	PZT Actuator	PZT Actuator with PDMS thin film	PZT Actuator with PMMA thin film
KW	0.139	0.195	0.13
Δt (K)	7.469	9.731	9.028
Δt (˚ F)	13.44	17.52	16.25
Q ($feet^3$/min)	32.68	35.14	25.28
Q (m^3/s)	0.015	0.017	0.012

CHAPTER 8.0 DESIGN AND SIMULATION OF MEMS BASED PRESSURE SENSOR

8.1 Introduction

Monitoring pressure and receiving feedback in micropumps specially during onsite applications is vital. Carrying out a design and simulation analysis for MEMS based pressure sensor is also very beneficial in this research. According to this, the design and simulation for a MEMS based pressure sensor shown in Figure 8.1 a was executed with the available resources. During the design and simulation, it is vital to consider microstructure, sensing elements, and the sensitivity enhancement. Since pressure sensors with piezo-resistive sensing are more sensitive to pressure variations in microfluidic applications, piezo-resistive pressure sensor is proposed for this requirement. Thus, the design concept of a piezo-resistive pressure sensor is shown in Figure 8.1 b.

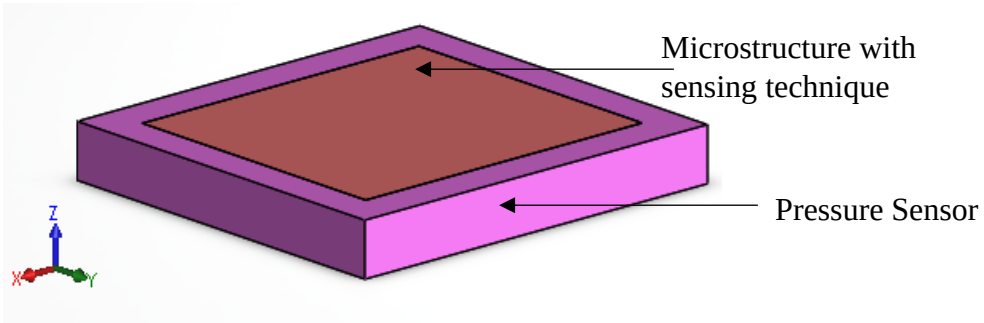

Figure 8.1 a: MEMS based pressure sensor – 3D model

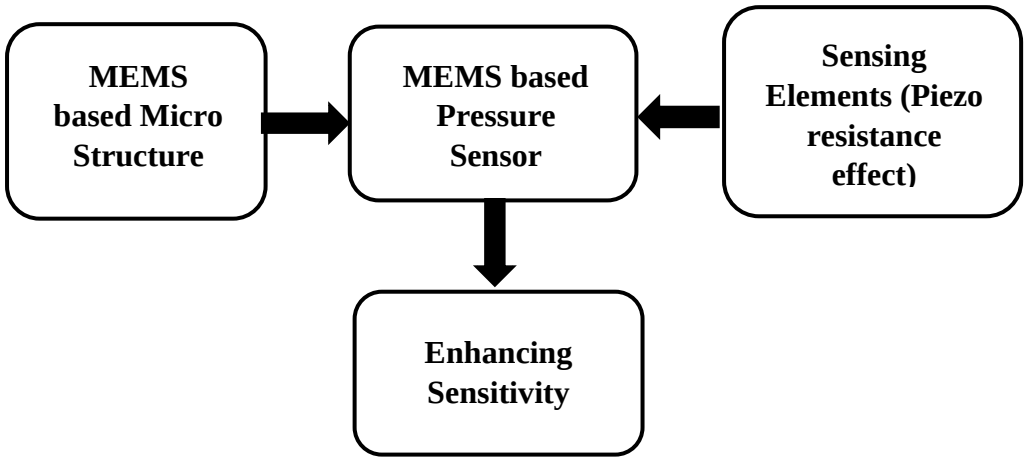

Figure 8.1 b: Design concept of MEMS based piezoresistive pressure sensor

Commonly, the thin elastic diaphragm and piezo-resistive sensing elements are the most important elements of a piezo-resistive pressure sensor. Hence, the designed pressure sensor comprised a diaphragm fixed around its perimeter and the sensing elements placed in a Wheatstone bridge circuit connection with p-type piezo-resistive element. When applying constant pressure on diaphragm back side, the diaphragm got deformed due to the variation of resistance in piezo-resistors. Hence the voltage variations and the sensitivity enhancement were obtained owing to the variation in resistance.

8.2 Available kinds of Diaphragms for Pressure Sensors

The design of pressure sensors mainly involves the geometrical considerations of membranes for better sensitivity enhancement. Flat type diaphragms and bossed or sculptured type diaphragms are mainly used in pressure sensors in various kinds of applications [64]. In case of low pressure like full scale of 500 Pa pressure monitoring applications, flat type diaphragms are not much favorable due to low sensitivity. In this sense, special kinds like sculptured diaphragms are very useful to get high sensitivity and linearity [64]. The Figure 8.2 a, Figure 8.2 b and Figure 8.2 c illustrate the circular flat type diaphragm, square flat type diaphragm and sculptured type diaphragms respectively.

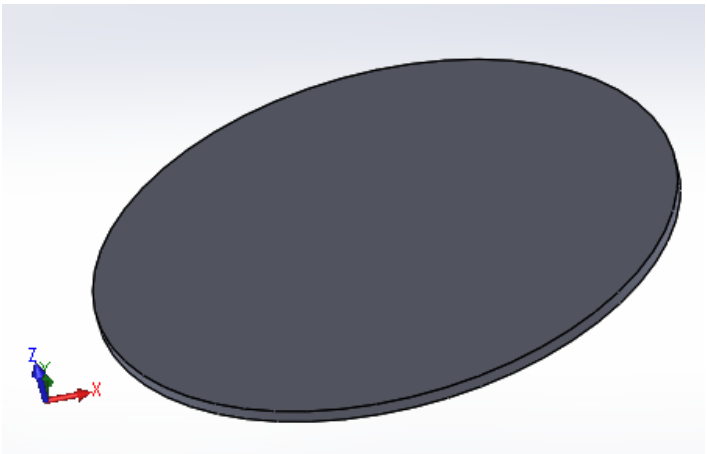

Figure 8.2 a: Circular flat type diaphragm

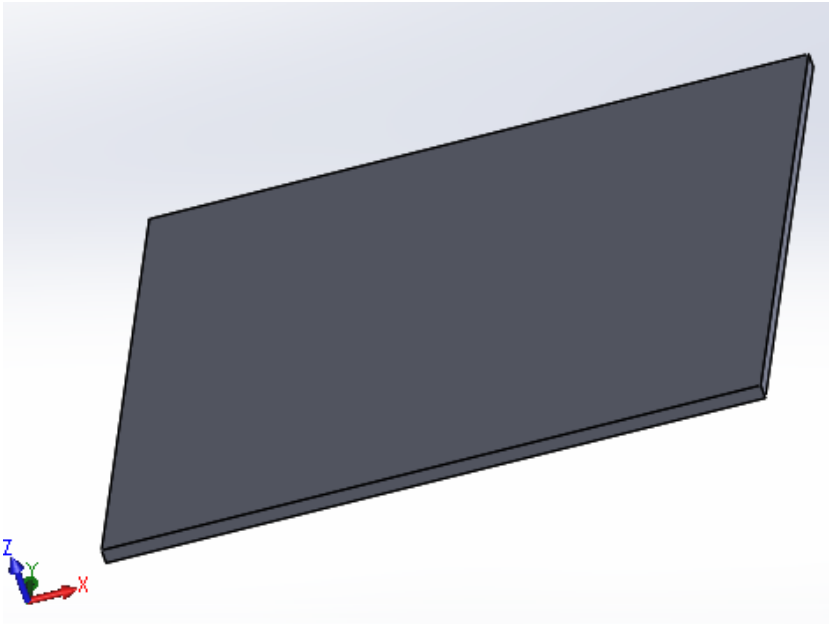

Figure 8.2 b: Square flat type diaphragm

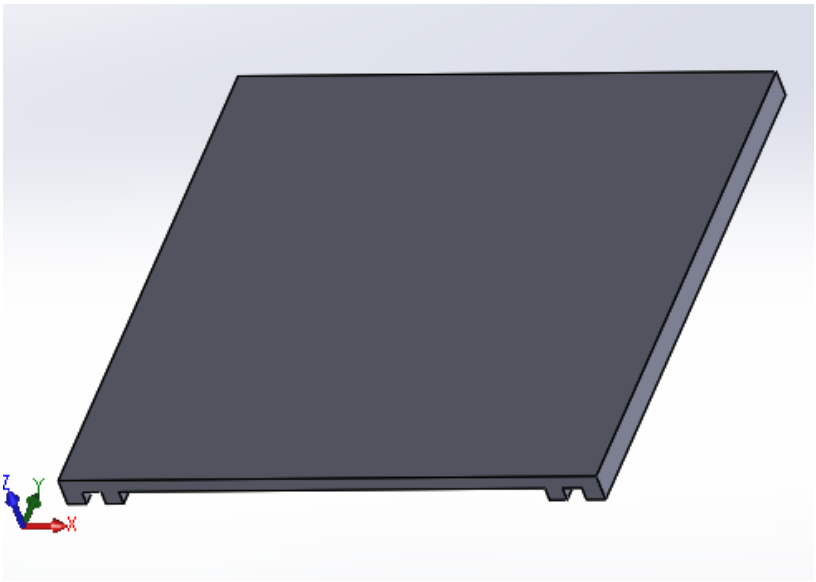

Figure 8.2 c: Sculptured type diaphragm

8.3 Thin Plate Deflection Theory

When applying a constant pressure "*p*" on a thin membrane, the thin plate deflection theory is defined in the following manner for three kinds of diaphragms namely, square type, circular type, rectangular type [104][105][106][107]:

8.3.1 Square type diaphragm

Consider the **s**quare diaphragm of side length "*a*" and the thickness of "*t*" as shown in Figure 8.3.1 fixed around its all four edges,

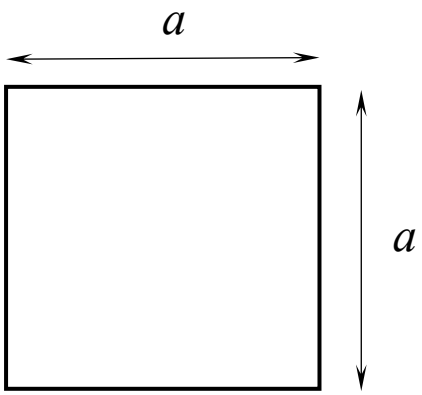

Figure 8.3.1: Square type diaphragm

The maximum deflection occurs at the center of the plate and it is expressed as:

$$W_{\max} = -\frac{0.0138pa^4}{Et^3} \qquad \text{(8.3.1 a)}$$

The maximum stress at the center of each edge and expressed as:

$$\sigma_{\max} = \frac{0.308pa^2}{t^2} \qquad \text{(8.3.1 b)}$$

Where, *t* –Plate thickness, *E* - Young's Modulus and *p* - Pressure loading respectively.

8.3.2 Circular type diaphragm

By considering thin circular diaphragm of radius "*r*" and thickness of "*t*" as shown in Figure 8.3.2 fixed around its perimeter [107]:

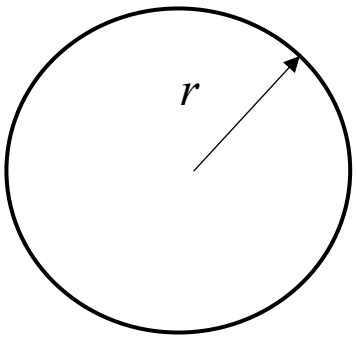

Figure 8.3.2: Circular type diaphragm

The maximum stresses along tangential and radial directions at the edge are described as:

$$(\sigma_{rr})_{\max} = \frac{3W}{4\pi t^2} \tag{8.3.2 a}$$

$$(\sigma_{\theta\theta})_{\max} = \frac{3\upsilon W}{4\pi t^2} \tag{8.3.2 b}$$

In addition, the maximum center deflection is expressed as:

$$W_{\max} = -\frac{3W(m^2-1)r^2}{16\pi E m^2 t^3} \tag{8.3.2 c}$$

Where, t - Thickness of the plate, E - Young's Modulus, υ - Poisons ratio

$m = 1/\upsilon$, $W = (\pi r^2)p$

8.3.3 Rectangular type diaphragm

The thin rectangular diaphragm with side lengths "a" and "b" ($a > b$) and thickness "t" shown in Figure 8.3.3 fixed around it's all edges,

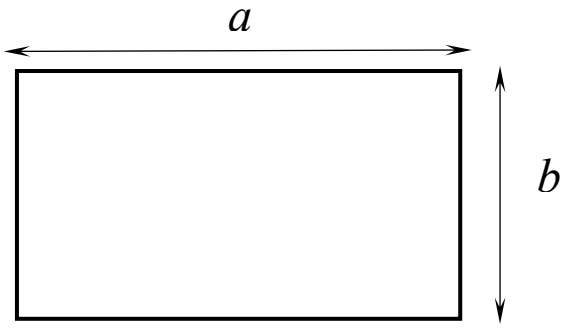

Figure 8.3.3: Rectangular type diaphragm

The supreme stress and deflection at the center of the lengthier side and at centroid are expressed as [104] [106],

$$(\sigma_{yy})_{\max} = \beta \frac{pb^2}{t^2} \tag{8.3.3 a}$$

$$W_{\max} = -\alpha \frac{pb^4}{Et^2} \tag{8.3.3 b}$$

Where, $W = (\pi r^2)p$, υ = poisons ratio, E = Young' modulus and $m = 1/\upsilon$.

Here the negative sign denotes the downward deflection and the α and β are determined from Table 8.3.3.

According to the thin plate deflection theory, the supreme deflection of diaphragm should be less than 20% of the diaphragm thickness. Also the diaphragm thickness should not go beyond 10% of the diaphragm length [3][108].

Table 8.3.3: Coefficients for supreme stress and deflection in Rectangular Plate [104] [105]

a/b	1	1.2	1.4	1.6	1.8	2	∞
α	0.0138	0.0188	0.0226	0.0251	0.0267	0.0277	0.0284
β	0.3078	0.3834	0.4356	0.4680	0.4872	0.4974	0.5000

8.4 Design and simulation of microstructure

8.4.1 Design of microstructure

Since the device is designed for microfluidics, it is necessary to design the appropriate diaphragm. Though there are various shapes of diaphragms discussed in literature, three kind of diaphragms are selected as an initial stage of this study [3][109]. In this sense, the three-dimensional mesh plots are obtained for three kinds of structures such as square, circular and cross section beam types. In order to reach maximum deflection with the variation of diaphragm length/radius and thicknesses, these mesh plots are plotted by using MATLAB as shown in Figure 8.4.1 a, Figure 8.4.1 b and Figure 8.4.1 c respectively.

According to the maximum deflection occurring parameters, the required diaphragms are decided. These parameters are illustrated in Table 8.4.1. Then these solid models of the respective diaphragms are modelled using SOLIDWORKS as shown in Figure 8.4.1 d, Figure 8.4.1 e and Figure 8.4.1 f respectively.

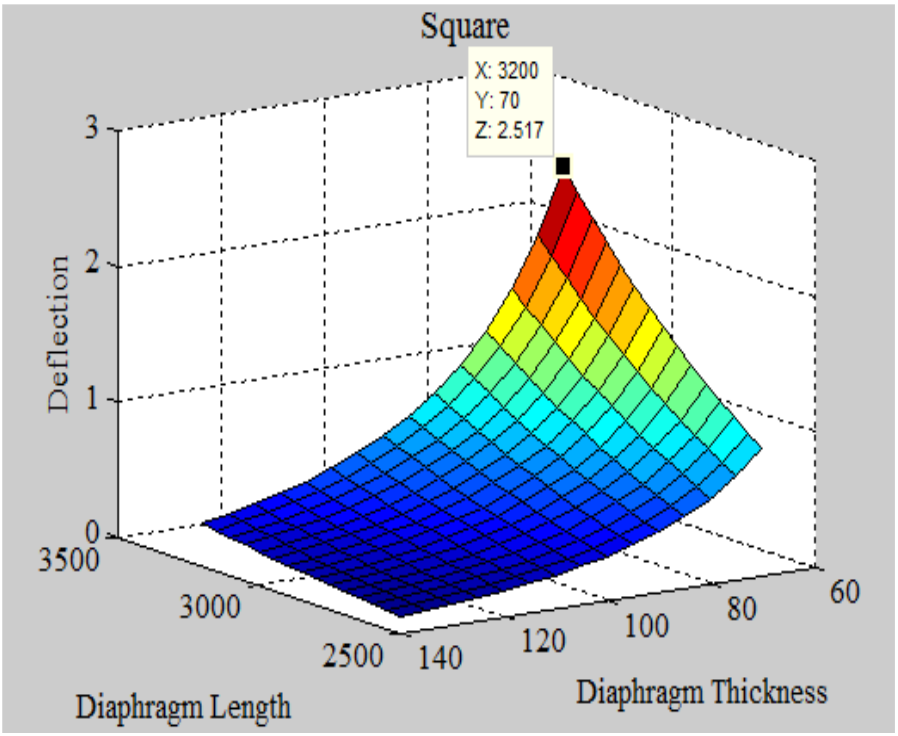

Figure 8.4.1 a: Three-dimensional mesh plot for square shaped diaphragm

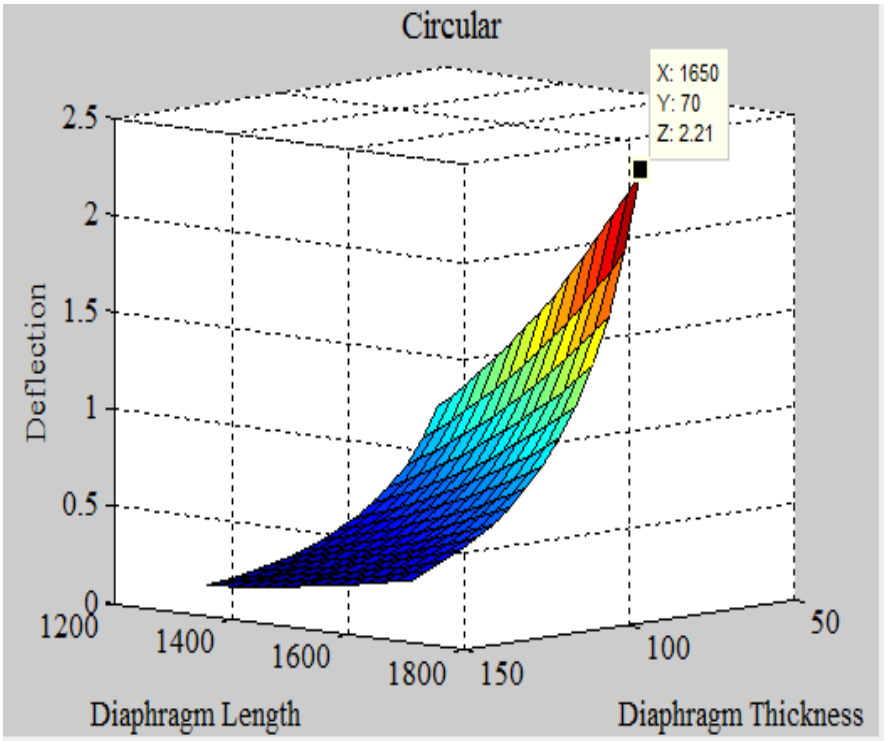

Figure 8.4.1 b: Three-dimensional mesh plot for circular shaped diaphragm

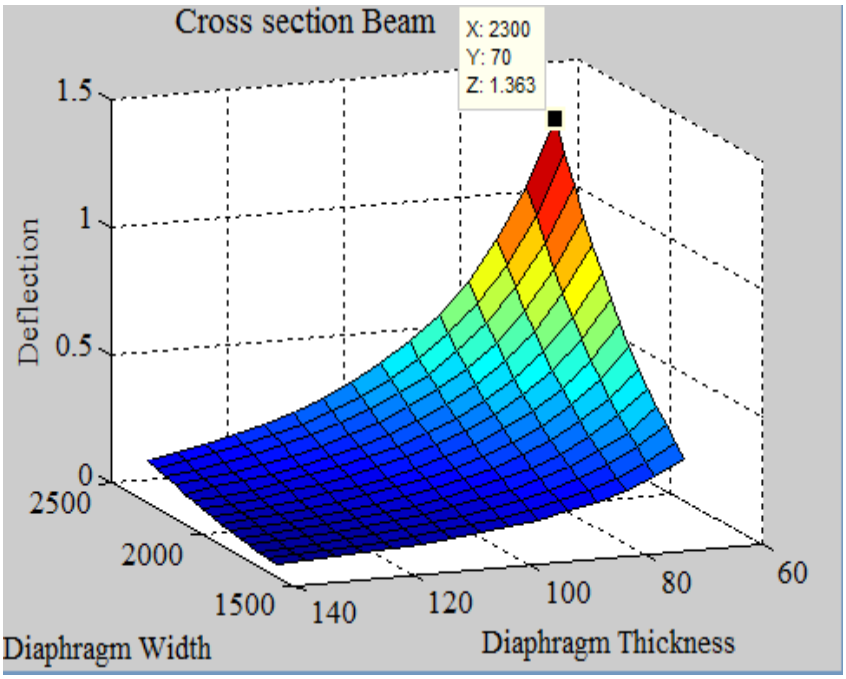

Figure 8.4.1 c: Three-dimensional mesh plot for cross sectional beam shaped diaphragm

Table 8.4.1: Proposed parameters of respective diaphragms

Diaphragm Geometry	Area/ (um x um)	Thickness/(um)
Square	3200 x 3200	70
Circular	Π x 1650^2	70
Cross Section Beam	5600 x 2300	70

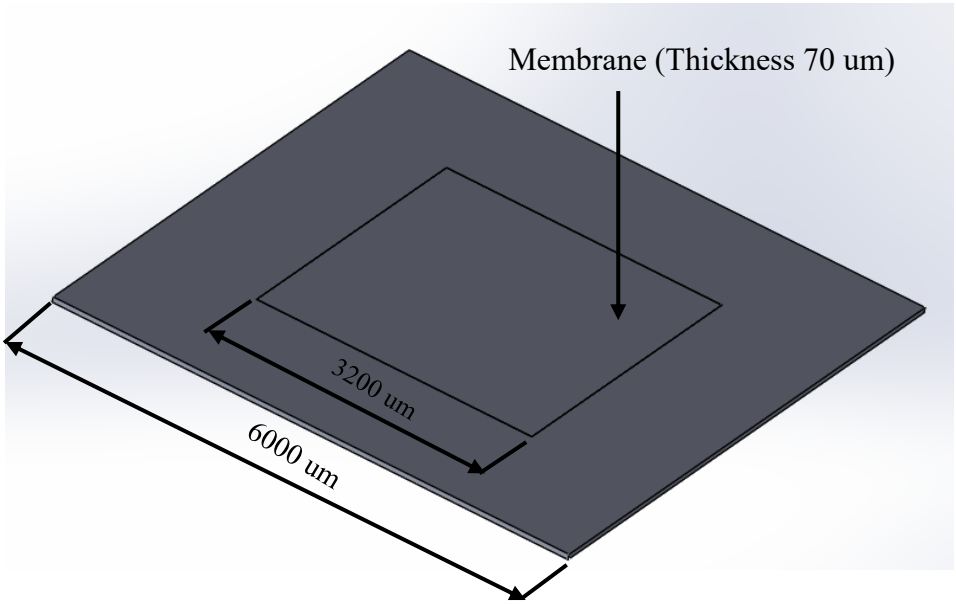

Figure 8.4.1 d: Proposed solid model for square diaphragm

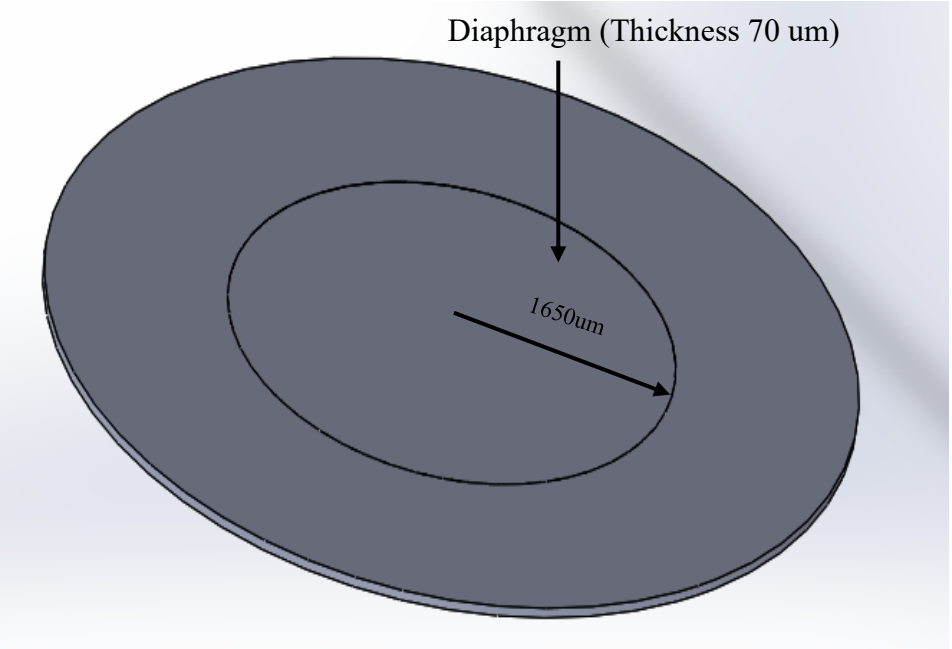

Figure 8.4.1 e: Proposed model for circular diaphragm

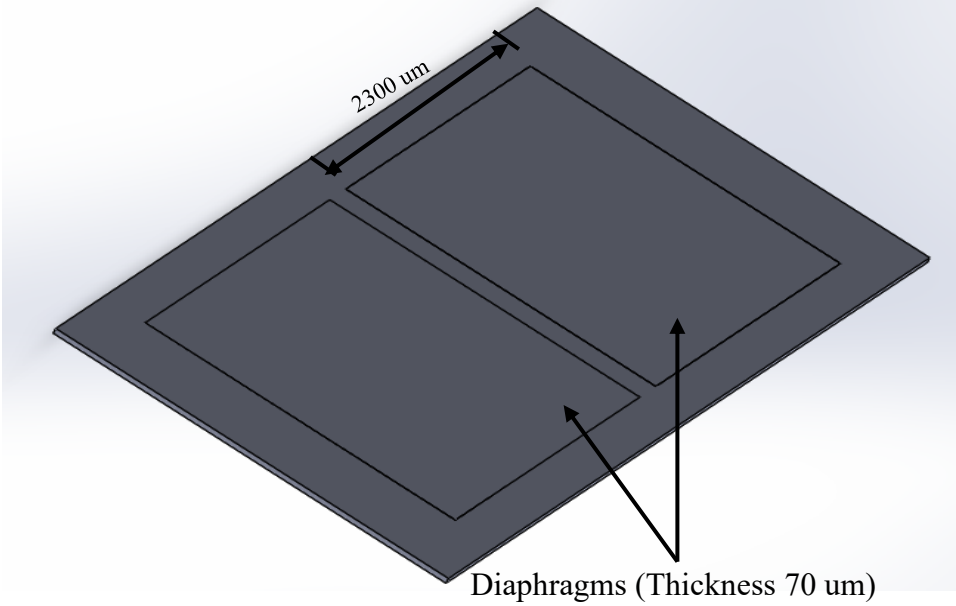

Figure 8.4.1 f: Proposed model for cross sectional beam diaphragm

8.4.2 Simulation Analysis of microstructure

In order to choose the suitable diaphragm geometry, the structural analysis is essential. Hence Finite Element Method (FEM) analyses were executed in COMSOL by defining the appropriate material properties to choose the relevant diaphragm for the respective pressure sensor. The appropriate material properties for this analysis is tabulated in Table 8.4.2. Thus, the deflection and stress over the given pressure were plotted as expressed in Figure 8.4.2 a, Figure 8.4.2 b, Figure 8.4.2 c, Figure 8.4.2 d, Figure 8.4.2 e and Figure 8.4.2 f respectively.

Table 8.4.2: Material properties of respective diaphragms

Property	Value
Young's Modulus	170 GPa
Poisson's ratio	0.28
Density	2330 kg/m^3

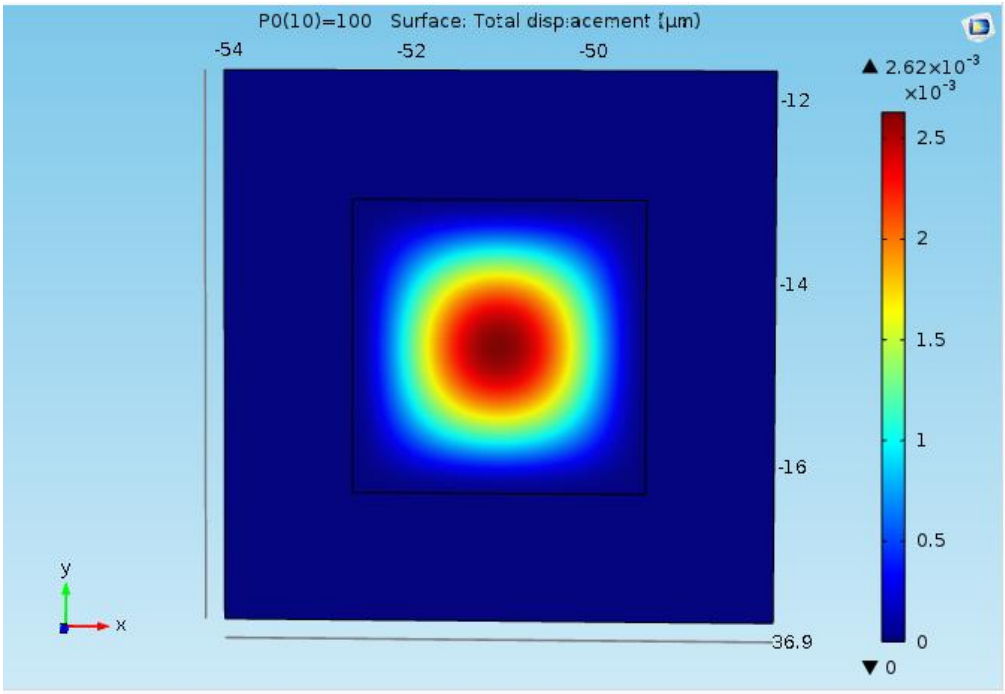

Figure 8.4.2 a: Deflection profile of square diaphragm

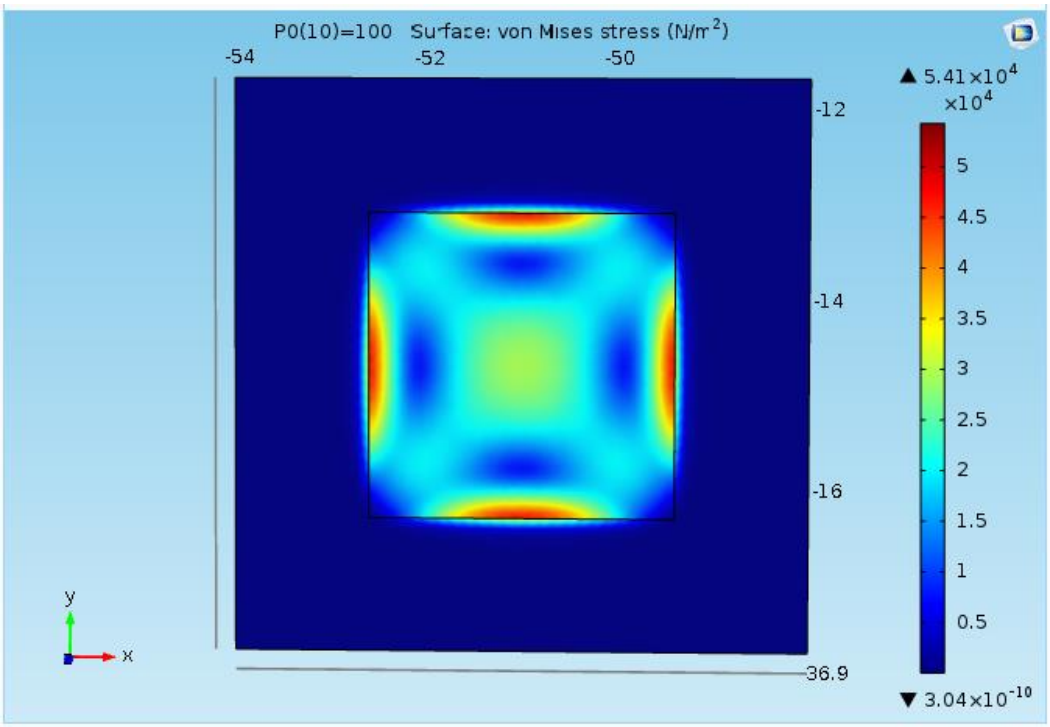

Figure 8.4.2 b: Stress profile of square diaphragm

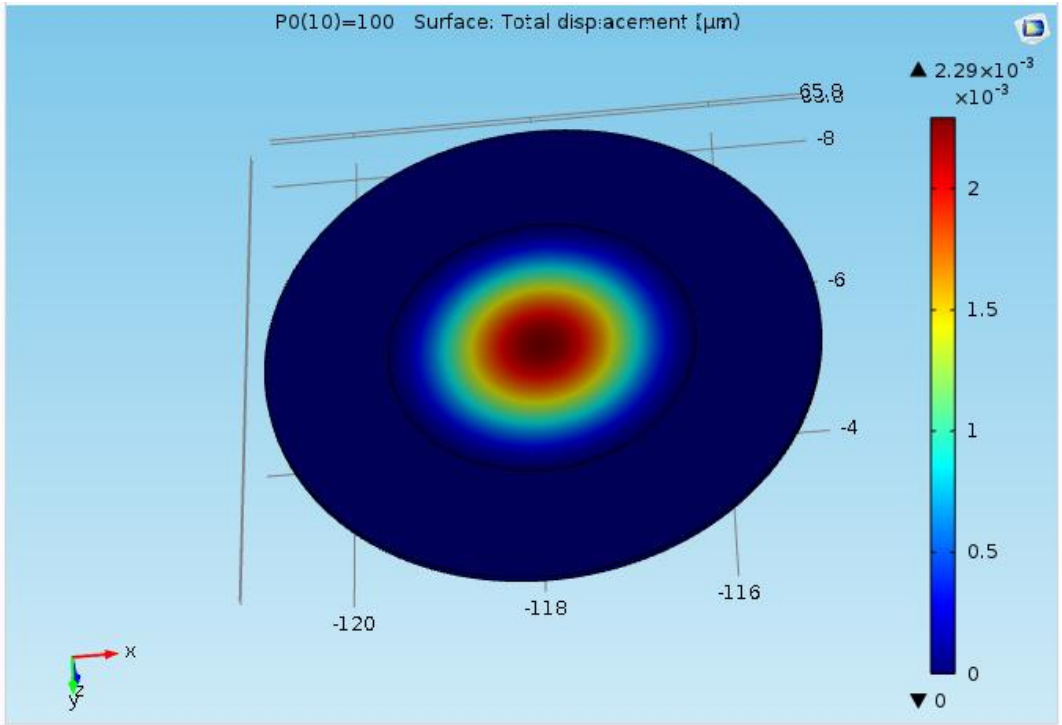

Figure 8.4.2 c: Deflection profile of circular diaphragm

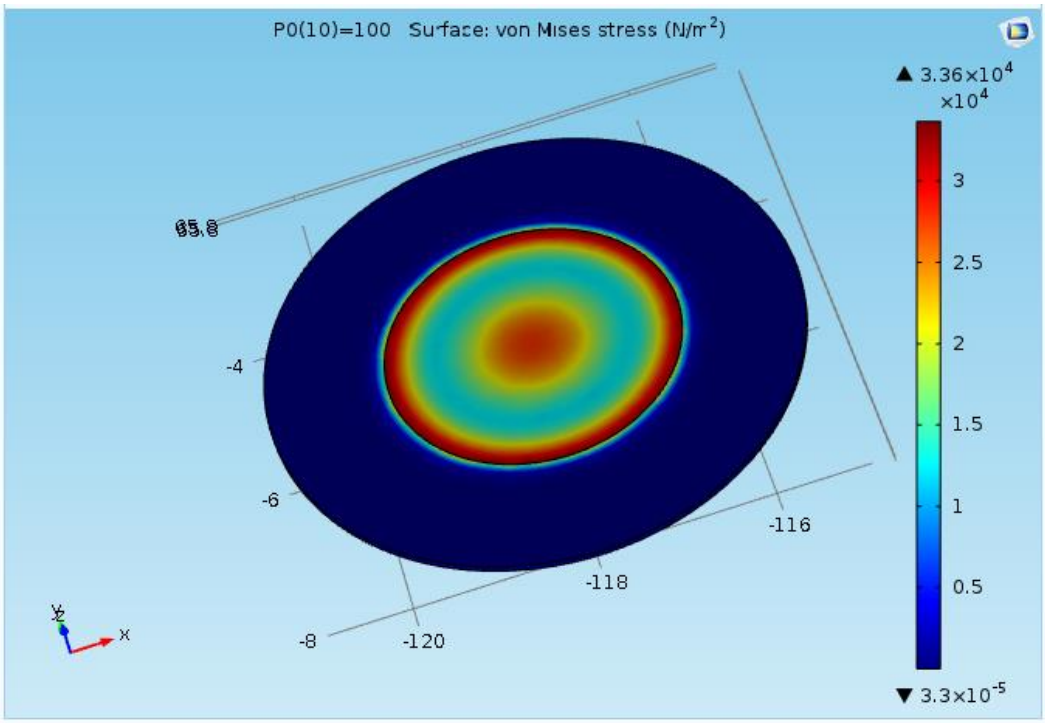

Figure 8.4.2 d: Stress profile of circular diaphragm

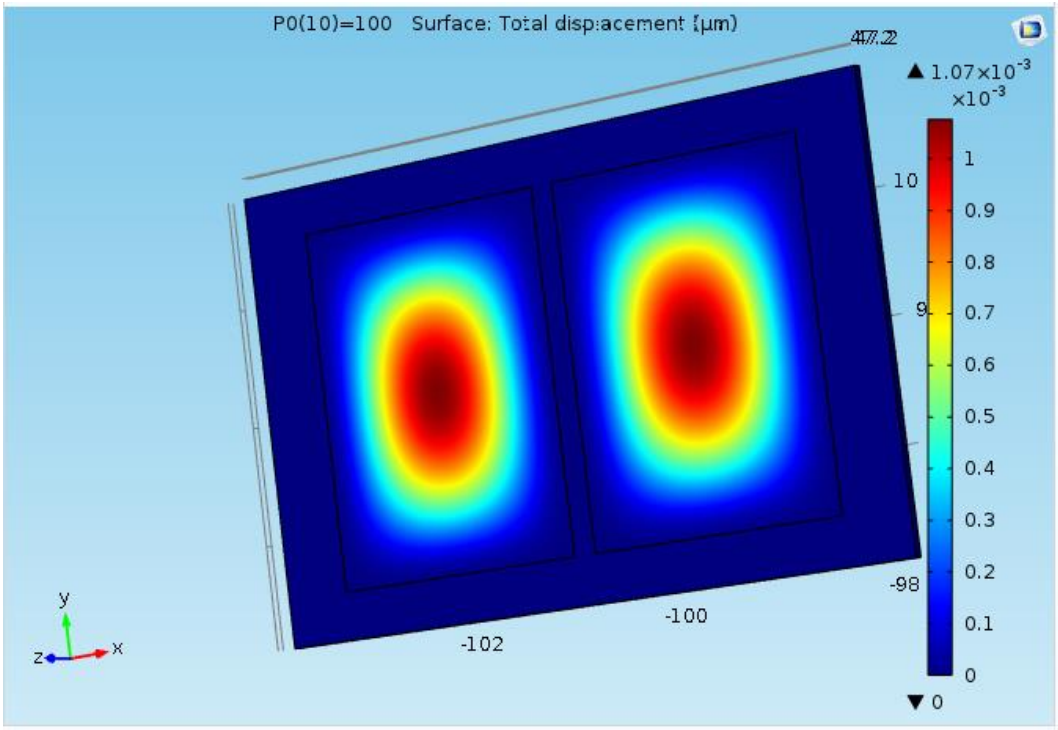

Figure 8.4.2 e: Deflection profile of cross-sectional beam diaphragm

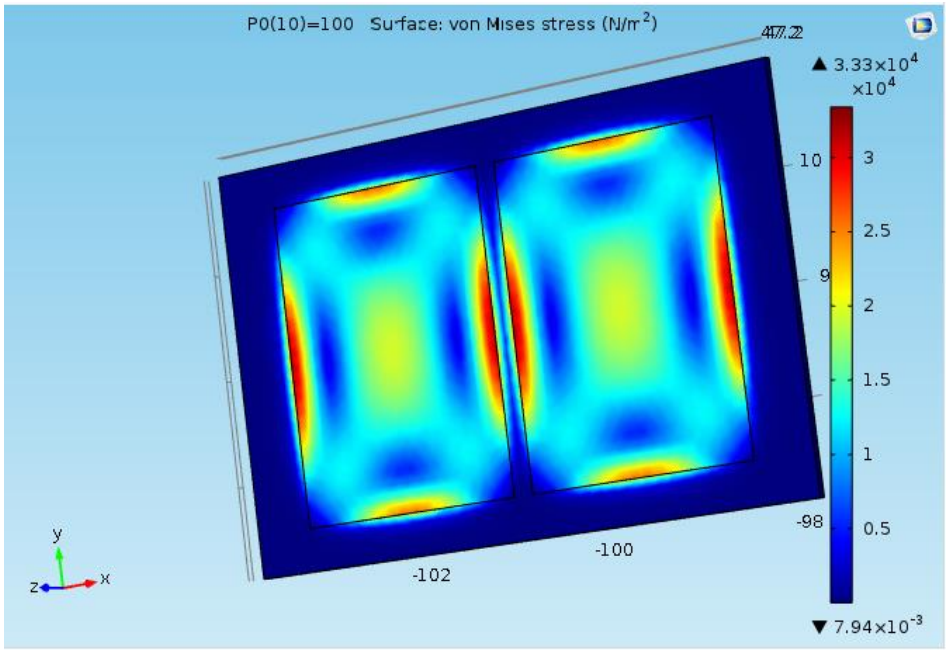

Figure 8.4.2 f: Stress profile of cross-sectional beam diaphragm

By using the structural simulation results, the variation of maximum deflection and stress for the given pressure were drawn in MATLAB as expressed in Figure 8.4.2 g and Figure 8.4.2 h accordingly.

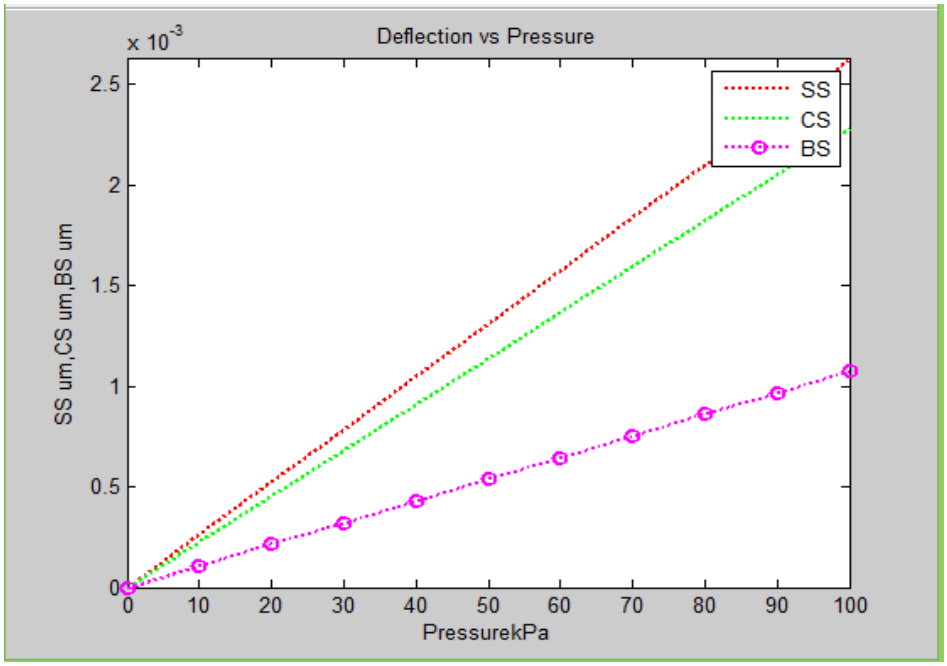

Figure 8.4.2 g: Deflection variation with pressure

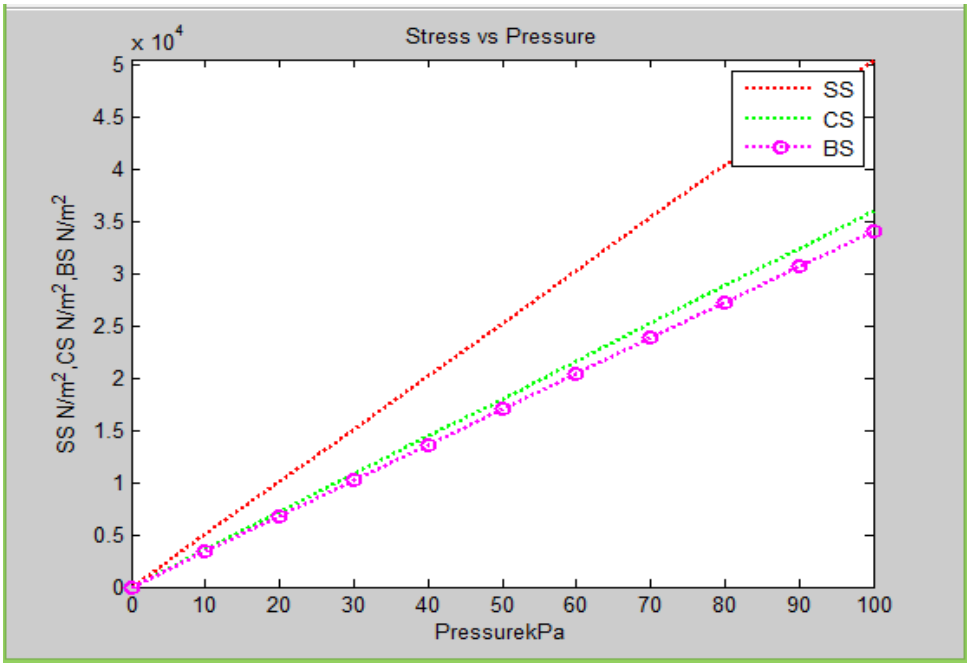

Figure 8.4.2 h: Stress variation with pressure

Even though the maximum stress must be less than 70 MPa (plastic yield strength of Silicon), all kinds of diaphragms fulfilled the above phenomenon [104]. As per plots obtained, all diaphragms satisfied the thin plate deflection principles. But the square membrane provided the maximum deflection and stress. Hence the respective design is developed with square membrane and the modal analysis was carried out by using Ansys to identify the dynamic properties of this square membrane under the frequency domain. The outcome of this analysis at different mode frequencies are plotted as illustrated in Figure 8.4.2 i, Figure 8.4.2 j, Figure 8.4.2 k and Figure 8.4.2 l. This analysis resulted that the supreme displacement occurs at the first mode frequency.

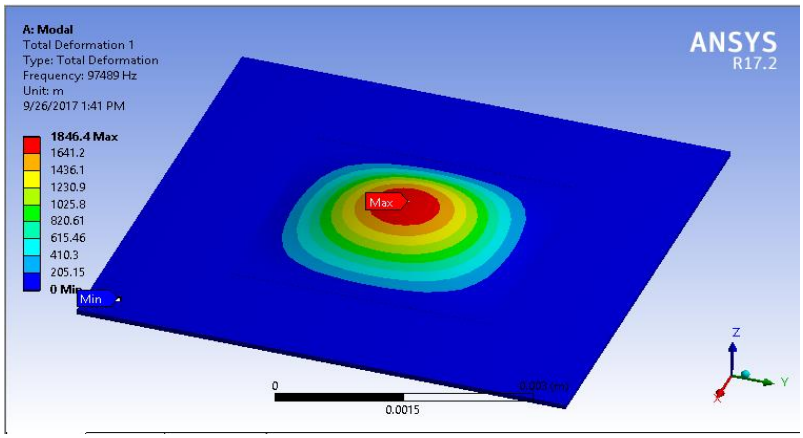

Figure 8.4.2 i: First Mode of Frequency of Modal Analysis

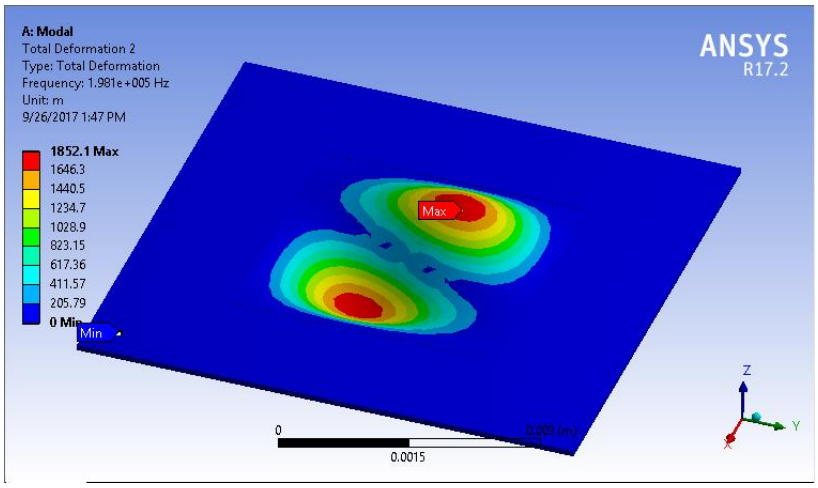

Figure 8.4.2 j: Second Mode of Frequency of Modal Analysis

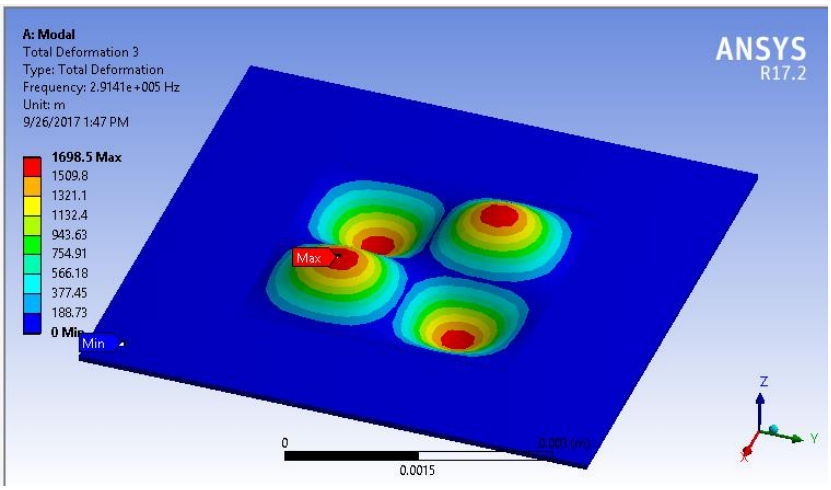

Figure 8.4.2 k: Third Mode of Frequency of Modal Analysis

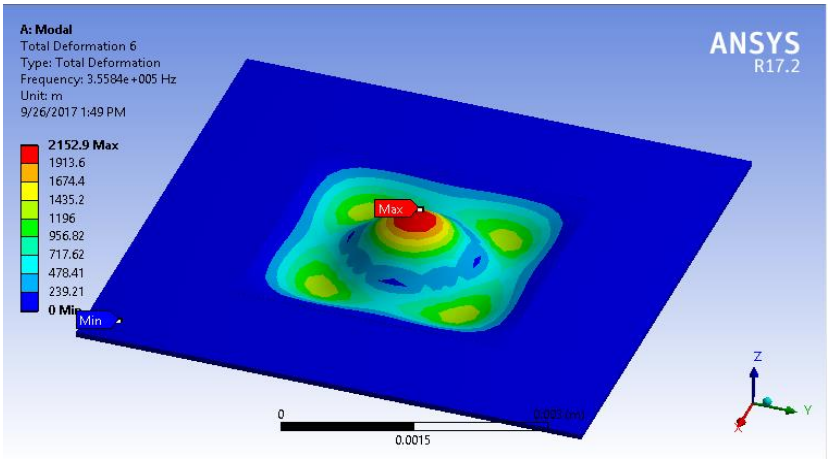

Figure 8.4.2 l: Sixth Mode of Frequency of Modal Analysis

8.5 Design and simulation analysis of sensing elements

Comparing with other sensing features discussed in literature, Piezo-resistive pressure sensors are very much useful in microfluidic requirements. Hence the operation principle of a piezo-resistive pressure sensor is expressed in Figure 8.5 a. In this case, the two terminal piezo-resistive sensing elements are selected due to the diverse properties such as linearity, high sensitivity, less stress development.

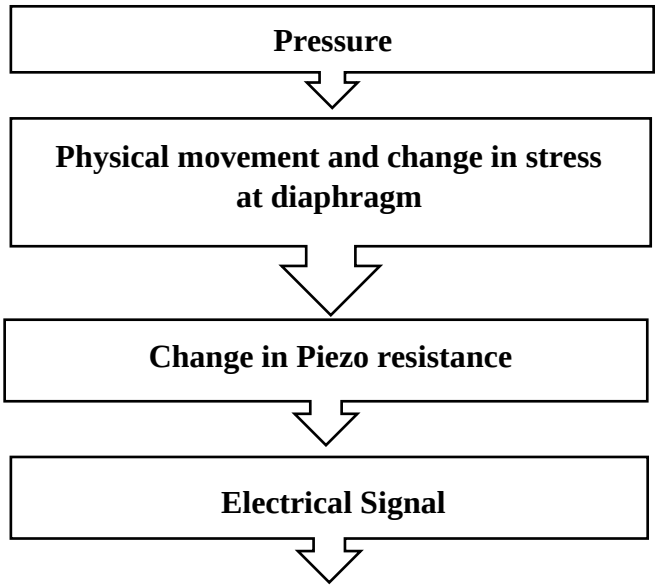

Figure 8.5 a: Operation principles of piezoresistive pressure sensor

The change in resistance of a stressed piezo-resistive material is described by [41] [62][64][108],

$$\frac{\Delta R}{R} = \frac{\Delta l}{l} - \frac{\Delta A}{A} + \frac{\Delta \rho}{\rho} \tag{8.5 a}$$

The geometrical deformations of length and cross section of resistors are described by the first two expressions of the aforementioned equation and these are insignificant for a stressed piezoresistors compared with the third expression. In addition, the resistivity change due to developed stress is defined by the piezoresistive coefficient π and the fractional change in resistivity per unit stress is also defined as follows [41][108][109].

$$\pi = \frac{\Delta \rho / \rho}{\sigma} \tag{8.5 b}$$

$$\frac{\Delta R}{R} = \pi_l \sigma_l + \pi_t \sigma_t \tag{8.5 c}$$

Where, ρ, σ, σ_l and σ_t are resistivity, stress, stress along the longitudinal direction as well as in transverse direction of the resistor respectively. π_l and π_t are the longitudinal and transverse piezoresistive coefficient termed as [64] [110]:

$$\pi_l = 1/2(\pi_{11} + \pi_{12} + \pi_{44}) \tag{8.5 d}$$

$$\pi_t = 1/2(\pi_{11} + \pi_{12} - \pi_{44}) \tag{8.5 e}$$

According to the respective design, p-type piezoresistive elements were placed on top of the n-type Si wafer. The typical piezoresistive coefficients for lightly doped Si are tabulated in Table 8.5 a.

Table 8.5 a: Distinctive parameters for Piezoresistive Coefficients of Lightly doped Si [60] [62] [64]

Doping Type	π_{11} ($10^{-11}Pa^{-1}$)	π_{12} ($10^{-11}Pa^{-1}$)	π_{44} ($10^{-11}Pa^{-1}$)
n-type	-102.2	53.4	-13.6
p-type	6.6	-1.1	138.1

Also placing piezo- resistive elements at highly stressed areas are desirable for obtaining virtuous output signal of the full Wheatstone bridge circuit. Thus, the plan view for the arrangement of piezoresistive elements and schematic diagram of

Wheatstone bridge are expressed in Figure 8.5 b and Figure 8.5 c respectively. Hence the variation in voltage and resistance are described by Equation (8.5 f) [109].

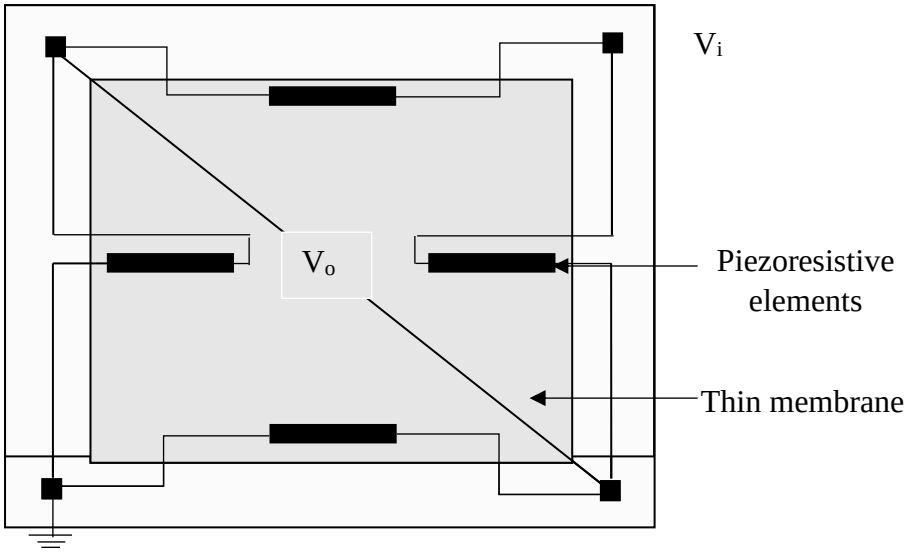

Figure 8.5 b: Arrangement of piezoresistive elements - Plan view

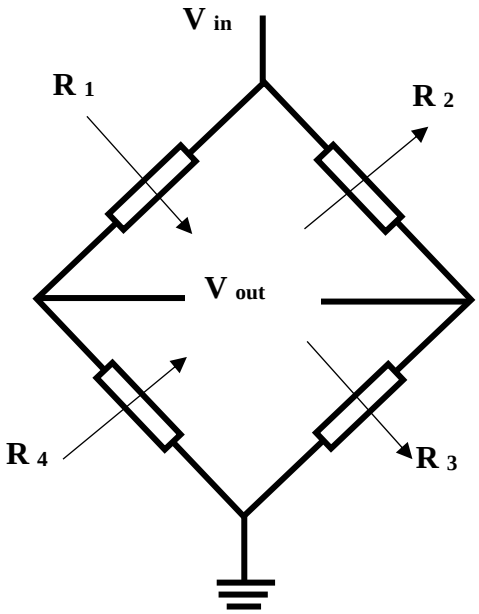

Figure 8.5 c: Wheatstone bridge circuit illustration [61]

$$\frac{\Delta R}{R} = \frac{V_{out}}{V_{in}} = \frac{1}{4}\left(\frac{\Delta R_1}{R_1} - \frac{\Delta R_2}{R_2} + \frac{\Delta R_3}{R_3} - \frac{\Delta R_4}{R_4} \right) \qquad (8.5\text{ f})$$

In addition, the resistor's value varies slightly due to piezoresistive effect and hence the variation in resistance with respect to the original resistor will be more obvious than with greater valued resistors. Therefore, the resistors are designed with thin sheets of materials as per sheet resistivity concept.

Theoretically analyzing piezo-resistance effect is necessary before moving to the fabrication stage. But resistive changes are anisotropic and this fluctuates with the longitudinal and transverse stresses, theoretical analysis is a challenge. Then the analysis was done by using coupled Field Analysis in COMSOL Multiphysics. As an initial step, the model is developed with the tabulated design parameters in Table 8.5 b. Then the Structural Mechanics and Piezo-resistivity physics are identified and FEM based piezoresistive-structural couple field analysis was performed. In this analysis piezoresistive physics for domain currents is selected and the required properties such as structural, electrical and piezoresistive of the designed model are well-defined. In addition, the entire diaphragm is designed by using the lightly doped n-type silicon and the piezoresistors are designed by using p type silicon.

Table 8.5 b: Proposed designed Factors of Piezo-resistive Pressure Sensor

Chip (μm x μm x μm)	6000x6000x70
Membrane (μm x μm x μm)	3200x3200x70
Piezoresistors (μm x μm x μm)	200x10x1
Sheet Resistivity (Ω/Sq)	100
Contact pads size(μm x μm x μm)	100x100x1
Applied load (kPa)	100
Supply voltage (V)	3

Then the electrical properties are determined by defining terminal and ground boundaries. At last, the model is meshed and simulated parametrically for the pressure range of 0 to100 kPa. The designed and meshed model are illustrated in Figure 8.5 d and Figure 8.5 e respectively. The displacement profile and the stress contours are also obtained for a specific pressure value and expressed in Figure 8.5 f and Figure 8.5 g respectively.

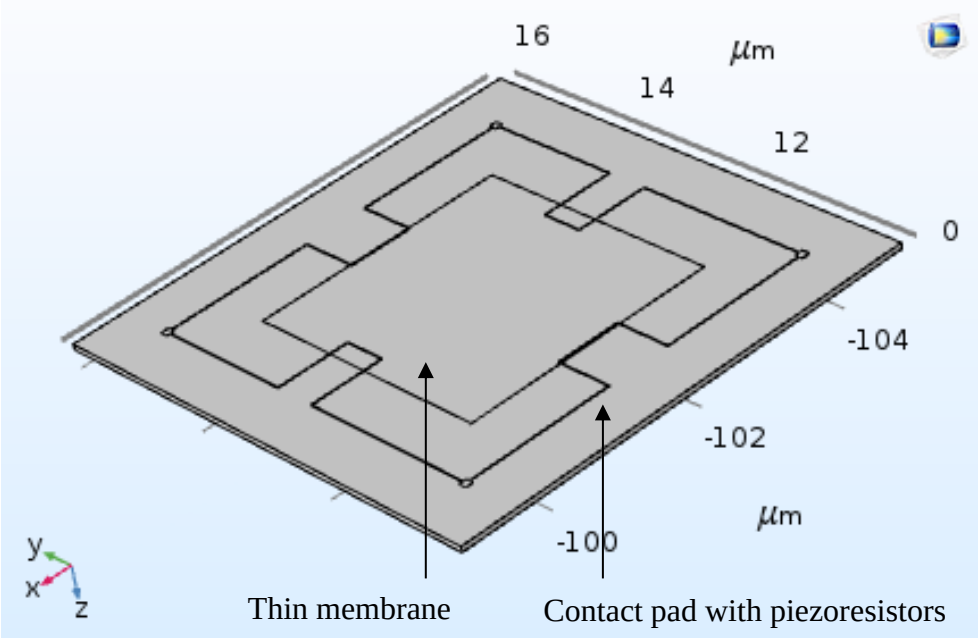

Figure 8.5 d: Piezoresistive pressure sensor- Designed Model

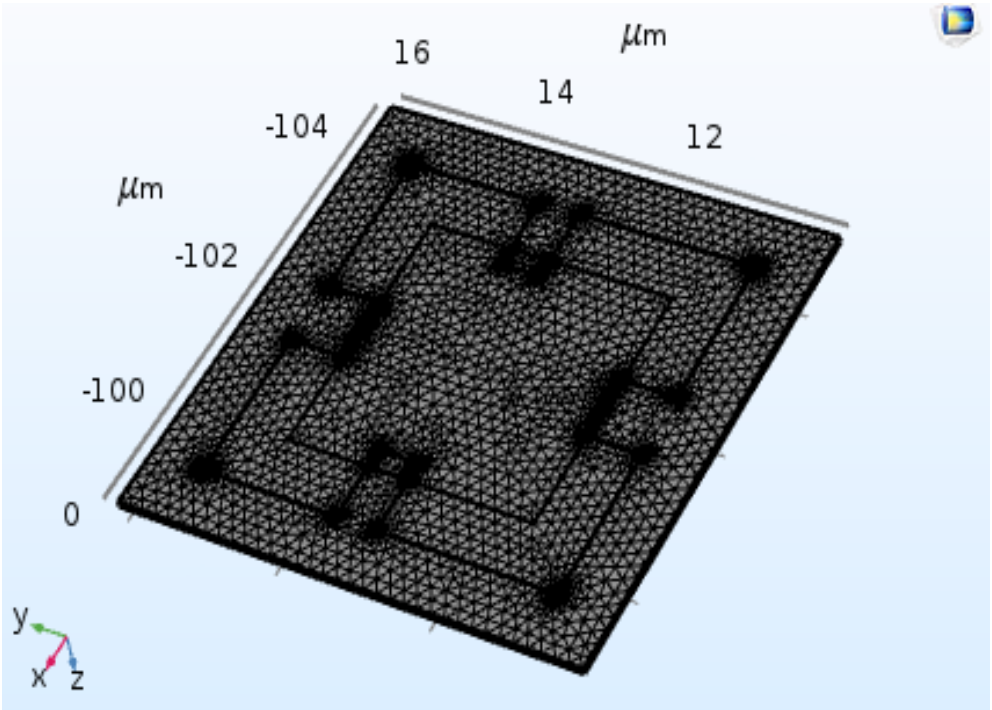

Figure 8.5 e: Piezoresistive pressure sensor – Meshed model

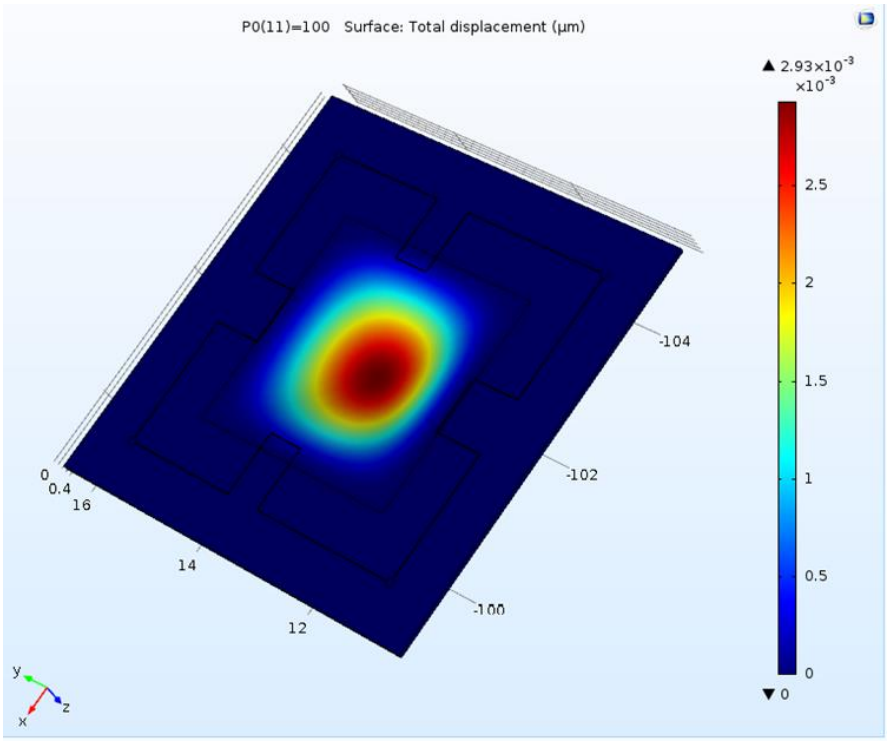

Figure 8.5 f: Displacement profile of piezo-resistive pressure sensor

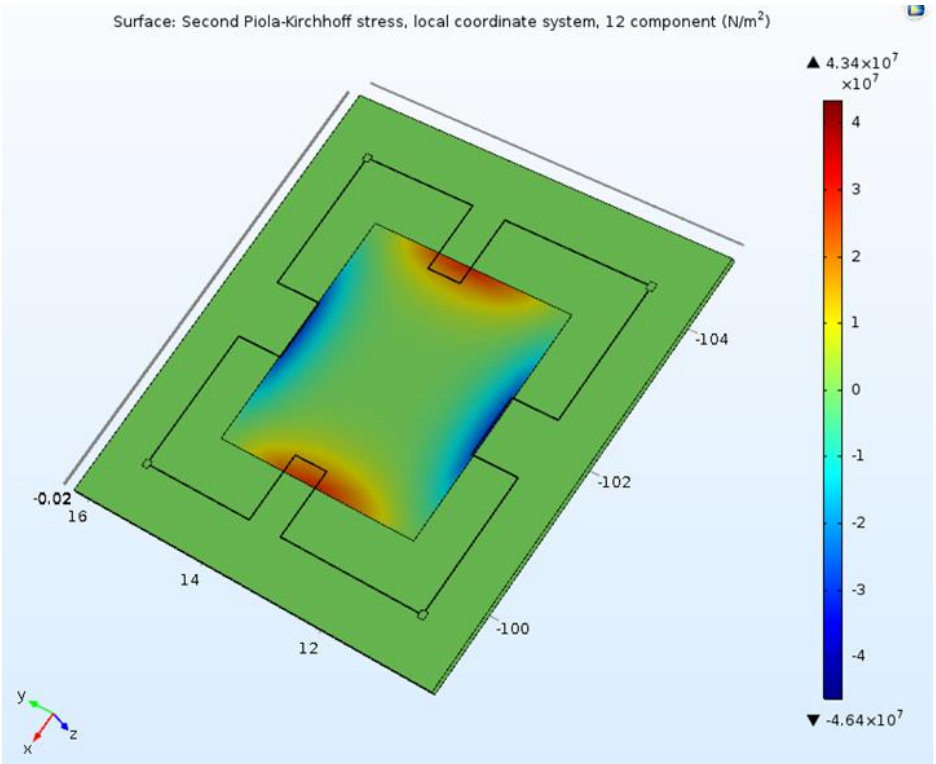

Figure 8.5 g: Stress profle of piezo-resistive pressure sensor

8.6 Sensitivity Enhancement

Sensitivity is an essential feature during the design of a piezoresistive pressure sensor. The sensitivity mainly depends on the change in voltage and the resistance with the variation in applied pressure. Hence it is termed as follows [41] [60] [64] [108],

$$S = \frac{\Delta V_{out}}{V_{in}} \frac{1}{\Delta P} = \frac{\Delta R}{\Delta P} \frac{1}{R} \qquad (8.6\ a)$$

Where, S- Sensitivity, ΔV_{out} –Output voltage, ΔP- Change in pressure and ΔR- Change in resistance respectively. Though the output voltage is an essential factor to compute the sensitivity, it is determined from the simulation results. Hence the sensitivity of the proposed design is determined for the specified pressure range. The variation of output voltage and sensitivity are tabulated as expressed in Table 8.6 for the given pressure parameters. According to this data, the variation of sensitivity with pressure is plotted and illustrated in Figure 8.6.

Table 8.6: Variation of output voltage and sensitivity with pressure

Pressure (kPa)	Output voltage (mV)	Sensitivity (mV/V)/(kPa)
0	39.214	-
10	39.172	1.3057
20	39.129	1.3043
30	39.087	1.3029
40	39.044	1.3015
50	39.002	1.3001
60	38.959	1.2986
70	38.916	1.2972
80	38.874	1.2958
90	38.831	1.2944
100	38.788	1.2929

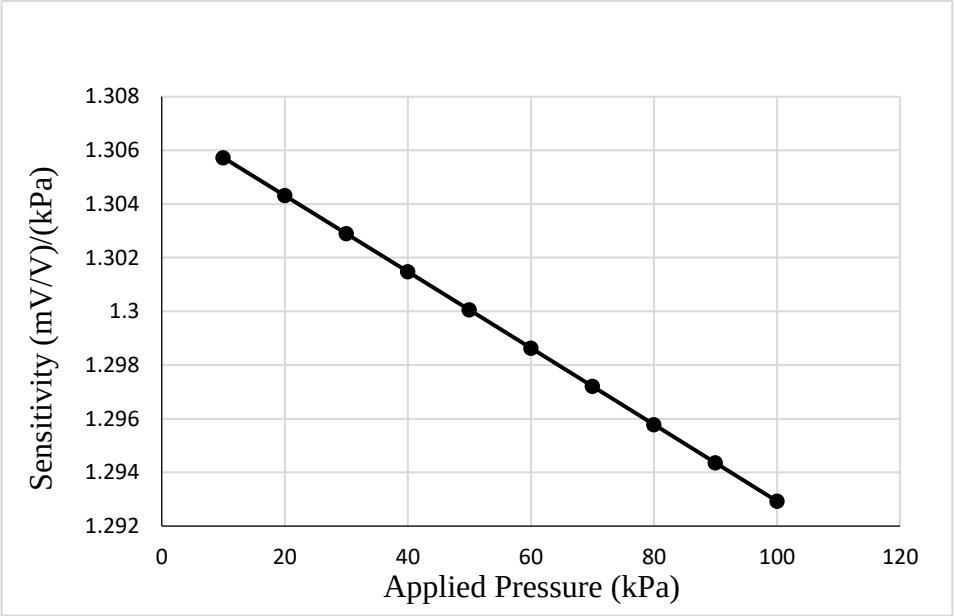

Figure 8.6: Variation of sensitivity with applied pressure

8.7 Thermo-mechanical effect in pressure sensors

Silicon based pressure sensors are widely used at different thermal environments. But the piezo-resistive coefficient and the doping concentration give measurable impacts with temperature and this leads to the change in resistance as well as the voltage output. Though change in voltage gives changes in sensitivity, considering the thermal effects on the sensitivity is necessary. Hence analyzing thermo-mechanical effects in piezo-resistive pressure sensors are very much useful.

8.7.1 Thermal effect on the Piezoresistive coefficient

In order to reach clear understanding about the variation of piezoresistive coefficient as well as the sensitivity with temperature and doping concentration, performing theoretical analysis is very much essential. Among the models developed and expressed in literature, Richter's model is the best one. Thus, the mesh plots are plotted using MATLAB according to Richter's model, for the variation of Piezoresistive coefficient with temperature and doping concentration as illustrated in Figure 8.7.1.

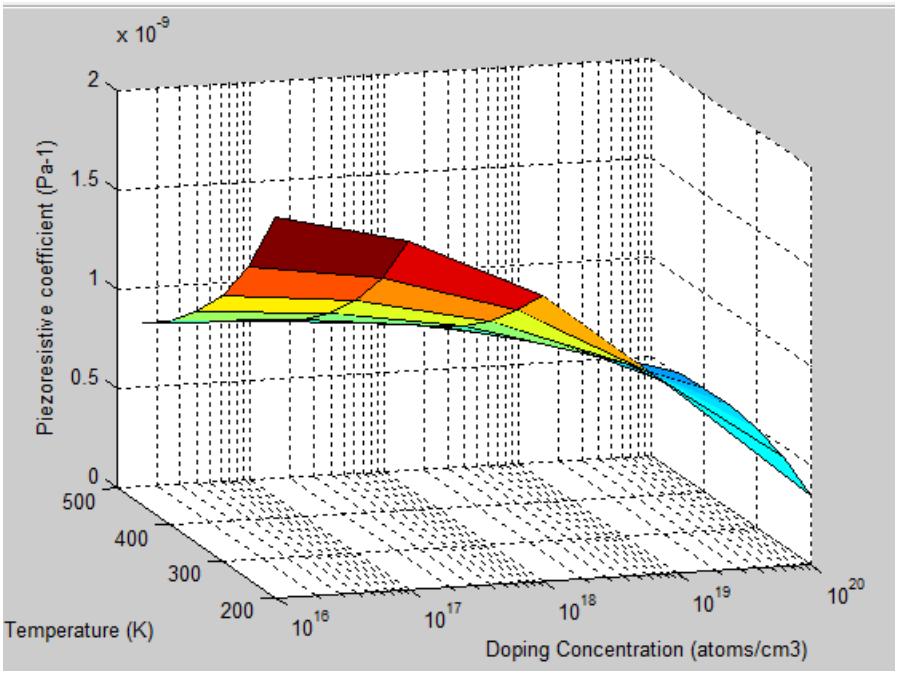

Figure 8.7.1: Variation of Piezoresistive coefficient with temperature and doping concentration

8.7.2 Thermal effect on the Sensitivity

Though the sensitivity of the pressure sensor always depends on the temperature and doping concentration, it is necessary to analyze thermal effect on the sensitivity too. When the membrane is subjected to a uniform pressure of *P*, the values of four resistances in Wheatstone bridge vary and an output voltage is developed. In addition, the tension also varies due to temperature and its law of variation with output voltage and sensitivity are expressed as [66][111] [112]

$$\frac{\Delta V}{V} = \frac{\pi_{44}(N,T)}{2} \; P\left(\frac{a}{h}\right)^2 \left(\sigma_{xx} - \sigma_{yy}\right) \qquad (8.7.2\text{ a})$$

$$S(T,N) = \frac{\pi_{44}(N,T)}{2}\left(\frac{a}{h}\right)^2 \left(\sigma_{xx} - \sigma_{yy}\right) \qquad (8.7.2\text{ b})$$

Here, π_{44} is the piezoresistive coefficient which depends on temperature and doping concentration, *a* is the diaphragm side length, h is the diaphragm thickness, σ_{xx} is the lateral stress and σ_{yy} is the transversal stress respectively.

In this sense, theoretically analyzing the sensitivity variation with temperature and doping concentration gives an overall idea to perform simulation analysis.

Hence, mesh plot for the variation of sensitivity with temperature and doping concentration is plotted by using MATLAB as expressed in Figure 8.7.2.

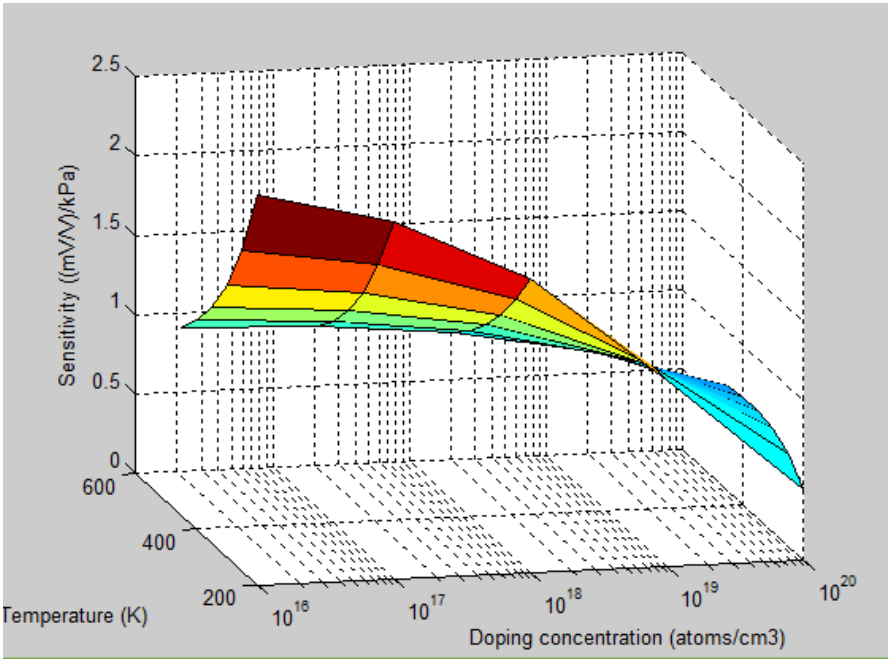

Figure 8.7.2: Variation of Sensitivity with temperature and doping concentration

8.7.3 Thermo-mechanical simulation

It is very much essential to analyze the thermo-mechanical behavior of piezoresistive pressure sensor using FEM to verify the results with theoretical analysis. Hence, Finite Element Analysis in COMSOL was used to simulate the effect of temperature and doping concentration on characteristics of the sensor output.

This analysis was carried out in COMSOL Multiphysics under Thermal stresses physics and stationery study step. In this sense, the piezoresistive pressure sensor model was meshed and simulated over the temperature ranges from 200 K to 450 K at the interval of 50 K. Based on the simulation analysis, the variation of central deflection with temperature is plotted and illustrated in Figure 8.7.3 a.

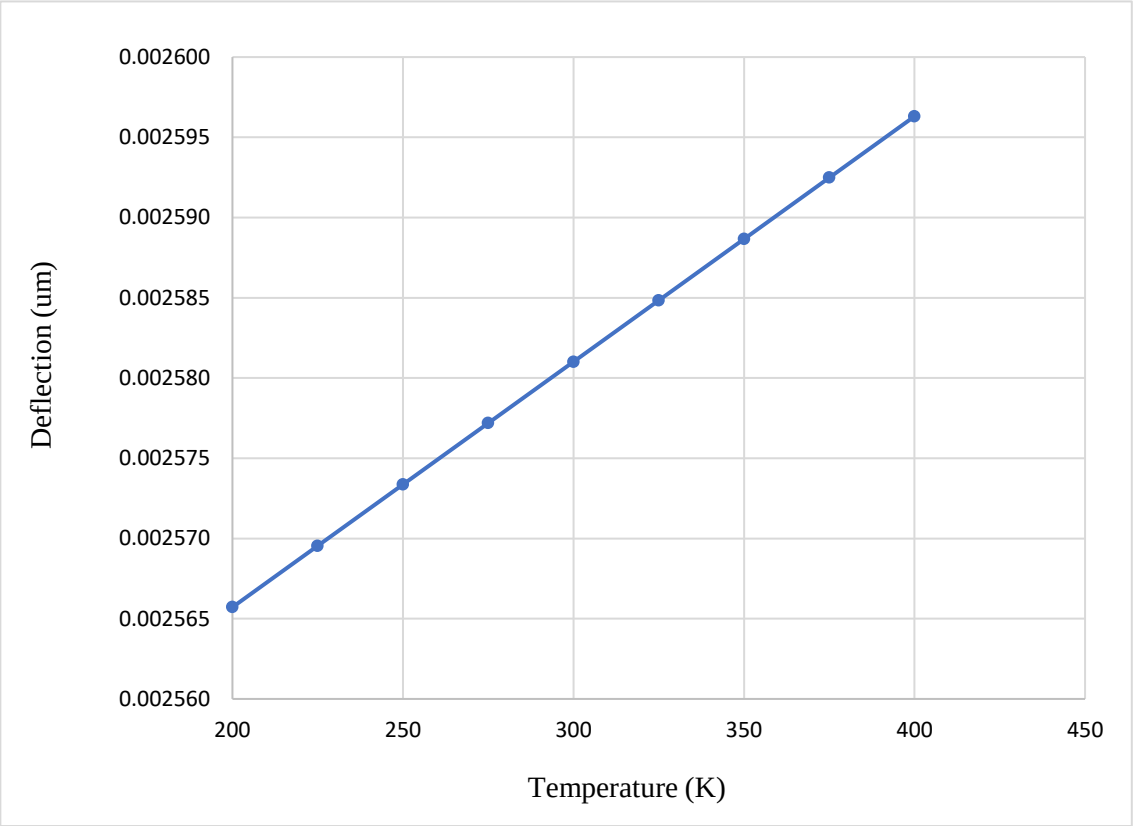

Figure 8.7.3 a: Variation of central deflection of the membrane with temperature

In order to analyze the sensitivity with temperature, stress plots are plotted and shown in Figure 8.7.3 b and Figure 8.7.3 c respectively. In addition, the variation of sensitivity with applied pressure at different temperatures with the piezoresistor doping concentration of 10^{18} [atoms/cm^3] are also obtained and shown in Figure 8.7.3 d. The variation of output voltage with doping concentration at different temperatures are obtained and illustrated in Figure 8.7.3 e. Further, the analysis was executed for the variation of temperature due to ohmic heating in a piezoresistive pressure sensor and expressed in Figure 8.7.3 f respectively.

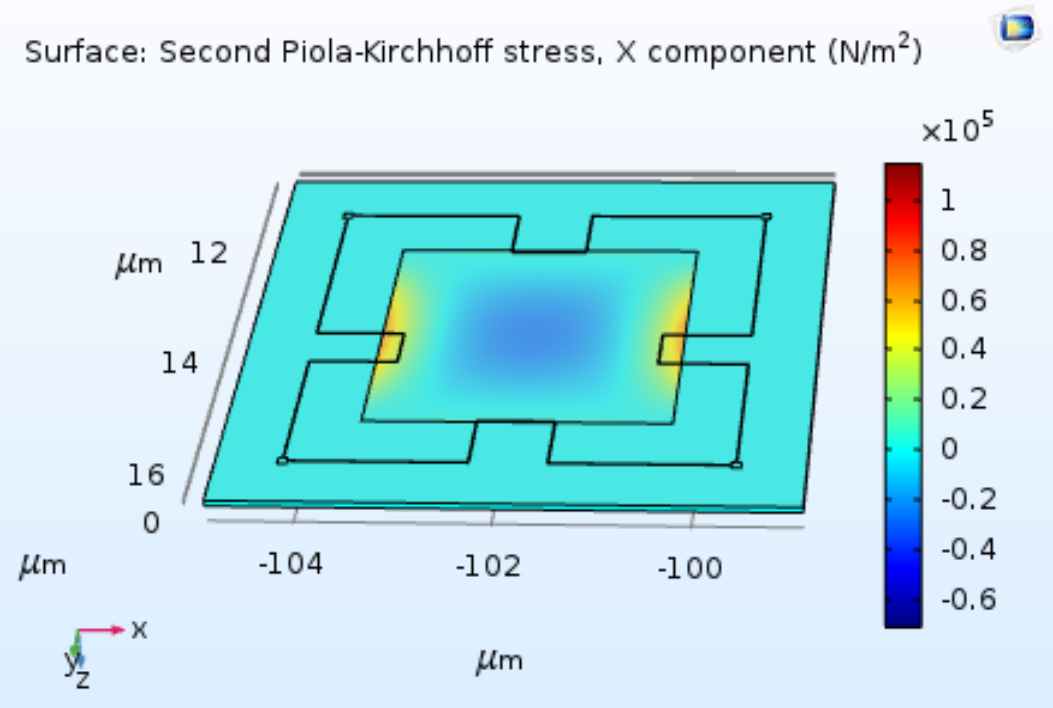

Figure 8.7.3 b: Normal stress of piezo-resistive pressure sensor at 100 kPa and 300K

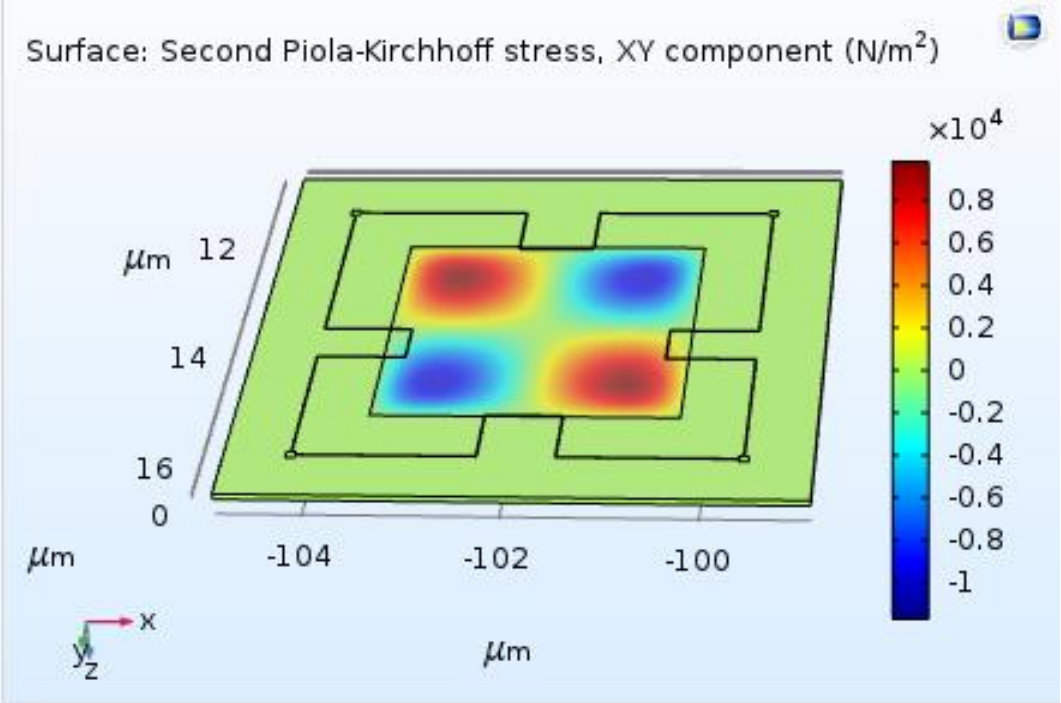

Figure 8.7.3 c: Shear stress of piezo-resistive pressure sensor
at 100 kPa and 300K

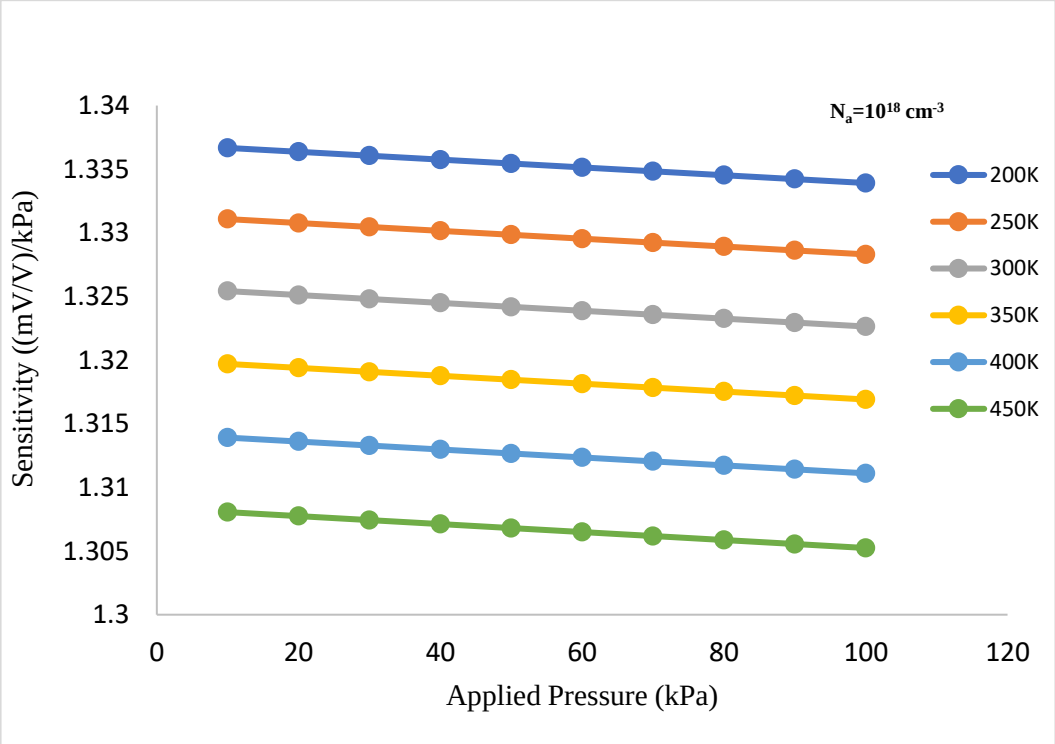

Figure 8.7.3 d: Variation of sensitivity with pressure at different temperatures

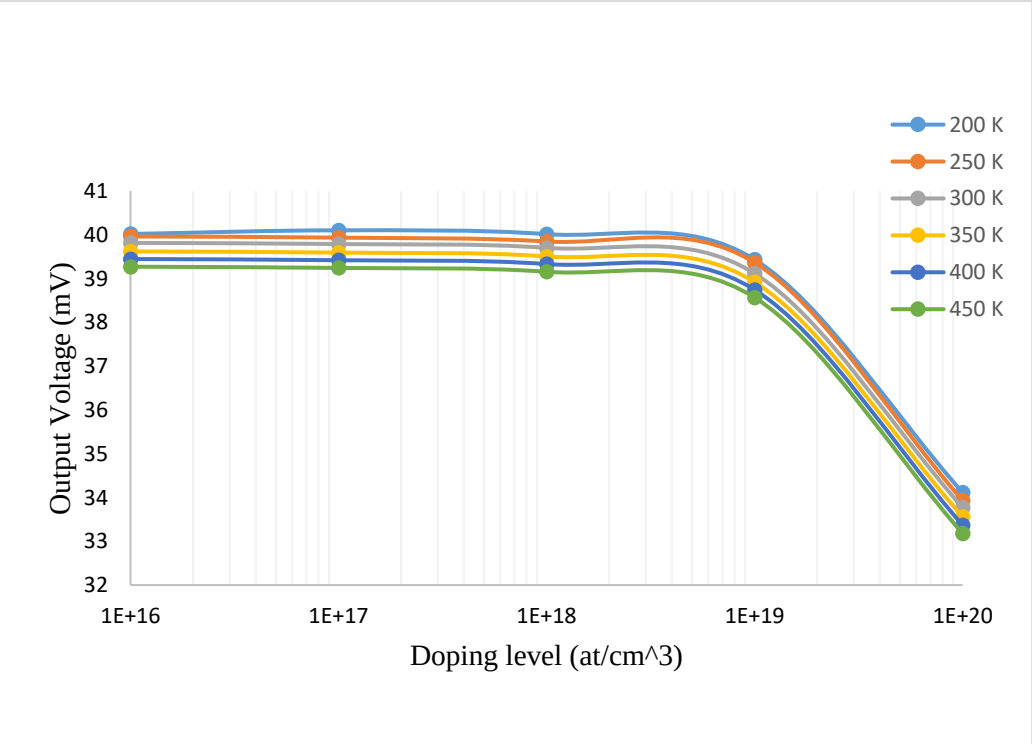

Figure 8.7.3 e: Variation of output voltage with doping concentration at different temperatures

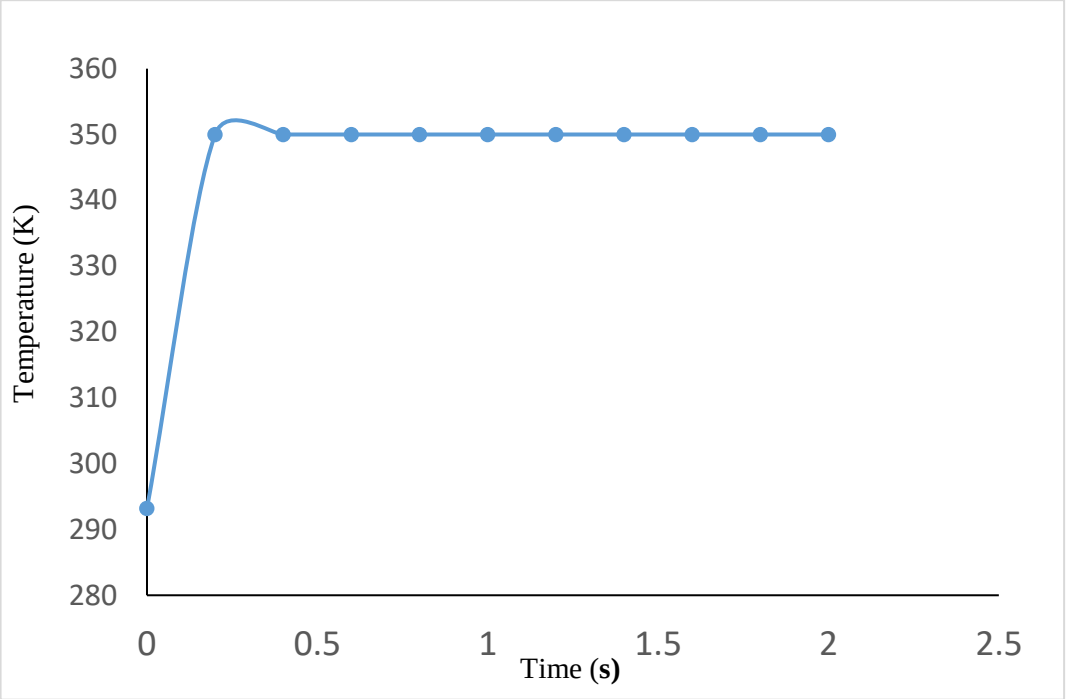

Figure 8.7.3 f: Temperature variation due to ohmic heating with time

CHAPTER 9.0 NUMERICAL SIMULATION OF MICROPUMP COUPLED WITH PRESSURE SENSOR

9.1 Introduction

As a completion of the theoretical design, it is necessary to perform a numerical analysis for the entire theoretical model as shown in Figure 9.1. Hence the complete numerical simulation analysis for the micropump coupled with pressure sensor was carried out with appropriate tools. Further, this analysis is an added advantage to decide the applicability of this device within prescribed pressure ranges.

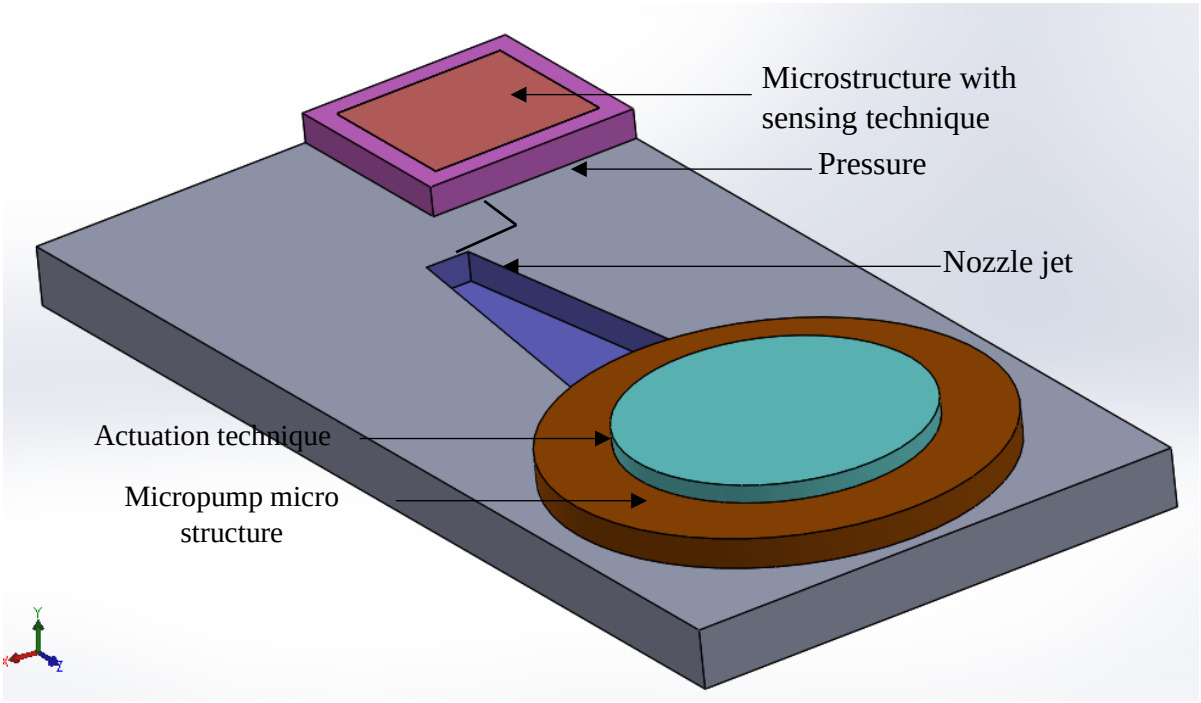

Figure 9.1: Entire Theoretical model – Micropump coupled with pressure sensor

9.2 Simulation Analysis of Micropump coupled with Pressure Sensor

From the numerical simulation analysis, the deflection and stress contours of the designed pressure sensor are obtained and expressed in Figure 9.2 a and Figure 9.2 b respectively.

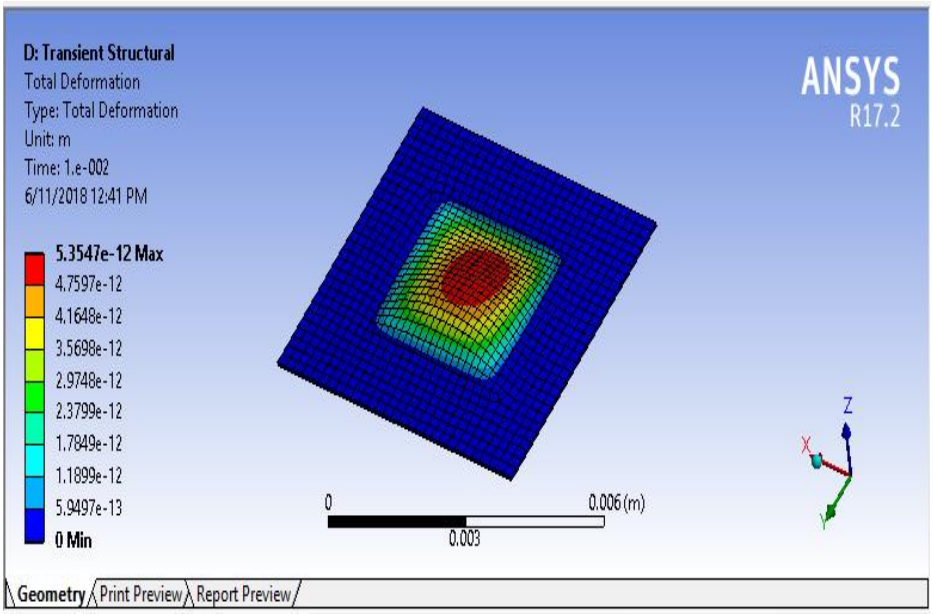

Figure 9.2 a: Deflection contours of designed pressure sensor

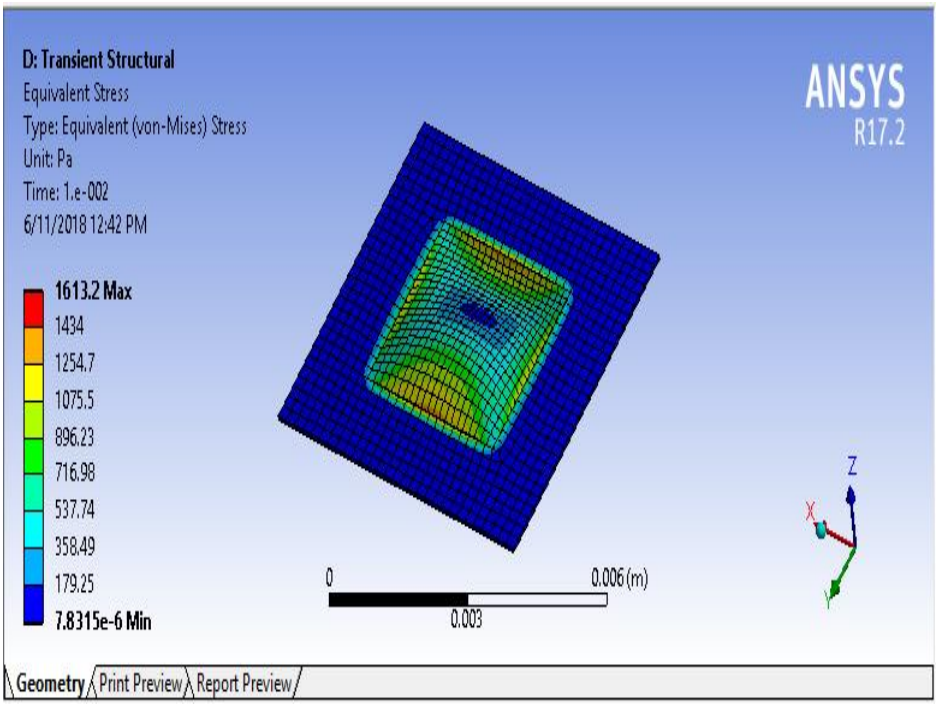

Figure 9.2 b: Von - mises stress contours of designed pressure sensor

The vital objective of this analysis is to reach the measurable sensitivity for the micropump discharge pressure with the designed pressure sensor. Thus, the piezoresistive-structural couple field analysis using COMSOL Multiphysics was done. From this analysis, the output voltage and the sensitivity are determined for the

respective discharge pressure values and tabulated in Table 9.2 a. Further, the variation of sensitivity with discharge pressure is plotted as illustrated in Figure 9.2 c.

Table 9.2 a: Variation of output voltage and sensitivity with discharge pressure

Discharge pressure (kPa)	Output voltage (mV)	Sensitivity ((mV/V)/(kPa))
50	39.1655	0.52221
75	39.1425	0.52190
100	39.1195	0.52159
125	39.0965	0.52129
150	39.0735	0.52098
175	39.0506	0.52067
200	39.0276	0.52037
225	39.0046	0.52006
250	38.9816	0.51975
275	38.9586	0.51945

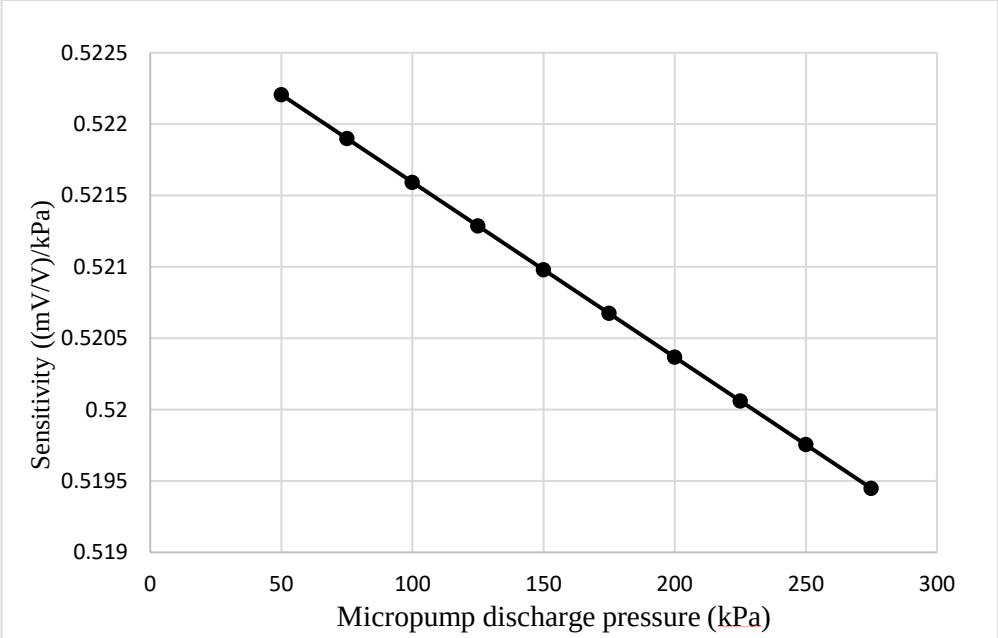

Figure 9.2 c: Variation of sensitivity with discharge pressure

CHAPTER 10.0 DISCUSSION

According to the simulation analysis of micropump, piezoelectric structural simulation reveals that the thin film deposition of polymers on PZT brass diaphragm improves the mechanical property as well as changes the resonant frequency of the diaphragm. Also, the thin film deposition of PMMA gives comparably maximum deflection as well as the maximum stress. But the resonant frequency of these diaphragms is considerably large. One the other hand, thin film deposition with PDMS gives the second most maximum deflection and maximum stress too. In addition, the resonant frequencies of these diaphragms are comparatively less and thin film deposition of 220 um PDMS gives the least natural frequency as 1568.4 Hz. In contrast the simple PZT actuated brass diaphragm relatively has less maximum deflection and stress values too. But the natural frequency is bit large. Hence the application of thin film polymer deposition on a PZT actuated brass diaphragm improves the mechanical properties of respective actuators and this thin film deposition techniques will be considered for future improvements as well.

As per the plots obtained in the simulation analysis of micropump, when the net flow rate varies with frequency the pump flow rate increases up to a maximum level at a specific frequency and then by increasing the frequency, the flow rate is again reduced. This happens due to the eigenfrequency of the piezoelectric diaphragm. This analysis will also be applicable to control the micropump flow rate. According to the test results obtained from the piezoelectrically actuated dual diaphragm valveless micropump, it is understood that the flow rate is increasing up to a specific point and then decreasing when the frequency varies from 0 Hz to a specific value. Thus, the maximum net flow rate of 512 ul /s at 100 Hz is attained. According to the respective plot for the variation of flowrate with discharge pressure head at constant applied frequency, the flow rate decays with the growing pressure head and this reaches 24 mm H_2O as the maximum pump head. This pump curve for the developed pump is necessary to understand the flow characteristics during the designing of micropumps for specific requirements.

As per the respective plots obtained for the variation of flowrate with frequency, the maximum flowrate for the respective frequency during the experiment is less than that of the simulation. This may occur due to several reasons. There may be a voltage drop

due to noises and interreferences at the signal generator. Hence the signal and the system amplitude are distorted. Therefore, it is difficult to get pure sinusoid wave form. Due to this wave form distortion, V_{rms} is reduced and the amplifier voltage is distorted. Further, the amplifier output might vary due to the internal impedance of the amplifier. In addition, the wires used to interconnect the whole circuit might have some internal resistances and this is also an essential factor in the output variation.

According to the respective plots for the thermo-elastic damping effects in PZT actuators, the Quality factor (Q) of PZT actuator varies with increasing mode frequency due to thermo-elastic damping effect and the Quality factor (Q) decreases with increasing temperature. Further, comparing with heat generation, heat dissipation is high at 200 K and decreasing with increasing temperature. Although comparing with heat generation, heat dissipation is less at 300 K. Hence 0.015 m^3/s of air cooling is necessary to operate the device at the ambient temperature. In addition, 0.017 m^3/s and 0.012 m^3/s of air cooling are necessary to operate the device with PDMS thin film coated PZT actuated diaphragm and PMMA thin film coated PZT actuated diaphragm at the ambient temperature.

In case of the structural simulation of pressure sensors, all three structures reach the supreme deflection on the center of the thin diaphragm and four edges of square membrane attain maximum stress parameters too. On the other hand, the circular membrane reaches supreme stresses along its perimeter and the two rectangular membranes attain supreme stresses along the edges. But the longer edges have higher value than the shorter edges in cross section beam membrane.

Even though all three membranes fulfil the basic thin plate deflection concepts, the square membrane provides the supreme parameters. Considering the operation of the diaphragm, it is much valuable to identify the maximum displacement mode frequency and hence this is determined as 97.489 kHz. As per the sensitivity analysis of the piezoresistive pressure sensor, the sensitivity has linear variation with specified pressure and this satisfies with the theoretical features. This data will also be necessary to vary the frequency to be applied to the pressure sensor diaphragm within the specified range.

The respective plots for thermo-mechanical analysis of piezoresistive pressure sensors reveal that the response of the sensor is decreasing with increasing temperature.

However, the response of the sensor is linear within the temperature range considered and it fits with theoretical equations. Further, the plot of variation of output voltage with doping concentration expresses that the increasing doping concentration lowers the output signal. But the output signal rapidly decreases when the doping level increases beyond 10^{19}[atom/cm^3]. Due to ohmic heating effect, the temperature of piezoresistive pressure sensor initially varies with the time and then it is constant.

The numerical simulation of pressure sensor coupled with the solution of fluid flow analysis reveal that the maximum deflection and stress obtained in the designed pressure sensor are within the range of allowable maximum deflection. In addition, the variation of sensitivity gives the linear variation over the range of micropump discharge pressure. Hence the designed pressure sensor seems very much suitable for the proposed micropump used in microfluidic applications.

Though miniaturization is very much useful for onsite microfluidic applications in biomedicine, this device can be further miniaturized with some limitations. Basically, the flow rate variation depends on the volume change of the pump chamber and the frequency. On the other hand, the volume changes mainly depend on the maximum amplitude of the PZT actuator and the radius of the PZT actuated diaphragm. Due to the miniaturization with the same PZT actuator, the flowrate will not have much impact unless otherwise changing the applied voltage for further increment of the amplitude of the PZT actuator. But there will be a maximum limitation for this applied voltage. If it is gone beyond that, the PZT disk would be highly susceptible to crack damage due to the large strain developed. Hence further studies will be carried out in future to analyze this maximum voltage for further miniaturization of this device with maximum flowrate.

Commonly, micropumps have many applications. Even though this proposed micropump can have the potential to develop with pressure feedback and monitoring system, this is mainly motivated for onsite microfluidic applications. Further studies will be carried out to analyze this device with bio-fluids as well.

CONCLUSION

Development of onsite microfluidic devices for biomedical applications are widespread and they are helpful to human to make their life easy and healthy. Amongst all of these microfluidic devices, fluid transmission applications micropumps are very much essential. On the other hand, there are various factors that have to be considered during the selection of micropumps for a certain microfluidic application. Among these factors, operating voltage, actuation techniques and flow rate are most critical to analyze the performance and suitability of micropumps for such applications. Hence, the main motive of this research is to design and fabricate a PZT based micropump for microfluidic applications.

As an initial stage of this research, the modelling and simulation studies were performed for a PZT actuated membrane. Then the design and simulation analysis were executed for a single diaphragm valveless micropump as well as dual diaphragm micropump. After that, a single diaphragm PZT actuated valveless micropump was fabricated with the optimal design features. As an improvement of this micropump, a dual diaphragm PZT actuated valveless micropump was also fabricated. The developed dual diaphragm micropump was tested for a constant applied frequency as well as at different discharge pressure head. The test results revealed that the flow rate decays with the growing pressure head and this pump curve for the developed pump is necessary to understand the flow characteristics during the designing of micropumps for specific requirements.

As for the benefit of microfluidic applications in biomedicine, modelling and simulation analysis were carried out for a PZT actuator with thin film deposition techniques of two kind of polymers namely PMMA and PDMS. Although thermal effects in micro scale devices are very much considerable, thermo-elastic damping analysis for PZT actuator as well as thin film deposited PZT actuators were also fulfilled.

The pressure feedback and monitoring of this micropump is also very much considerable during the microfluidic application. Therefore, a model was designed and simulated for a MEMS based piezoresistive pressure sensor. In this sense, an analysis was done for three different diaphragm geometries by varying the dimensional

parameters. According to the results obtained in FEM analyses, the square type diaphragm is chosen as best diaphragm geometry. In addition, simulation analysis revealed that the square type piezoresistive pressure sensors have better sensitivity for a wide range of pressure values. Not only from the FEM analysis, but also this square type membrane with piezoresistive sensing would be the best selection over other diaphragms by comparing the fabrication costs, transduction techniques and microfluidic applications. In addition, thermo mechanical analysis was also carried out to simulate the effect of temperature and doping concentration on the characteristics of proposed pressure sensor. To analyze the applicability of this device with pressure feedback, numerical simulation analysis was carried out for a micropump coupled with pressure sensor.

Even though this proposed micropump is mainly motivated in the field of microfluidic applications in biomedicine, material selection for this should be reviewed in a proper manner to choose the compatible material for the specific application. Henceforth, further research studies will also be performed in miniaturizing the device to micro scale with the most suitable biocompatible materials.

References

[1] F. R. Munas, Y. W. Ranjith Amarasinghe, and D. Dao, "Review on MEMS based Micropumps for Biomedical Applications," *Int. J. Innov. Res. Sci. Eng. Technol. (An ISO Certif. Organ.*, vol. 3297, no. 7, pp. 5602–5615, 2007. (Available at:http//www.ijirset.com)

[2] A. Nisar, N. Afzulpurkar, B. Mahaisavariya, and A. Tuantranont, "MEMS-based micropumps in drug delivery and biomedical applications," *Sensors Actuators, B Chem.*, vol. 130, no. 2, pp. 917–942, 2008.

[3] F. Abhari, H. Jaafar, and N. A. Md Yunus, "A comprehensive study of micropumps technologies," *Int. J. Electrochem. Sci.*, vol. 7, no. 10, pp. 9765–9780, 2012.

[4] F. R. Munas,G. Melroy, C. B. Abeynayake, H. L. Chathuranga, R. Amarasinghe, P. Kumarage, V. T. Dau, and D. V.Dao, "Development of PZT actuated valveless micropump," *MDPI Sensors (Switzerland)*, vol. 18, no. 5, 2018. doi:10.3390/s18051302 (Available at: http//www.mpi.com/journals/sensors)

[5] R. Zengerle, J. Ulrich, S. Kluge, M. Richter, and A. Richter, "A bidirectional silicon micropump," "*Sensors and Actuators, A Phys."*, vol. 50, no. 1–2, pp. 81–86, 1995.

[6] Z. X. Zou, Y. Z. Ye, Y. Zhou, and Y. Yang "A novel thermally actuated silicon micropump," in *Proceedings of the 1997 International Symposium on Micromechatronics and Human Science*, 1997, no. 5, pp. 231–234.

[7] H. Yang, T. H. Tsai, and C. C. Hu, "Portable valve-less peristaltic micropump design and fabrication," *DTIP MEMS MOEMS - Symp. Des. Test, Integr. Packag. MEMS/MOEMS*, no. April, pp. 273–278, 2008.

[8] P. K. Podder, D. P. Samajdar, D. Mallick, and A. Bhattacharyya, "Design and simulation of micro-pump, micro-valve and micro-needle for biomedical applications," *CODEC 2012 - 5th Int. Conf. Comput. Devices Commun.*, vol. 3, pp. 1–4, 2012.

[9] M. Pandey and P. Upadhyay, "Design and Simulation of valve less PZT micropump for drug delivery system," *Int. J. Adv. …*, vol. 3, no. 2, pp. 92–100, 2012.

[10] S. Li, S. Chen, "Analytical Analysis of a circular PZT actuator for valveless micropumps," *Sens. Actuators A*, vol. 104, pp. 151–161, 2003.

[11] P. Woias, "Micropumps - Past, progress and future prospects," *Sensors Actuators, B Chem.*, vol. 105, no. 1, pp. 28–38, 2005.

[12] W. J. Spencer, W. T. Corbett, L. R. Dominguez, and B. D. Shafer, "An Electronically Controlled Piezoelectric Insulin Pump and Valves," *IEEE Trans. Sonics Ultrason.*, vol. 25, no. 3, pp. 153–156, 1978.

[13] J. G. Smits, "Piezoelectric micropump with three valves working peristaltically," *Sensors Actuators A. Phys.*, vol. 21, no. 1–3, pp. 203–206, 1990.

[14] R. Mishra, T. K. Bhattacharyya, and T. K. Maity, "Design and Simulation of Microfluidic Components towards Development of a Controlled Drug Delivery Platform," *2016 29th Int. Conf. VLSI Des. 2016 15th Int. Conf. Embed. Syst.*, no. 1, pp. 583–584, 2016.

[15] E. M. Garcell, "Analysis and Simulation of MEMS Comb-Actuators," pp. 1–23, 2012.

[16] M. J. Simon, V. M. Bright, R. Radebaugh, and Y. C. Lee, “An analytical model for a piezoelectric axially driven membrane microcompressor for optimum scaled down design,” *J. Mech. Des. Trans. ASME*, vol. 134, no. 1, pp. R35–R64, Jun. 2012.
[17] M. W. Ashraf, S. Tayyaba, and N. Afzulpurkar, “Micro Electromechanical Systems (MEMS) based microfluidic devices for biomedical applications,” *Int. J. Mol. Sci.*, vol. 12, no. 6, pp. 3648–3704, Jan. 2011.
[18] S. K. Jha and V. C. Jha, “Design and Fabrication of a Three Dimensional Valveless Micropump with Shape Deposition Manufacturing Process”, *Int. J. Res. Eng. Appl. Sci. (IJREAS)*, vol. 2, no. 2, pp. 805–824, 2012 ISSN : 2249-3905.
[19] M. J. Simon, V. M. Bright, R. Radebaugh, and Y. C. Lee, “An analytical model for a piezoelectric axially driven membrane microcompressor for optimum scaled down design,” *J. Mech. Des. Trans. ASME*, vol. 134, no. 1, 2012.
[20] K. Mahija, B. G. Pushpalatha, and J. J. Jijesh, “Mems Based Drug Delivery System,” *Int. J. Electro Signal and Sys. (IJESS).*, vol. 1, no. 2,pp. 91–95, 2012.
[21] K. Yoshida, T. Muto, J. W. Kim, and S. Yokota, “An ER microactuator with built-in pump and valve,” *Int. J. Autom. Technol.*, vol. 6, no. 4, pp. 468–475, 2012.
[22] J. M. Anderson and J. J. Langone, “Issues and perspectives on the biocompatibility and immunotoxicity evaluation of implanted controlled release systems,” *J. Control. Release*, vol. 57, no. 2, pp. 107–113, 1999.
[23] A. F. M. Shukur, N. Sabani, B. N. Taib, M. A. M. Azidinab, and M. M. Shahiminab, “Performance characteristics of valveless and cantilever-valve micropump,” *Proc. SPIE 8923, Micro/Nano Mater. Devices, Syst.*, vol. 89234B, pp. 1–9, 2013.
[24] C. G. J. Schabmueller, M. Koch, M. E. Mokhtari, A. G. R. Evans, N. M. White, A. Brunnschweiler, and H. Sehr, “Self-aligning gas/liquid micropump,” *J. Micromechanics Microengineering*, vol. 12, no. 4, p. 420, 2002.
[25] Grundfos, *Pump Handbook*, Design of Pumps and Motors, Grandfos Pumps Corporation, 2014.
[26] “Bartels Micropump.”[online] Available: http:// www.bartels-mikrotechnik.de › index.php › products › micropumps
[27] “PiezoelectricPump.”[Online].Available:http://www.dolomite-microfluidics.com/.
[28] C. P. Cartin, “Design, Fabrication, and Testing of a PDMS micro pump with moving membranes,” 2012.
[29] S. Yang, X. He, S. Yuan, J. Zhu, and Z. Deng, “A valveless piezoelectric micropump with a Coanda jet element,” *Sensors Actuators, A Phys.*, vol. 230, pp. 74–82, 2015.
[30] R. S. Jiaqi Wang, Kean C. Aw*, “Optimization of valveless micro pump for drug delivery,” in *Proceedings of the 9th IEEE InternationalConference on Nano/Micro Engineered and Molecular Systems, Hawaii, USA*, 2014.
[31] A. S. Manolis and T. A. Manolis, “Totally Implantable Artificial Heart: Still a Major Challenge,” *Rhythmos*, vol. 9, no. 1, pp. 1–3, 2014.
[32] A. K. Agarwal, J. Atencia, D. J. Beebe, and H. R. Jiang, “Design of microfluidic impellers capable of bi-directional pumping under a single rotating magnetic

actuation," *2007 20th IEEE Int. Conf. Micro Electro Mech. Syst. - MEMS '07*, pp. 667–670, 2007.
[33] M. I. Younis, S. L. Hendricks, and D. J. Leo, "Modeling and Simulation of Microelectromechanical Systems in Multi-Physics Fields," 2004.
[34] M. L. Roukes and R. Lifshitz, "Thermoelastic damping in micro- and nanomechanical systems," *Phys. Rev. B*, vol. 61, pp. 5600–5609, 2000.
[35] P. Ronkanen, P. Kallio, M. Vilkko, and H. N. Koivo, "Self Heating of Piezoelectric Actuators : Measurement and Compensation," *Proceedings of the IEEE International Symposium on Micro-Nanomechatronics and Human Science, Nagoya, Japan, p. 313-318, 2004.*
[36] A. H. Nayfeh and M. I. Younis, "Modeling and simulations of thermoelastic damping in microplates," *J. Micromechanics Microengineering*, vol. 14, no. 12, p. 420, 2004.
[37] B. Kim, C. M. Jha, T. White, R. N. Candler, M. Hopcroft, M. Agarwal, K. K. Park, R. Melamud, S. Chadorkar, and T. W. Kenny, "Temperature Dependence of Quality Factor in MEMS Resonators," *J. Microelectromechanicalsystems*, vol. 17, no. 3, pp. 755–766, 2008.
[38] K. L. Turner, D. R. Clarke, and N. C. Macdonald, "Santa Barbara Energy Dissipations in MEMS Resonators : Fluid Damping of Flexural Resonators and Thermoelastic Damping A dissertation submitted in partial satisfaction of the requirements for the degree Doctor of Philosophy in Mechanical Engineering by Weibin Zhang Committee in charge : Professor Hyongsok Soh," no. December, 2006.
[39] C. Zener, "Internal friction in solids: II. General theory of thermoelastic internal friction," *Phys. Rev*, vol. 53, no. 1, pp. 90–99, 1938.
[40] C. Zener, "Internal friction in solids," *Phys. Rev*, vol. 52, pp. 230–235, 1937.
[41] F. R. Munas, Y. W. R. Amarasinghe, and P. Kumarage, "Design and Simulation of MEMS Based Piezoresitive Pressure Sensor for Microfluidic Applications," in *2018 Moratuwa Engineering Research Conference (MERCon)*, 2018, pp. 215–220.
(Available at: https://ieeexplore.ieee.org/xpl/mostRecentIssue.jsp)
[42] J. W. Judy, "Microelectromechanical systems (MEMS): Fabrication, design and applications," *Smart Mater. Struct.*, vol. 10, no. 6, pp. 1115–1134, 2001.
[43] M. Asadnia, A. G. P. Kottapalli, Z. Shen, J. Miao, and M. Triantafyllou, "Flexible and surface-mountable piezoelectric sensor arrays for underwater sensing in marine vehicles," *IEEE Sens. J.*, vol. 13, no. 10, pp. 3918–3925, 2013.
[44] A. P. Dabrowski and L. J. Golonka, "High pressure sensor with PZT transducer in LTCC package," *Procedia Eng.*, vol. 87, pp. 1099–1102, 2014.
[45] E. Teomete, "Measurement of crack length sensitivity and strain gage factor of carbon fiber reinforced cement matrix composites," *Meas. J. Int. Meas. Confed.*, vol. 74, pp. 21–30, 2015.
[46] D. Dumont-Fillon, H. Tahriou, C. Conan, and E. Chappel, "Insulin micropump with embedded pressure sensors for failure detection and delivery of accurate monitoring," *Micromachines*, vol. 5, no. 4, pp. 1161–1172, 2014.
[47] S. Fournier and E. Chappel, "Modeling of a Piezoelectric MEMS Micropump Dedicated to Insulin Delivery and Experimental Validation Using Integrated

Pressure Sensors: Application to Partial Occlusion Management," *J. Sensors*, vol. 2017, 2017.
[48] J. R. Lake, K. C. Heyde, and W. C. Ruder, "Low-cost feedback-controlled syringe pressure pumps for microfluidics applications," *PLoS One*, vol. 12, no. 4, pp. 1–12, 2017.
[49] J. Wang, C. Zhao, G. H. Zhao, X. F. Jin, S. M. Zhang, and J. B. Zou, "All-quartz high accuracy MEMS pressure sensor based on double-ended tuning fork resonator," *Procedia Eng.*, vol. 120, pp. 857–860, 2015.
[50] H. Schmid-Engel, S. Uhlig, U. Werner, and G. Schultes, "Strain sensitive nano-cermet thin films for high temperature pressure and force sensors," *Sensors Actuators A Phys.*, vol. 206, pp. 17–21, 2013.
[51] J. Cheng, M. Sundholm, B. Zhou, M. Hirsch, and P. Lukowicz, "Smart-surface: Large scale textile pressure sensors arrays for activity recognition," *Pervasive Mob. Comput.*, vol. 30, pp. 97–112, 2016.
[52] A. Arogbonlo, C. Usma, A. Z. Kouzani, and I. Gibson, "Design and Fabrication of a Capacitance Based Wearable Pressure Sensor Using E-textiles," *Procedia Technol.*, vol. 20, pp. 270–275, 2015.
[53] H. K. Lee, J. Chung, S. Chang, and E. Yoon, "Normal and shear force measurement using a flexible polymer tactile sensor with embedded multiple capacitors," *J. Microelectromechanical Syst.*, vol. 17, no. 4, pp. 934–942, 2008.
[54] P. Rey, P. Charvet, M. T. Delaye, and H. S. Abou, "A High Density Capacitive Pressure Sensor Array for Fingerprint Sensor Application," *IEEE Int. Solid-State Sensors Actuators Conf.*, vol. 2, pp. 1453–1456, 1997.
[55] X. Huang and D. Zhang, "A high sensitivity and high linearity pressure sensor based on a peninsula-structured diaphragm for low-pressure ranges," *Sensors Actuators, A Phys.*, vol. 216, pp. 176–189, 2014.
[56] A. Aqilah, A. Jaffar, S. Bahari, C. Y. Low, and T. Koch, "Resistivity characteristics of single miniature tactile sensing element based on pressure sensitive conductive rubber sheet," *Proc. - 2012 IEEE 8th Int. Colloq. Signal Process. Its Appl. CSPA 2012*, vol. 12, pp. 223–227, 2012.
[57] K. Noda, Y. Hashimoto, Y. Tanaka, and I. Shimoyama, "MEMS on robot applica- tions," in *Proceedings of the Solid-State Sensors, Actuators and Microsystems Conference (TRANSDUCERS). International*, 2009, pp. 2176–2181.
[58] W. P. Eaton and J. H. Smith, "Micromachined pressure sensors: review and recent developments," *Smart Mater. Struct.*, vol. 6, pp. 30–41, 1997.
[59] V. Balaji and K. N. Bhat, "A Comparison of Burst Strength and Linearity of Pressure Sensors having Thin Diaphragms of Different Shapes," *J. Isss*, vol. 2, no. 2, pp. 18–26, 2013.
[60] S. Santosh Kumar, A. K. Ojha, R. Nambisan, A. K. Sharma, and B. D. Pant, "Design and Simulation of MEMS Silicon Piezoresistive Pressure Sensor for Barometric Applications," *Int. Conf. Adv. Recent Technol. Electr. Electron.*, pp. 339–345, 2013.
[61] B. Ziaie, A. Baldi, and M. Z. Atashbar, *Hand Book of Nanotechnology: Introduction to Micro Nano Fabrication, Part A Nanostructures, Micro-/Nanofabrication and Materials Springer,*. ISBN 978-3-540-01218-4. Springer-Verlag Berlin.

[62] J. C. Doll and B. L. Pruitt, *Microsystems and Nanosystems: Piezoresistor Design and Applications,* ISBN 978-1-4614-8516-2 ISBN 978-1-4614-8517-9(eBook).
doi:10.1007/978-1-4614-8517-9

[63] R. Amarasinghe, D. V. Dao, T. Toriyama, and S. Sugiyama, "Design and fabrication of a miniaturized six-degree-of-freedom piezoresistive accelerometer," *J. Micromechanics Microengineering*, vol. 15, no. 9, pp. 1745–1753, 2005.

[64] K. N. Bhat, "Silicon micromachined pressure sensors," *J. Indian Inst. Sci.*, vol. 87, no. 1, p. 115, 2012.

[65] A. Beddiaf and F. Kerrour, "Study of the Impact of Thermal Drift on Reliability of Pressure Sensors," *J. Eng Sci and Tech.* vol. 12, no. 10, pp. 2677–2690, 2017.

[66] B. Abdelaziz, K. Fouad, and S. Kemouche, "The Effect of Temperature and Doping Level on the Characteristics of Piezoresistive Pressure Sensor," *J. Sensor Tech.*, vol.4, pp. 59–65, 2014. http://dx.doi.org/10.4236/jst.2014.42007.

[67] Y. Kanda, "Piezoresistance Effect of Silicon," *Sensors Actuators A Phys.*, pp. 83–91, 1991.

[68] K. K. Ng and S.M. Sze, "*Physics of Semiconductor Devices*.," 3rd Edition, JohnWiley & Sons, New York, 2007.

[69] M. A. Green, "Intrinsic concentration, effective densities of states, and effectivemass in silicon.," *J. Appl. Phys*, vol. 6, pp. 2944–2954, 1990.

[70] O. H. J. Richter, J. Pedersen, M. Brandbyge, E.V. Thomsen, "Piezoresistance in p-type silicon," *J. Appl. Phys*, vol. 023715, 2008.

[71] C. Jenke, J. P. Rubio, S. Kibler, J. Häfner, M. Richter, and C. Kutter, "The combination of micro diaphragm pumps and flow sensors for single stroke based liquid flow control," *Sensors (Switzerland)*, vol. 17, no. 4, pp. 14–16, 2017.

[72] Z. G. Feng and E. E. Michaelides, "Proteus: A direct forcing method in the simulations of particulate flows," *J. Comput. Phys.*, vol. 202, no. 1, pp. 20–51, 2005.

[73] S. W. Van Der Merwe, A. A. Groenwold, P. W. Loveday, and G. D. Thiart, "A MEMS Based Valveless Micropump for Biomedical Applications," *7th South Afri.. Conf. Computational. Appl. Mech(SACAM).*, January, 2010.

[74] P. Gowdhaman, V. Annamalai, and O. P. Thakur, "Piezo, ferro and dielectric properties of ceramic-polymer composites of 0-3 connectivity," *Ferroelectrics*, vol. 493, no. 1, pp. 120–129, 2016.

[75] Q. Li, L. Chen, M. R. Gadinski, S. Zhang *et al.*, "Flexible high-temperature dielectric materials from polymer nanocomposites," *Nature*, vol. 523, no. 7562, pp. 576–579, 2015. doi:10.1038/nature14647

[76] C. He. and W. G. Chen, "Preparation and application of piezoelectric materials and its research status," in *Proc.of Funt. Mate*, 2010, pp. 11–13.

[77] M. Ghosh and M. G. Rao, "Growth mechanism of ZnO nanostructures for ultra-high piezoelectric coefficient," *Materials Express*, 2013, vol. 3, no. 4, pp. 319–327.

[78] R. Li, J. Zhou, H. Liu, and J. Pei, "Effect of polymer matrix on the structure and electric properties of piezoelectric lead zirconatetitanate/polymer composites," *Materials (Basel).*, vol. 10, no. 8, 2017.

[79] M. F. Lin, V. K. Thakur, E. J. Tan, and P. S. Lee, “Surface functionalization of $BaTiO_3$ nanoparticles and improved electrical properties of $BaTiO_3$/Polyvinylidene fluoride composite,” *RSC Adv.*, vol. 1, no. 4, pp. 576, 2011.

[80] Y. Mengyao, W. Wei. et al, “Research Progress and Development Trend of Smart Transmission Line Technologies,” *Xiandai Huagong/Modern Chem. Ind.*, vol. 2, no. 4, pp. 0–4, 2011.

[81] V. Tiwari, and G. Srivastava. “Structural, dielectric and piezoelectric properties of 0–3 PZT/PVDF composite,” *Ceram. Int*, pp. 41, 8008–8013, 2015. ISSN :0272-8842 Doi: 10.1016/j.ceramint.2015.02.148

[82] V. T. Dau, T. X. Dinh, R. Sakamoto, O. Tomonori, and S. Sugiyama, “A valve-less micro pump with pzt diaphragm,” *Proceedings of the* 12th *Int. Conf. Miniaturized. Sys. Chemi. Life Sci. USA*, 2008, pp. 1369–1371.

[83] J. J. Rojas and J. E. Morales, “Design and Simulation of A Piezoelectric Actuated Valveless Micropump,” in *Proceedings of the COMSOL Conference, Boston, MA, USA*, 2015, no. 1, pp. 3–6, 2015.

[84] V. T. Dau, T. X. Dinh, and S. Sugiyama, “A MEMS-based silicon micropump with intersecting channels and integrated hotwires,” *J. Micromechanics Microengineering*, vol. 19, no. 12, 2009.

[85] V. T. Dau, T. X. Dinh, T. Katsuhiko, and S. Susumu, “A cross-junction channel valveless-micropump with PZT actuation,” *Microsyst. Technol.*, vol. 15, no. 7, pp. 1039–1044, 2009.

[86] V. T. Dau, T. X. Dinh, Q. D. Nguyen, R. Amarasinghe, K. Tanaka, and S. Sugiyama, “Microfluidic valveless pump actuated by electromagnetic force,” *Proceedings of IEEE Sensors*, 2009, pp. 679–682.

[87] T. X. Dinh, N. T. M. Le, V. T. Dau, and Y. Ogami, “A dynamic model for studying valveless electromagnetic micropumps,” *J. Micromechanics Microengineering*, vol. 21, no. 2, p. 21, 2011.

[88] N. Q. Dich, T. X. Dinh, P. H. Pham, and V. T. Dau, “Study of valveless electromagnetic micropump by volume-of-fluid and OpenFOAM,” *Jpn. J. Appl. Phys.*, vol. 54, no. 5, 2015.

[89] G. Melroy, C. B. Abeynayake, and H. L. chathuranga,"Design and Development of a Micropump for Biomedical Applications," BSc thesis, Dept of Mec. Engineering, UOM, SriLanka, May 2017.

[90] S. S. Krishna, N. V. S. A. Sai, and K. S. Rao, “Design and Simulation of MEMS 3D Piezoelectric Accelerometer,” in *Proceedings of the COMSOL Conference, Boston, MA, USA*, 2014, vol. 2, no. 2, pp. 77–81.

[91] W. Malalasekera, H. K. Versteeg, and H. K. Versteeg, *An introduction to computational fluid dynamics : the finite volume method*. Prentice Hall: Englewood Cliffs, NJ, USA, 2007.

[92] M. J. Simon, V. M. Bright, R. Radebaugh, and Y. C. Lee, “An analytical model for a piezoelectric axially driven membrane microcompressor for optimum scaled down design,” *J. Mech. Des. Trans. ASME*, vol. 134, no. 1, pp. 14, R35–R64, 2012.

[93] E. R. K. Comeford, S. Elliot, and S. Nivers, “Application and Design of Acrylic Microfluidic Chips,” *Project Report, Worcestor Polytechnic Institute*, 2017.

[94] A. Bamshad, A. Nikfarjam, and H. Khaleghi, “A new simple and fast thermally-

solvent assisted method to bond PMMA-PMMA in micro-fluidics devices," *J. Micromechanics Microengineering*, vol. 26, no. 6, 2016.
[95] A. M. G. Borges, L. O. Benetoli, M. Licinio *et al.*, "Polymer films with surfaces unmodified and modified by non-thermal plasma as new substrates for cell adhesion," *Mater. Sci. Eng. C*, vol. 33, no. 3, pp. 1315–1324, 2013.
[96] J. Shi, Z. Luo, D. Zhu, and S. P. Beeby, "PDMS/PVA composite ferroelectret for improved energy harvesting performance," *J. Phys. Conf. Ser.*, vol. 773, no. 1, 2016.
[97] G. da S. Padilha, V. M. Giacon, and J. R. Bartoli, "Effect of solvents on the morphology of PMMA films fabricated by spin-coating," *Polímeros*, vol. 27, no. 3, pp. 195–200, 2017.
[98] E. Mohajerani, F. Farajollahi, R. Mahzoon, and S. Baghery, "Morphological and thickness analysis for PMMA spin coated films," *J. Optoelectron. Adv. Mater.*, vol. 9, no. 12, pp. 3901–3906, 2007.
[99] H. Q. Zhang, Y. Jin, and Y. Qiu, "The optical and electrical characteristics of PMMA film prepared by spin coating method," *IOP Conf. Ser. Mater. Sci. Eng.*, vol. 87, no. 1, 2015.
[100] D. Meyerhofer, "Characteristics of resist films produced by spinning," *J. Appl. Phys.*, vol. 49, no. 7, pp. 3993–3997, 1978.
[101] D. F. S. Petri, "Characterization of spin-coated polymer films," *J. Braz. Chem. Soc.*, vol. 13, no. 5, pp. 695–699, 2002.
[102] D. W. Schubert, "Spin coating as a method for polymer molecular weight determination," *Polym. Bull.*, vol. 38, no. 2, pp. 177–184, 1997.
[103] A. F. Dário, H. B. MacIa, and D. F. S. Petri, "Nanostructures on spin-coated polymer films controlled by solvent composition and polymer molecular weight," *Thin Solid Films*, vol. 524, no. 1, pp. 185–190, 2012.
[104] A. Nallathambi, and T. Shanmuganantham, "Sensors & Transducers Design of Diaphragm Based MEMS Pressure Sensor with Sensitivity Analysis for Environmental Applications," vol. 188, no. 5, pp. 48–54, 2015.
[105] A. Mishra, I. Bahal, J. Arya, A. Pandey, and S. Urooj, "Sensitivity Analysis of MEMS Based Piezoresistive Sensor Using COMSOL Multiphysics," *Proceedings of the 3rd International Conference on Frontiers of Intelligent Computing: Theory and Applications (FICTA) 2014: Volume 1*, 2015, pp. 59–67.
[106] T. R. Hsu, "MEMS & Microsystem: Design and Manufacture," Tata McGraw-Hill, 2002, pp. 34–47, 271–300.
[107] U. Sampath Kumar and N. Jagadesh Babu, "Design and Simulation of MEMS Piezoresistive Pressure Sensor to Improve the Sensitivity," vol. 3, no. 3, pp. 153–155, 2015.
[108] T. G. P. Priyadarshana, H. M. D. P. Wijethunge, B. C. C. P. Jayasekara, and Y. W. R. Amarasinghe, "Design and Optimization of a MEMS Based Piezoresistive Pressure Sensor for Flash Flood Level Measurement," pp. 55–61, 2012.
[109] Y. Kanda, "Piezoresistance effect of silicon," *Sensors Actuators A. Phys.*, vol. 28, no. 2, pp. 83–91, 1991.
[110] C. S. Smith, "Piezoresistance effect in germanium and silicon," in *Physical Review*, vol. 94, no. 1, 1954, pp. 42–49.

[111] M. Mohammadi, A.R., Bennington, C.P.J. and Chiao, “Development of a Combined Piezoresistive Pressure and Temperature Sensor Using a Chemical Protective Coating for Kraft Pulp Digester Process Monitoring,” *J. Micromechanics Microengineering*, vol. 21, 2011.
[112] B. Othmani, R., Benmoussa, N. and Benyoucef, “The Thermal Drift Characteristics of Piezoresistive Pressure Sensor,” *Phys. Procedia*, vol. 21, pp. 47–52, 2011.

Appendix A: Production drawings of micropump

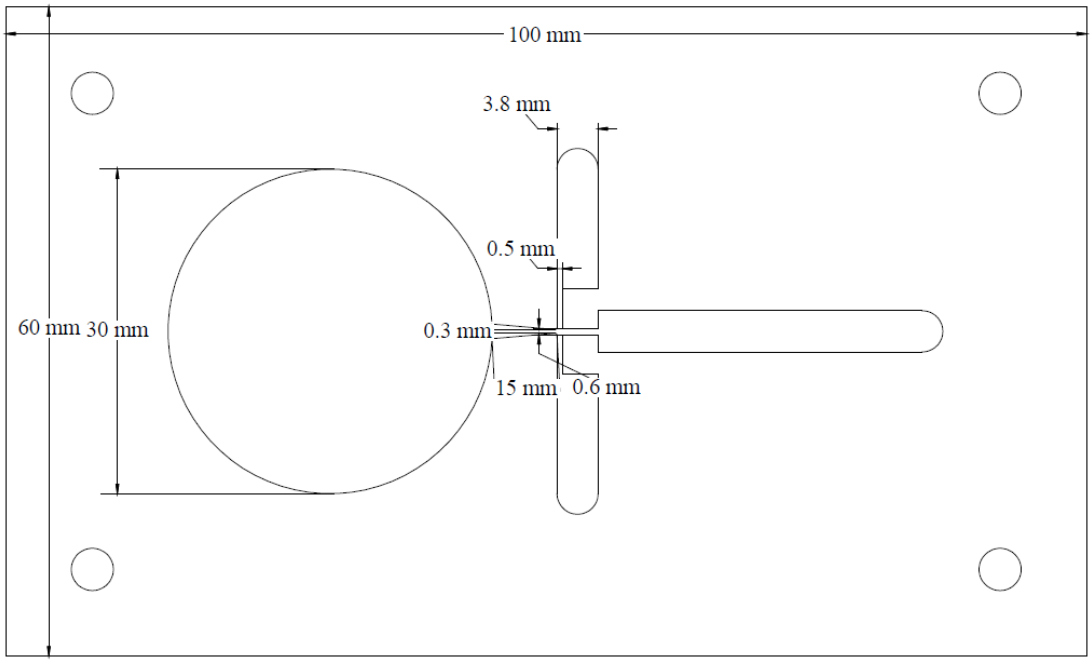

Details of Microfluidic channels and pump chamber

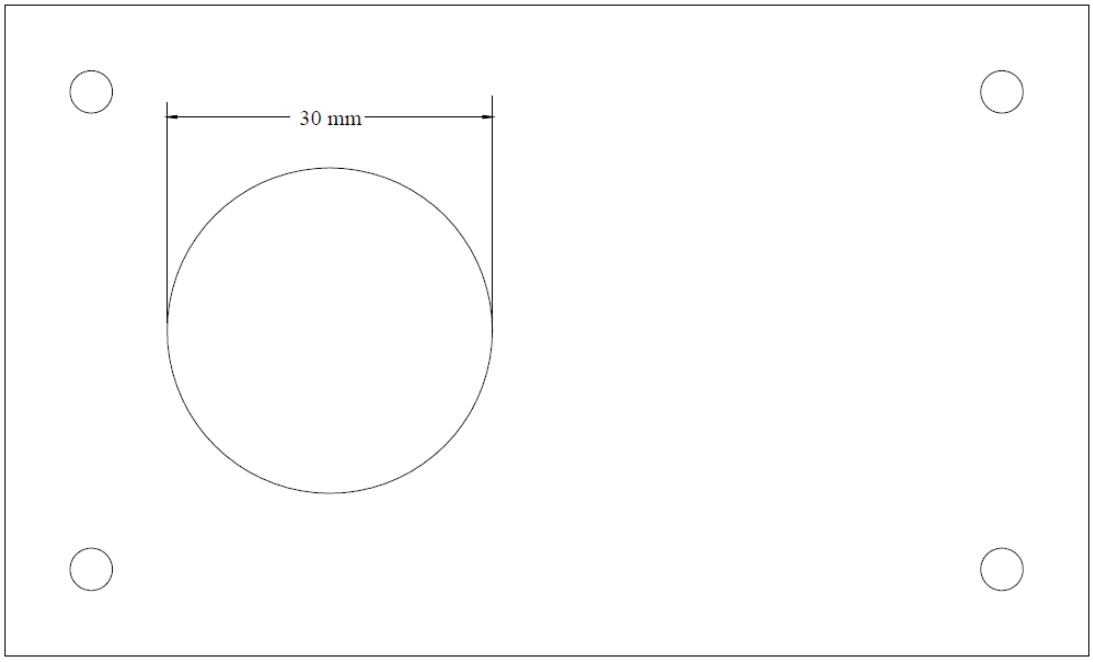

Layers for pump chamber

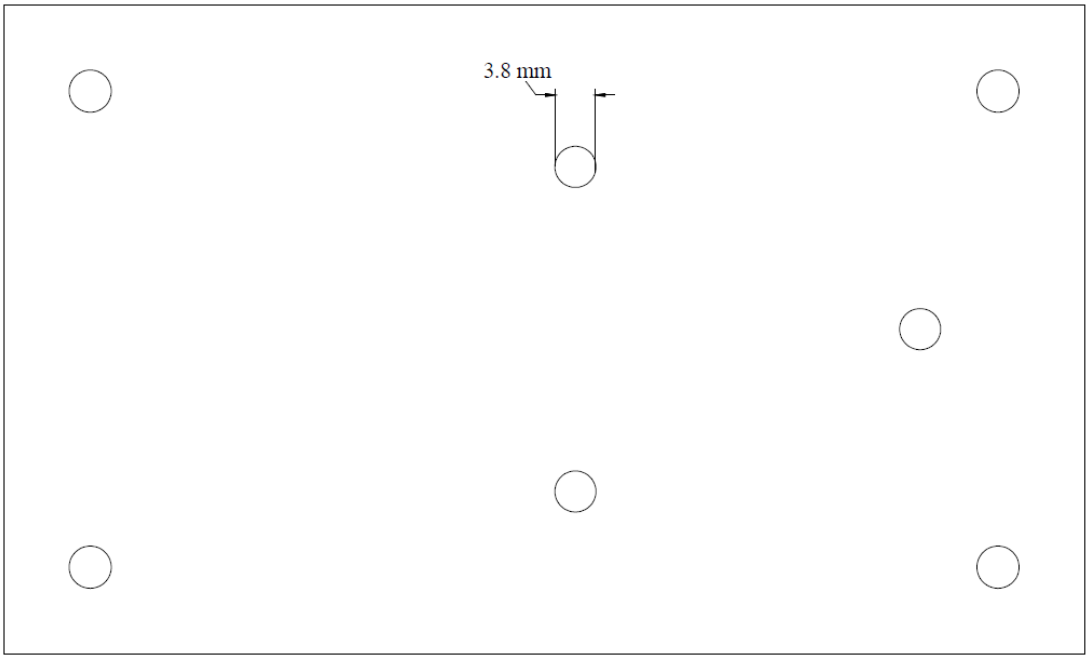

Details of inlet/outlet ports

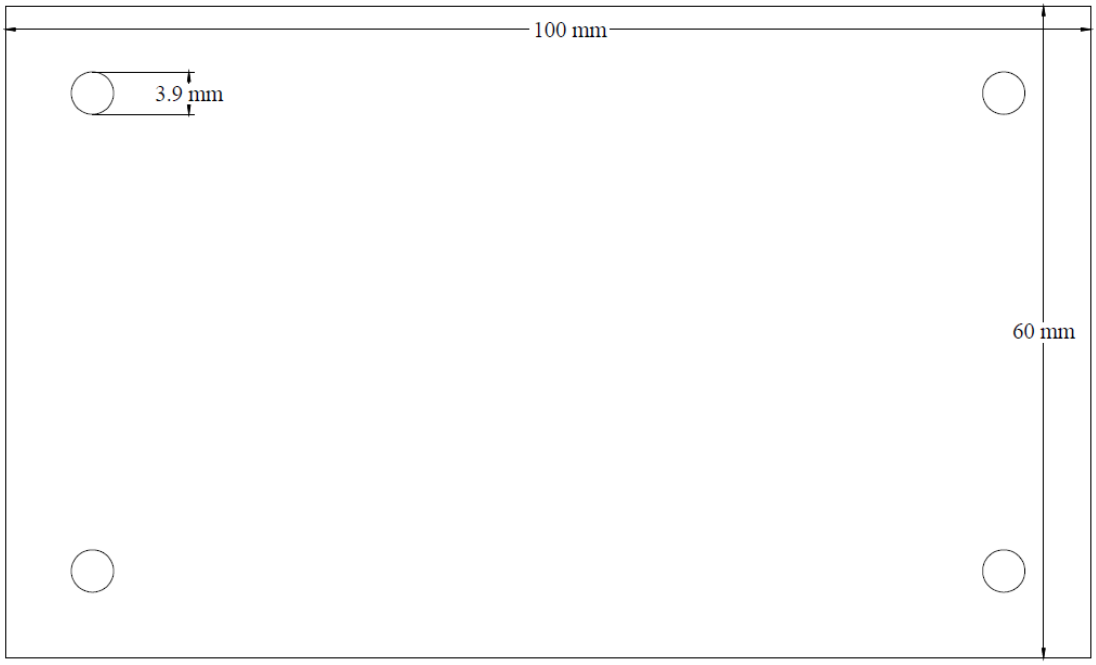

Detailed dimensions of PMMA sheets

Appendix B: Arduino Code of Graphical User Interface[89]

```
#define PWMoutPin1 7
#define PWMoutPin2 8
void setup() {
  pinMode(PWMoutPin1, OUTPUT);
  pinMode(PWMoutPin2, OUTPUT);
}
void loop() {
  int val = analogRead(1);
  val = map(val, 0, 1023, 25, 1000);
  digitalWrite(PWMoutPin1, HIGH);
  digitalWrite(PWMoutPin2, LOW);
  delay(val);
  digitalWrite(PWMoutPin1, LOW);
  digitalWrite(PWMoutPin2, HIGH);
  delay(val);
}
```

```
#include <AD9850.h>
const int W_CLK_PIN = 7;
const int FQ_UD_PIN = 8;
const int DATA_PIN = 9;
const int RESET_PIN = 10;
double freq = 1000;
double trimFreq = 124999500;
int phase = 0;
void setup(){
  DDS.begin(W_CLK_PIN, FQ_UD_PIN, DATA_PIN, RESET_PIN);
  DDS.calibrate(trimFreq);
```

```
}
void loop(){
  DDS.setfreq(freq, phase);
  while(1);
}
```

AD9850.h Arduino library has been provided in https://github.com/F4GOJ/AD9850

Appendix C: Overall design of the signal conditioning circuit[89]